THE CLASSICAL THEORY OF FIELD EVAPORATION

BY

RANAJIT KUMAR BISWAS

Submitted for the

Degree of Doctor of Philosophy

at the

University of Aston in Birmingham

OCTOBER 1987

THE UNIVERSITY OF ASTON IN BIRMINGHAM

THE CLASSICAL THEORY OF FIELD EVAPORATION

BY

RANAJIT KUMAR BISWAS

Submitted for the
Degree of Doctor of Philosophy
at the
University of Aston in Birmingham
OCTOBER 1987

SUMMARY

The field evaporation literature has been carefully analysed and is shown to contain various confusions. After redefining consistent terminology, this thesis investigates the mechanisms of field evaporation, in particular, the relevance of the theoretical mechanisms by analysing available experimental data. A new formalism (The "extended image-hump formalism") is developed and is used to devise several tests of whether the Mueller mechanism is operating. The general conclusion is that in most cases the Mueller mechanism is not operating and escape takes place via Gomer-type mechanisms.

Keywords

CHARGED SURFACES, FIELD-ION EMISSION, FIELD EVAPORATION, MUELLER MECHANISM, EXTENDED IMAGE-HUMP FORMALISM

DEDICATION

In loving memory of my father, Sri Parimal Chandra Biswas, who would have been very happy to see this work of mine completed.

ACKNOWLEDGEMENTS

The supervisor of this project was Dr. R. G. Forbes, and I would like to acknowledge my sincere gratitude to him for his guidance, help and encouragement with this work; I am specially grateful for his efforts to maintain close contact with me after he had left the University of Aston in Birmingham to take up an appointment in the University of Surrey.

I am also grateful to Professor T. Mulvey for his guidance and continued interest in the subject, and also for being my supervisor during the time of writing up the thesis.

I thank my parents for their encouragement and moral support throughout my education.

Finally, I am especially grateful to my wife Ira, my son Buro and my daughter Ria for their patience and unfailing support during my years as a research student.

CONTENTS

LIST OF FIGURES

LIST OF TABLES

CHAPTER 1

INTRODUCTION AND BASIC CONCEPTS

1.1 Field evaporation

Atoms may be removed in the form of ions by applying a high electric field to a metallic surface. This process is known as field desorption; it was discovered by Mueller (1941) when he applied a high voltage to a pointed barium-covered tungsten emitter.

The desorption process that involves the field-induced emission of ions from their own lattice is known as "field evaporation". Field evaporation is important in several contexts:

1. In the field-ion techniques, field evaporation is used as the tip smoothing process that prepares perfectly clean surfaces. Also, by using a controlled layer-by-layer evaporation process, the interior of a specimen tip can be observed in atomic detail (cf. Mueller 1960).

2. Field evaporation is also of significance as the emission mechanism in atom probe field-ion microscopy (cf. Mueller et. al, 1968) and in related techniques such as field desorption microscopy (cf. Walko and Mueller, 1972). In the atom-probe microscope, layer-by-layer evaporation is used to provide information about the chemical composition of the emitter.

3. Field evaporation is the emission mechanism in certain

experiments which investigate surface atomic behaviour. Examples are: Plummer and Rhodin's (1968) experiment, in which the binding energies of transition- metal elements deposited on tungsten were measured, and Ernst's (1979) experiments on rhodium, from which surface-atom vibrational frequencies were deduced (Ernst and Block, 1980).

4. Field evaporation is also presumed to be the emission mechanism in liquid metal field-ion sources (cf. Swanson, 1980). These sources have considerable technological potential in the areas of ion lithography, selective area ion milling, microcircuit fabrication, and in scanning ion-beam instruments.

1.2 Background to field evaporation theory

The wide applications of field evaporation make it useful to have a good understanding of the theoretical principles involved. However, for many years no unified theory has existed, possibly because of the complex nature of the field evaporation process. The opinions of different authors concerning field evaporation phenomena have often been divergent, and there seem to have been misconceptions about some basic aspects of the field evaporation process.

Some basic questions in field evaporation theory to which there seem no widely accepted answers are:

1. What precisely are the factors that affect the shape of field-evaporated emitter end-forms?

2. What is the bonding state of a metal atom at a charged surface, and how should such atoms be treated? In practice,

the bound atom is sometimes treated as neutral and sometimes as partly ionic.

3. How is the charged, structured surface of a real emitter to be modelled? And how does one determine the position of the emitter´s electrical surface? (For a definition of ´electrical surface´, see section 2.6).

4. What is the exact nature of the initial escape process involved in field evaporation? This issue has been incompletely resolved for a long time, and the true nature of the potential structure in which the desorbing atom moves is still unknown.

5. Precisely what mechanisms are involved in the high temperature field evaporation process, for example in the pulsed-laser atom probe (cf. Kellogg and Tsong, 1980)?

As part of the attempt to find solutions to such problems, it seems useful to try to develop a better understanding of the basic mechanism of conventional low-temperature (near 80 K) refractory metal field evaporation. This is our objective here.

Field evaporation was for a long time assumed to be a single-stage process, i.e. the observed evaporation charge-state was assumed to be identical with that immediately after escape. But, following the recent work by Ernst and by Kingham (see section 3.8 for more details), it is now thought that, for most metals, field evaporation is a two-stage process: first a metal atom escapes as a singly charged or possibly doubly charged ion, and subsequently it may be post-ionised into higher charge states.

Important experimental features of field evaporation (e.g. the field sensitivity) are, however, determined by the initial escape process. So it is useful to look at this in slightly more detail.

The determining features of the escape stage are: (a) the

charge state in the bonding situation before escape; (b) the charge state immediately after escape; (c) the nature of the intermediate step(s) and of the potential barrier over which the nucleus of the evaporating atom escapes.

1.3 Escape mechanisms

For the escape mechanism two principal alternatives have often been considered: (1) The Mueller (or 'image-hump') mechanism; (2) Gomer-type mechanisms, also called surface charge-exchange mechanisms.

The Mueller mechanism (Mueller 1956, 1960) is based on ionic evaporation over a Schottky potential saddle. In the presence of an applied field, a protruding surface atom is assumed to be initially bound either neutral or partially ionized. As it moves away from the surface a change in charge state occurs between the bonding point and the escape point. Escape then occurs, over an image hump, with the ion in a constant well-defined charge state.

Charge-exchange type mechanisms were first discussed by Gomer (1961) and Gomer and Swanson (1963), who treated field evaporation as a special case of field desorption. In Gomer-type mechanisms the desorbate is again assumed initially bound in a neutral or partially ionized state; however, in this mechanism it is assumed that ionization and escape occur together, ionization taking place as the escaping atom nucleus goes over some form of potential hump.

There are two variants of Gomer-type mechanism: 'Charge hopping', in which the ionization process is pictured as a sharp 'hop' by the electron involved; and 'charge draining', in which

the ionization process is pictured as a slow draining of electron charge out of the escaping atom. The existence of these two possibilities was first pointed out by Gomer and Swanson, and was re-emphasised by Forbes (1981); discussion of charge draining has recently been taken further by Chibane (1985).

A third possible escape mechanism has sometimes been discussed. This is traditionally called the ionic bonding mechanism; it assumes that the escaping atom is initially bound as an ion, and then escapes over an image hump without any change in charge state.

The 'ionic bonding' mechanism has never been seriously considered as a field evaporation escape mechanism, but controversy over the choice between the Mueller mechanism and Gomer-type escape mechanisms has continued for many years.

1.4 Aims and structure of the thesis

Mueller's image-hump theory is the most easily understood treatment of field evaporation. It is often used for predicting evaporation fields, probably because the associated mathematics is extremely simple; and in its basic form the image-hump model can predict evaporation fields quite well.

However, considerable difficulties arise when more sophisticated versions of the model are examined in detail. There is a definite uncertainty about the behaviour of the atomic nucleus prior to evaporation, and there are uncertainities about the charge-state of the evaporating ion and the predicted distance of the hump from the metal's electrical surface (see 2.6). When repulsive interactions of the type proposed by Brandon (1964) are

taken into account, no hump may even exist in the ionic potential curve. This has long been recognised as a possibility, and will be conclusively demonstrated in chapter 5.

Although one or the other of the Gomer-type mechanisms is considered to be a better physical description of field evaporation, the associated mathematics has, until recently, contained errors. These have been due to a mathematical oversight in the conventional analysis, as pointed out by McKinstry (1973) and Forbes (1978b).

Both models of field evaporation have however been widely used, leading to different interpretations of field evaporation data. This situation is generally unsatisfactory. If we do not know what mechanism of field evaporation is operative, then we cannot obtain reliable atomic level information from theoretical interpretation of evaporation experiments.

The central objective of this work is to re-examine the evidence and classical arguments about field evaporation, within the one-dimensional framework in which the theory has commonly been formulated, with a view to establishing which mechanism of field evaporation operates for any given material. In practice, since work on Gomer-type mechanisms of field evaporation has been carried out in parallel with this work (by Chibane 1985), a main consideration has been to devise a series of tests to show that in most cases the Mueller mechanism cannot be operating. In consequence, the possibility of evaporation via the Mueller mechanism is put aside.

The central difficulty with this endeavour must also be stated at this stage. For simplicity, the conventional theory, and the corresponding arguments here, make two major assumptions. First,

that a one-dimensional model is adequate; second, that a classical potential model is sufficient. Neither of these things has been properly established, and part of this work has been to examine these assumptions.

It must also be appreciated that other important work on field evaporation was in progress in parallel with the author's effort:

(1) Kingham was developing his theory of post ionization.

(2) Chibane was showing that the charge-hopping model fits experimental data adequately.

(3) Forbes was developing tests relating to field evaporation.

The structure of the thesis is thus as follows:

This chapter (chapter 1) has introduced the phenomenon of field evaporation and its usefulness and appplication in various contexts. It has also pointed out a few underlying questions that are associated with the background of field evaporation theories, and has very briefly described the postulated escape mechanisms of field evaporation.

In the field evaporation literature, terminologies, definitions and units of measurement of the field evaporation parameters are sometimes inconsistent and confused. So, in chapter 2, the terminologies, definitions and units of measurement are resolved and brought together into a single place to make the field evaporation theories easier to follow in the context of this thesis.

Chapter 3 is mainly devoted to reviewing field evaporation literature prior to 1980. In particular we look at the two main postulated mechanisms of field evaporation; how these are used in the literature to interpret various phenomena of field evaporation; and how relevant experimental data may be used to

distinguish between the mechanisms.

The review of the field evaporation literature indicates that the Mueller mechanism of field evaporation may not be compatible with the available experimental data. In 1982, Forbes, Biswas and Chibane (1982) reanalysed Tsong's (1978b) field sensitivity data for the six refractory metals, Mo, Rh, Hf, W, Ir and Pt and reported that the Mueller mechanism was not compatible with the field sensitivity data. Chapter 4 includes a revised analysis of the field sensitivity data for these six refractory metals, and uses the "extended image-hump formalism" to carry out further tests on field sensitivity for the same species to demonstrate inconsistencies in the image-hump formalisms.

Evidence against the Mueller mechanism is now convincing enough to make one doubtful if any Schottky-hump would really exist in the ion potential energy curve when repulsive forces between ion-core electrons and the metal's substrate electrons were taken into account. This was first suspected by Brandon (1964). In chapter 5, we mathematically demonstrate that the Mueller mechanism cannot be a plausible physical process by which field evaporation may occur because the image-hump disappears for the tip-metal at a much lower field than either the experimental evaporation field or the theoretically calculated field using the simple image-hump formalisms.

In chapter 6, we collect more evidence against the Mueller mechanism from the development of field evaporation work since 1980 and establish various criteria, based on the "extended formalism", to see if the Mueller mechanism can be a plausible field evaporation mechanism.

In chapter 7, we reassess the situation and draw comparisons

among the tests we have adopted, to determine their relative merits and reliabilities to help us to resolve whether to accept or reject the Mueller mechanism of field evaporation in any particular case. In this chapter, we also discuss the possibility of a non-linear trajectory for ion emission that involves rolling of atoms along the structured emitter-surface prior to ionisation, followed by emission. We also discuss the possible usefulness of the quantum mechanical treatment in field evaporation theories. We then draw things together with concluding remarks and suggest possible further work on field evaporation.

CHAPTER 2

DEFINITIONS AND TERMINOLOGY FOR FIELD EVAPORATION THEORY

2.1 Introduction

In the last fifty years, field evaporation theories and experiments have developed into a complicated branch of physics using various terminologies, definitions, and units of measurements. But until now, these matters have been left in a disorganised fashion in field evaporation literature. A newcomer in this branch of science who is about to embark in the study of field evaporation needs to acquaint himself/herself with all the relevant definitions and technical details, and to grapple with the many inconsistencies in the literature.

In this thesis I have endeavoured to use a consistent set of definitions and terminology, based mainly on the approaches of Forbes, as used in various papers. The purpose of this chapter is to bring together into a single place all these definitions and terminologies

2.2 Electrical Units.

The equations used in this thesis are based on the international system of measurement, i.e. four electric dimensions are used. The literature of field evaporation often uses other systems, based on

c.g.s. units. Where reference is made to earlier work, in this thesis, equations have where necessary been converted to the international system form.

We are, however, dealing with atomic level phenomena. The SI base units are, in this context, sometimes inconveniently large; it is often convenient to use the following atomic level units.

For charge: the proton charge, e

(1 e = 1.602189 10^{-19} C)

For energies: the electronvolt, eV

(1 eV = 1.602189 10^{-19}J)

For distance: the nanometre, nm

(1 nm = 10^{-9} m)

For electric field strength: V/nm

(1 V/nm = 10^{9} V/m)

The factor $4\pi\varepsilon_0$ where ε_0 is the electric constant, often appears in the theory. In terms of these units the values of $4\pi\varepsilon_0$ and $(16\pi\varepsilon_0)^{-1}$ are:

$4\pi\varepsilon_0$= 0.694456 eV V^{-2} nm^{-1}

$(16\pi\varepsilon_0)^{-1}$ = 0.359994 eV^{-1} V^2 nm

2.2.1 Definition and units of polarisability

The SI quantity 'polarisability', which we denote in this thesis by b, is defined in terms of the dipole moment p induced by the local field F^{loc} acting on an atom:

$$b = p/F^{loc} \qquad (2.1)$$

From this it may be deduced that the polarisation energy U of a

neutral atom in a field F^{loc} is:

$$U = -(1/2) \quad b\,(F^{loc})^2 \qquad (2.2)$$

The SI unit of polarisability is J V^{-2} m^2. However, this unit is inconveniently large in the context of atomic phenomena. A much more convenient unit is the meV V^{-2} nm^2. From equation (2.2) it is readily seen that if b is in meV $V^{-2}nm^2$ and F^{loc} is in V nm^{-1}, then U is obtained directly in meV and is simply expressed in eV , which is the unit usually required.

For historical reasons, however, field-ion literature often uses the quantity 'Gaussian polarisability', expressed in $Å^3$. Gaussian polarisability (which we denote here by b_s) is related to the SI quantity polarisability by:

$$b_s = b/4\pi\varepsilon_0$$

The relationships between the various polarisability units are:

$$1 \text{ meV } V^{-2} \text{ nm}^2 = 1.602189 \quad 10^{-40} \text{J } V^{-2} m^2$$

$$1\text{meV } V^{-2} \text{ nm}^2 = 4\pi\varepsilon_0 \times 1.43998 \text{ Å}^3$$

2.3 Evaporation rate-constants and fluxes

The basic configuration of a field ion microscope is shown in Fig. (2.1).

The field ion emitter is a sharp metal point whose tip radius lies in the range 20 nm to 100 nm under most experimental conditions. When a high positive voltage V is applied to this

emitter with respect to some remote counter-electrode, a strong electric field is developed in the vicinity of the emitter, whose magnitude, F, is given by (Gomer 1961):

$$F = V/k_E R_E \qquad (2.3)$$

where R_E is the tip radius of the emitter, and k_E is a semi-constant of value approximately 5. Under the conditions of field ion microscopy, the field F = 20 - 60 V/nm.

The shape of a field ion emitter endform is slightly flattened, not hemispherical at the apex, and the field over the surface is not uniform . Regions of high electric field occur over the more sharply curved portions of the endform, and in particular over each protruding surface atom.

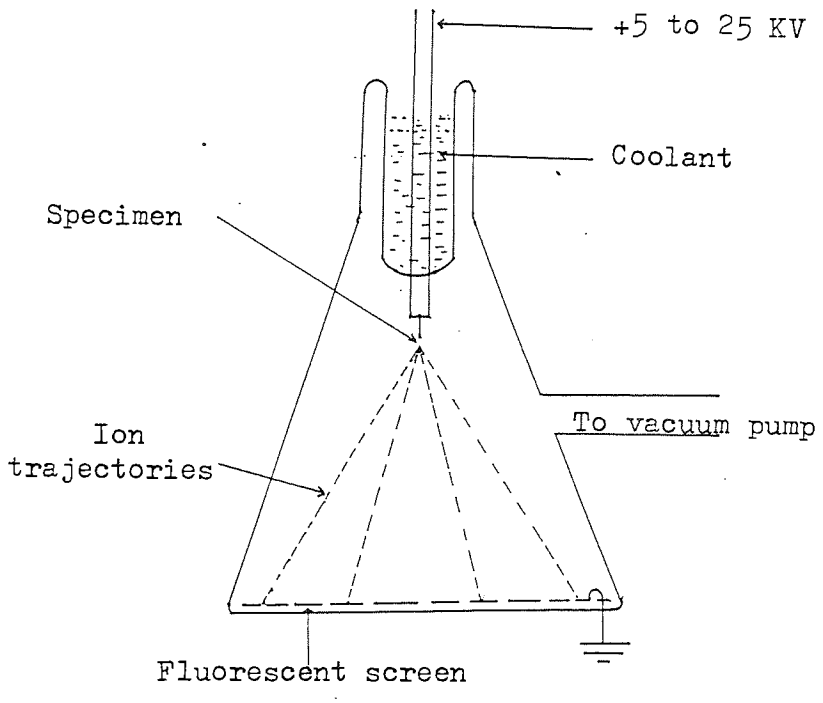

Fig. (2.1) A schematic field-ion microscope tube.

Thus different surface atoms are exposed to electric fields of different strengths. The protruding atoms, in particular the kink

site atoms as shown in Fig. (2.2) are at high risk of field evaporation.

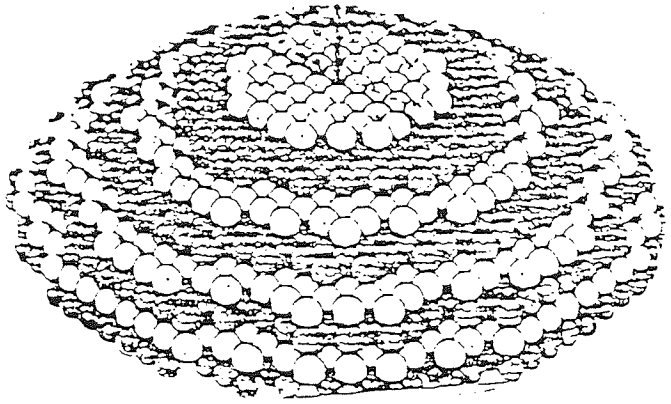

Fig. (2.2) The ball model.
The kink-site atoms(shown in white) are at high risk of field evaporation.

Low-temperature field evaporation is a single body process, involving the detachment of single metal atoms from the field-ion emitter. The field evaporation rate-constant 'k' determines how quickly an individual atom evaporates. k is measured in s^{-1}, and for the evaporation of a single atom from a given site it is given by:

$$k = A \exp(-Q_n/k_B T) \qquad (2.4)$$

where A is a semi-constant known as the 'field evaporation pre-exponential', k_B is the Boltzmann constant, T is the thermodynamic temperature and Q_n is the activation energy relevant

to the site in question.

At a field-ion emitter surface, some atoms are more exposed to the field than others, so for a given applied voltage there will be a spread of rate-constants. In order to overcome statistical problems, we assume that only a limited population of the surface atoms is 'at high risk' of field evaporation and that each of these 'high risk' atoms has the same rate-constant. In practice it is observed from low-temperature field-ion microscope experiments that only the kink-site atoms are at high risk of evaporation.

Thus the total evaporation flux J (i.e. the count of ions evaporated per unit time) is given by:

$$J = n_{hr}\, k_{hr} \qquad (2.5a)$$

where n_{hr} is the amount of material (or count of atoms) at high risk of evaporation and k_{hr} is the corresponding rate-constant. n_{hr} is expressed in 'atoms' or 'layers' , and J is correspondingly expressed in 'atoms/s' or 'layers/s'. Suitable values for n_{hr} are thought to lie in the range of 0.01 to 0.1 layers, i.e. between 1% and 10% of the surface atoms are taken to be at high risk of evaporation.

It is necessary to point out here that in early literature confusion often occurs between J and k_{hr}, and both quantities are sometimes called "evaporation rate". We shall adopt the view here that "evaporation rate" is not a technical term referring to a single physical quantity, but is a general phrase referring to both J and k_{hr}.

Combining the previous two equations we obtain:

$$J = n_{hr}\ A \exp(-Q_n/k_B\ T) \qquad (2.5b)$$

We refer to this equation as the "emission equation"

2.4 Surface-atom binding energy and the initial bonding state.

Fig. (2.3) represents schematically the potential energy variation with the position of a bound neutral atom, in the absence of a field (i.e F=0). The well depth Λ^0 is the neutral atom binding energy in zero field.

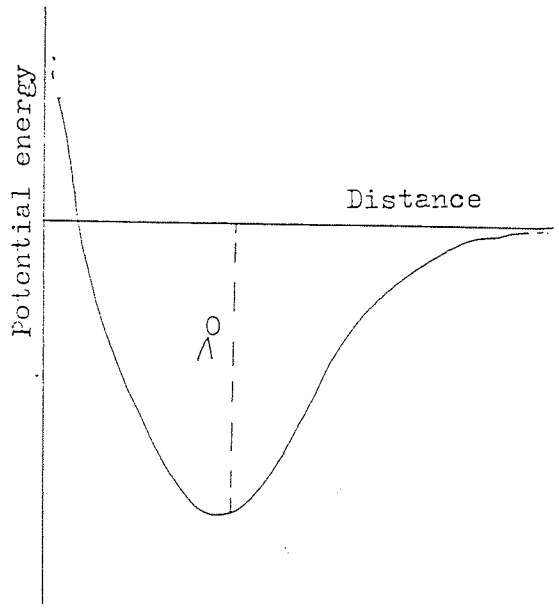

Fig. (2.3) Potential energy curve for a bound neutral in the absence of a field.

This curve is also shown in Fig. (2.4), where it is marked $U_0(F = 0)$. We also show the potential energy variation for a neutral atom in the presence of a field. This curve is marked $U_0(F)$; it is slightly lower than the F=0 curve because of field induced (polarisation) contribution to the binding potential of a

neutral atom. The inner part of this 'polarised neutral' curve is, however, somewhat hypothetical. This is because, in the case of metallic adsorption in the presence of a field, the surface atom is presumed to be partially ionic. Consequently, there will be a further field induced contribution to the binding potential of atom, because it is partially charged.

The lowest curve, marked U_α in Fig. (2.4) corresponds to the equilibrium state of a partially charged ion.

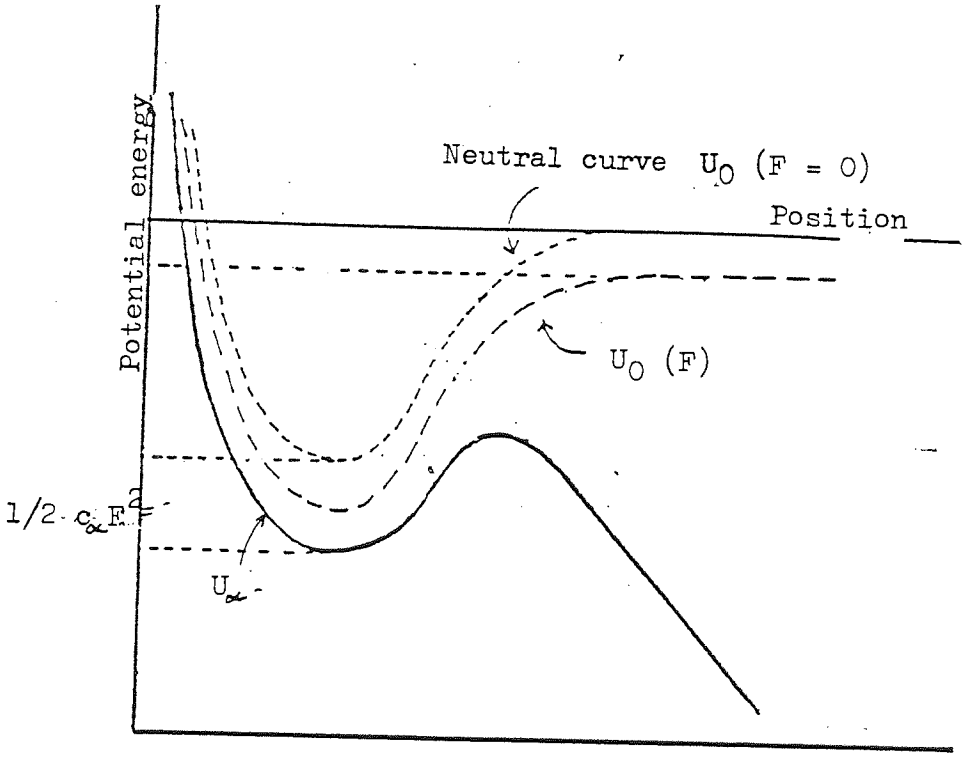

Fig. (2.4) U_α -potential energy curve of a partially ionized atom, and its initial bonding state.

The binding energy of a surface atom is defined as the work necessary to detach it from the surface as a neutral and remove it to a point in remote field free space.

In the case of the metal atom in a field, the field induced

contribution ($\Delta\Lambda$) to the binding energy, may in a first approximation be written in the form (cf. Forbes and Chibane 1982a):

$$\Delta\Lambda = (1/2)\, c_\alpha F^2 \qquad (2.6)$$

The zero-field binding energy then changes to the value Λ^F, where:

$$\Lambda^F = \Lambda^0 + (1/2)\, c_\alpha F^2 \qquad (2.7)$$

In the above equation F denotes the external field somewhat above the surface atom in question, and c_α is a coefficient (usually assumed constant) associated with the field induced modification of electronic charge distribution of the bound atom. It should be emphasised that c_α is not the physical quantity called 'polarisability', even though in the literature it is often given this name. Two considerations are involved. First, it should be noted that c_α is not defined in terms of the local field F^{loc} acting on the atom in question, but in terms of the external field F.

The other difficulty relates to the electronic state of atoms at a charged surface. Field evaporation literature, for simplicity, has often pretended that a field-evaporating atom is a polarised neutral atom. In reality, as already indicated, because the metal surface is electrically charged, the surface atoms must be partially ionic. So U_α has two components, due to orbital-polarisation energy and charge-transfer polarisation energy. Forbes and Chibane (1982a) have shown that it is reasonable to expect an F^2-form for the charge-transfer component

as well as for the orbital component. Hence we may write:

$$c_\alpha = c_\alpha \text{ (orb.)} + c_\alpha \text{ (ch.t.)} \qquad (2.8)$$

Both components seem to contribute significantly to c_α. Manifestly, this c_α is not a textbook polarisability, but is a parameter associated both with polarisation and partial ionization. In what follows we call c_α the F^2- energy coefficient.

In our theory, we assume an F^2 form for $\Delta\Lambda$, as in equation (2.6), even though the atom is partially ionized. This assumption has been described in the literature as "taking the surface atom to be primarily neutral".

We must also comment briefly on the the presumed constancy of c_α in equation (2.7). This is the assumption that has invariably been made in all classical analysis of field evaporation. In reality, both the orbital polarisation and the charge transfer components of the bonding potential will vary with position. In past work, it has been assumed that the bonding position is independent of field, at least to a good approximation. But this may not be a particularly good assumption as has been shown by recent work of Kreutzer (1986).

If the bonding position were itself a significant function of field then the c_α that appears in equation (2.7) would probably be a field dependent quantity. This possibility has come to seem more important recently (Forbes 1986) than it did previously. Reliable calculations of the position dependence of c_α are not yet available. In this thesis, possible field dependence in the value of c_α is disregarded, as in all previous classical analyses of field evaporation.

2.5 The classical ion potential energy

We now consider how to formulate and define ionic potential energies.

Field-ion theory defines a reference zero of energy by using the situation where the desorbed entity is in a neutral state (and in its ground state), and in field-free space remote from the emitter, at position R say. We may formulate this in the equation:

$$U_0^R = 0 \tag{2.9}$$

Symbols of the type U_n^s give the potential energy of the desorbate (or, strictly, of the emitter-plus-desorbate system) when the desorbate in an n-fold-charged state, and some defined reference point within the desorbate is at position s. For an atom or an atomic ion it is convenient to take the atomic nucleus as the reference point. U_0^R thus denotes the potential of a neutral particle at point R in remote field-free space.

The general quantity U_n^s can be defined formally by:

$$U_n^s - U_0^R = W \tag{2.10}$$

where W is the work necessary to create an n-fold ion at point s, from the corresponding neutral atom at point R. The detailed expression for the ion potential energy U_n^s is obtained by

considering all the contributions to this work, and results (cf. Forbes 1982a) in the following formal expression:

$$U_n^s = (H_n - n\phi^E) + n\delta^s + S_n(x,F) \qquad (2.11)$$

Here: n is the ion charge number; H_n is the energy needed to form an n-fold ion from the neutral, in remote field-free space, being given by the sum of the first n free-space ionization energies; ϕ^E is the relevant local emitter work-function; δ^s is a small correction due to patch and/or surface fields; and $S_n(x,F)$ is the 'variable part' of the ion potential energy, expressed as a function of field F and the distance x of point s from the emitter's electrical surface. We look more closely at the definition of x in the next section. The correction term δ^s is invariably ignored in the literature, and we shall follow this procedure.

$S_n(x,F)$ is usually expressed (in a classical approximation) as the sum of four terms corresponding to the following effects:

Electrostatic potential energy: $-neFx$

Correlation potential energy: $-n^2.e^2/16\pi\varepsilon_o x$

Ionic polarization energy: $-(1/2)c_n F^2$

Repulsive-interaction energy: $+G/x^t$

In these expressions: e is the elementary charge; t is the repulsive power law exponent; and G is the corresponding coefficient. Hence we obtain the following as the usual "full" expression for S_n:

$$S_n(x,F) = -neFx - n^2e^2/16\pi\varepsilon_o x - (1/2)c_n F^2 + G/x^t \qquad (2.12)$$

The corresponding ion potential energy is given from equation

(2.11), ignoring the term in δ^s, as

$$U_n(x,F) = (H_n - n\phi^E) - neFx - n^2e^2/16\pi\varepsilon_0 x - (1/2)\, c_n F^2 + G/x^t \qquad (2.13)$$

We also need to introduce a new quantity $W_n(x,F)$ to represent ion potential energy measured relative to the bottom of the atomic bonding well. Since the well bottom has potential energy U_α^B equal to $-\Lambda^F$, we obtain:

$$W_n(x,F) = U_n^s - U_\alpha^B = \Lambda^F + U_n^s \qquad (2.14a)$$

Hence, from eq.(2.10), ignoring the δ^s term, we obtain:

$$W_n(x,F) = (\Lambda^F + H_n - n\phi^E) + S_n(x,F) \qquad (2.14b)$$

Note that, in this expression, x is a free variable.

2.6 Electrical Surface and Related Matters.

As just shown, the 'variable part' $S_n(x,F)$ of the ion potential energy contains various terms that depend on the parameter x that is described as 'distance measured from the electrical surface'. In particular, S_n included the electrostatic energy component u =-neFx. In the theory to be developed later, we shall encounter terms such as $neFa_n$, where a_n is 'the distance, from the electrical surface, of the bonding point for an n-fold ion', and to evaluate such terms we need a value for a_n.

Obviously, it is first necessary to define and locate the origin of x.

The concept of electrical surface may be defined self-consistently as follows.

Consider an emitter that is macroscopically flat, and let v be the electrostatic potential energy of an electron in the vicinity of the emitter. By convention we take v to be zero inside the emitter. Outside the emitter, away from the immediate vicinity of the surface, v varies linearly with distance, as shown in Fig. (2.5). This linearity is a consequence of classical electrostatics.

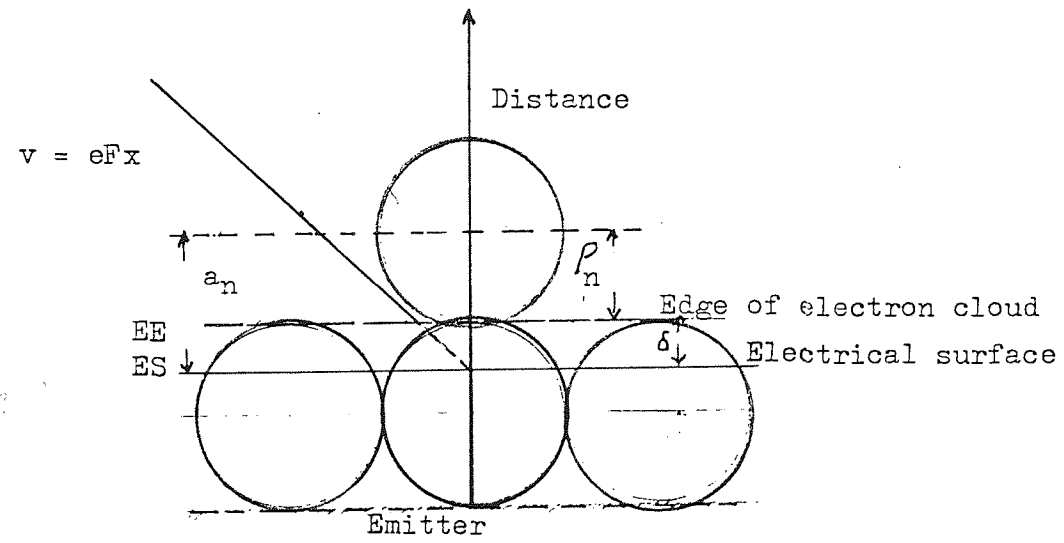

Fig. (2.5) The 'electrical surface'

If we extrapolate this linear variation back towards the emitter, then v becomes zero at a certain position. This position is called the 'electrical surface' and defines the origin of x. When x is measured from this origin, v has the form eFx (u the form -neFx) at sufficiently large distance from the surface.

It can also be shown, at least in the context of some surface

models (for example that of Lang and Kohn 1973), that the correlation-energy component in S_n does have the limiting form $-n^2.e^2/16\pi\varepsilon_o x$, if x is measured from the electrical surface as defined above.

In the equations the repulsive potential is, for convenience, written in the form G/x^t. This is a useful first approximation, but there is rather less scientific justification for this choice, and we look later in the thesis at the consequences of choosing an alternative form for the repulsive interaction.

One feature of the literature deserves note here. In the literature many workers, in particular Mueller and Tsong (e.g. 1974), use a coordinate system in which the origin of coordinates is taken in a plane that is on the vacuum side of our electrical reference surface by a small distance. This distance is often denoted by λ^{-1}. Equations in the Mueller and Tsong form can be obtained from our equations by replacing our 'x' by 'x + λ^{-1}'. There is, however, no advantage in using the more complicated form.

The question remains of determining a_n. This is illustrated in Fig.(2.5), which illustrates the situation of a bound atom or ion, of radius ρ_n which we can assume to be known, approximately. We suppose that the external particle comes to rest when its outer electrons are in contact with the 'electron edge' EE of the emitter, and we denote the distance between EE and the electrical surface ES by δ. If we cannot determine a_n directly from experiment, then we may be able to estimate it via a knowledge of δ. Various models have been used in past work (Gomer and Swanson 1963, Theophilou and Modinos 1972, Mueller and Tsong 1969, Lang and Kohn 1973). We have in practice taken a_n to be

roughly equal to the neutral-atom radius, if n = 1 or 2.

2.7 Field evaporation activation energy.

The field evaporation activation energy is defined as the amount of energy that a bound surface atom should acquire in order to escape from the surface of a material as an n-fold ion.

If we let p denote the position of the 'point of escape' at the top of the activation energy hump, then the activation energy Q_n is given in terms of W_n by:

$$Q_n(F) = W_n(x^p, F) \tag{2.15}$$

Using eq.(2.7) for Λ^F, we may combine equations(2.12) and (2.14) to obtain a 'full' form of the activation energy:

$$Q_n(F) = (\Lambda^0 + H_n - n\phi^E) + (1/2)(c_\alpha - c_n)F^2 - neFx^p - n^2e^2/16\pi\varepsilon_0 x^p + G/(x^p)^t \tag{2.16}$$

The first bracketed quantity in this equation is a constant typical of the species in question, and it is often written K_n, i.e.

$$K_n = \Lambda^0 + H_n - n\phi^E \tag{2.17}$$

We thus obtain as the most familiar form for $Q_n(F)$:

$$Q_n(F) = K_n + (1/2)(c_\alpha - c_n)F^2 - neFx^p - n^2e^2/16\pi\varepsilon_0 x^p + G/(x^p)^t \tag{2.18}$$

These equations show activation energy as a function of

charge-state n and field F, because the quantity x^p is also a function of n and F; however, they are implicit, rather than explicit, equations.

What we need in field evaporation theory is activation energy as an explicit function of field, and to obtain this we need to introduce the relationship between x^p and F, which Forbes (1977) calls the 'subsidiary condition'. In general there may be no explicit expression for x^p in terms of F, and so the most general form of subsidiary condition has to be written:

$$G' (x^p, F) = 0 \qquad (2.19)$$

where G' is some function.

From the point of view of mathematical analysis, the different mechanisms of field evaporation are associated with different subsidiary conditions, and we now look at the commonly used conditions.

2.8 Escape mechanisms

2.8.1 The Mueller mechanism

In the Mueller mechanism, it is assumed that ionization precedes escape and that escape of the ion occurs over a Schottky hump.

With the Mueller mechanism, the condition for an ion to be at the top of the Schottky hump is expressed in the form:

$$\left(\partial W_n / \partial x\right)\Big|_{x_m^{Sh}} = \left(\partial S_n / \partial x\right)\Big|_{x_n^{Sh}} = 0 \qquad (2.20)$$

where x_n^{Sh} is the position of the Schottky hump for a n-fold ion, as shown in Fig.(2.6).

Accordingly, the activation energy Q_n (F) necessary for an atom, bound as a neutral, to escape over the Schottky hump as an n-fold ion is given in the form:

$$Q_n(F) = W_n (x_n^{Sh}, F) = (\Lambda^F + H_n - n\phi^E) + S_n (x_n^{Sh}, F) \qquad (2.21)$$

The Mueller mechanism has been analysed using various different mathematical formalisms, corresponding to different choices of terms in S_n (x,F).

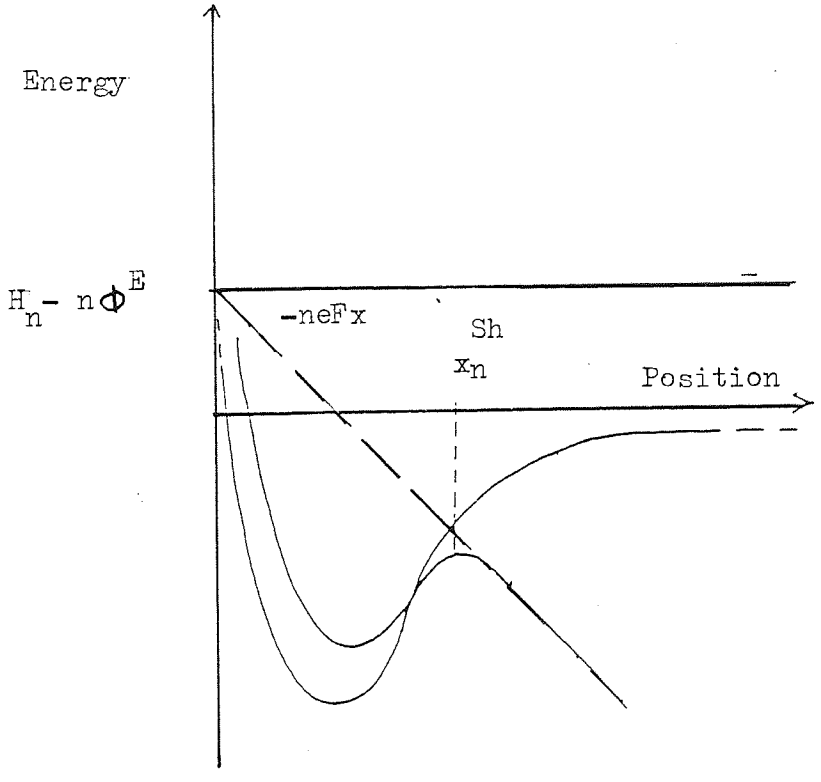

Fig.(2.6) The Mueller mechanism

In the 'basic' formalism, the F^2 and repulsive terms in

$S_n(x,F)$ are ignored. If the F^2-term is included then the expression for $S_n(x,F)$ corresponds to the 'standard' formalism, and $S_n(x,F)$ has the form:

$$S_n(x,F) = - neFx - n^2e^2/16\pi\varepsilon_0 x - (1/2)c_n F^2 \qquad (2.22)$$

The basic and standard formalisms are together known as 'simple' formalisms.

In the 'extended' formalisms, $S_n(x,F)$ includes the repulsive interaction term. In chapter (5), we have dealt with the matter in great detail in the analysis of the Mueller mechanism.

In the 'standard' formalism, we apply condition (2.20) to equation (2.22), to obtain:

$$x_n^{Sh} = (1/2)(ne/4\pi\varepsilon_0)^{1/2} F^{-1/2} \qquad (2.23)$$

Then using equations (2.21), (2.22) and (2.23) to eliminate x_n^{Sh}, the following formula is obtained for the activation energy (in the standard formalism):

$$Q_n(F) = K_n - (n^3e^3F/4\pi\varepsilon_0)^{1/2} + (1/2)(c_\alpha - c_n)F^2 \qquad (2.24)$$

where K_n as before is given by:

$$K_n = \Lambda^0 + H - n\phi^E \qquad (2.25)$$

In the basic formalism, the F^2-term is omitted.

2.8.2 Gomer-type mechanisms: Charge-hopping

As indicated in chapter 1, the Gomer-type mechanisms involve simultaneous ionization and escape, as the evaporating entity crosses an activation energy barrier; and there are two notable variants of this process, namely the 'charge hopping' and 'charge draining' mechanisms.

With the charge-hopping mechanism, ionization and escape occur simultaneously at the crossing point x^{cr} of the atomic and ionic curves. It is assumed that the motion of the ion is relatively fast, and the electron transfer occurs in a sharp hopping transition. Fig.(2.7) shows the point x^{cr}.

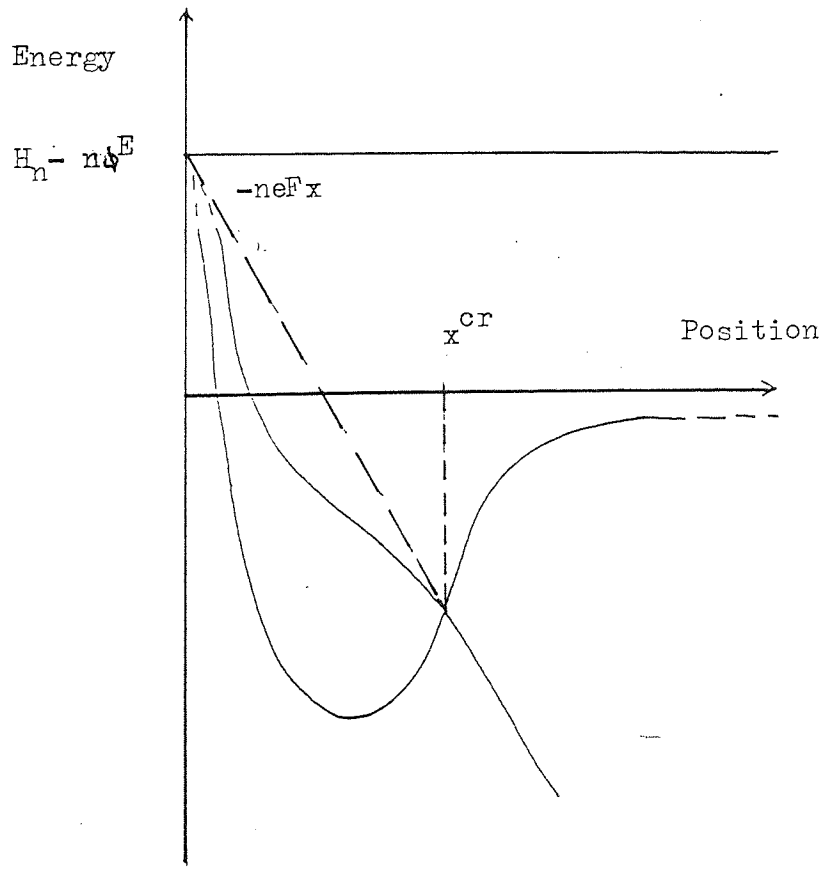

Fig. (2.7) The charge-hopping mechanism

For this mechanism, most pre-1978 treatments used the subsidiary condition:

$$x^p = x^{cr} = \text{const.} \qquad (2.26)$$

But it was argued by McKinstry (1972) and Forbes (1978b) that this condition was unsatisfactory and needed to be replaced by one involving the field dependence of x^{cr}. There was not necessarily any analytic formula for x^{cr} in terms of F, and hence the most general form of the subsidiary condition would be as in equation (2.19), namely:

$$G'(x^{cr}, F) = 0$$

In practice, a condition of the form:

$$W_n(x^{cr}, F) = V(x^{cr}) \qquad (2.27)$$

has been used in recent work (e.g. Forbes 1978b). V(x) is the potential energy of the bound atom, measured relative to the level of the bottom of the potential energy well, and can be approximated as a parabola, Morse potential, or other form. This approach has been called (Forbes et al. 1984) a 'curve-intersection formalism'. Given an expression (or in the case of numerical analysis a value) for x^p, activation energy is then determined from equation (2.16).

2.8.3 Gomer-type mechanisms: charge draining.

In this mechanism, the atom field evaporates as it is ionized through slow draining out of electrons. Fig.(2.8) is probably the best diagram to discuss the charge-draining mechanism. The curves U_0(F=0), $U_0(F)$ and U_α have been previously introduced as in fig.(2.4).

The evaporating atom, in the presence of a field, conforms to the curve U_α . As the atom moves away from the surface, charge drains out of it, and at high enough fields for evaporation to occur it goes over the activation energy hump in a partially charged state. Subsequently, ionization is completed via further charge draining.

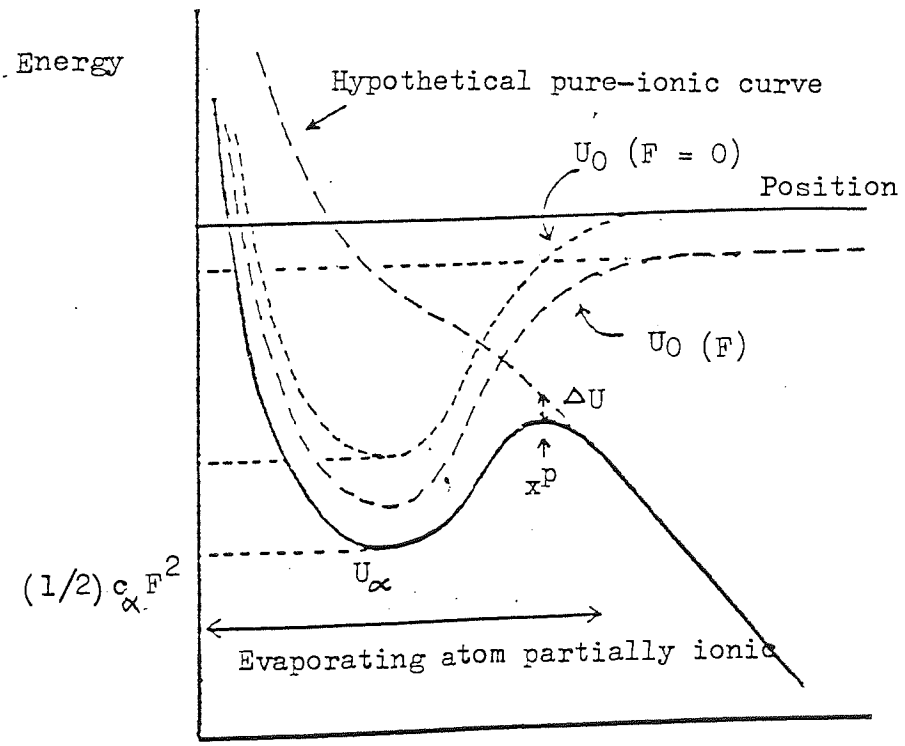

Fig. (2.8) The charge-draining mechanism

The resulting desorbate is an ion with charge ne , and it then conforms to the standard ionic potential energy curve, marked U_n in fig(2.8).

The charge-draining mechanism is plausible when the atom-surface distance is relatively small, as it is at the high field characteristic of conventional field evaporation. In this case, the ionic potential energy at x^p, relative to the bottom of the bonding well, can be written formally as:

$$W_n(c.d.) = W_n (x , F) - \Delta U \qquad (2.28)$$

where ΔU is the difference between the level of the top of the hump and the value $U_n(x^p,F)$ of the pure n-fold ionic potential.

In principle, a subsidiary condition for charge-draining is derived by assuming escape to occur at the top of the hump in fig.(2.8), which leads to:

$$dW_n(x,F)/dx - d\Delta U/dx = 0 \qquad (2.29)$$

But one should point out that a satisfactory analytical expression for ΔU is yet to be found.

2.9 Regimes

The equation (2.4) for rate-constant k is applicable to single-atom evaporation only at sufficiently high temperatures. At intermediate temperatures, there is a regime in which an

Arrhenius form of equation for k may be used, but the pre-exponential is a sensitive function of field and temperature.

At very low temperatures, such that $k_B T \ll h\nu$, where ν is the atomic vibration frequency, nearly all the desorption takes place out of the ground state, and the rate-constant is given by an the equation of the form:

$$k = \nu \exp(-a' Q^{3/2}) \qquad (2.30)$$

where a' is a coefficient relating to the details of the evaporation situation.

These regimes have been postulated in the analysis of the charge hopping mechanism of field evaporation by Gomer and Swanson (1963), in the analysis of the Mueller mechanism by Ehrlich and Kirk (1968), and in the analysis of the ionic bonding mechanism by Tsong (1968).

The transition temperature T^c at which the thermally-activated regime changes to an intermediate temperature regime is of particular interest in connection with some of the arguments in this thesis. Experiments on field evaporation should not be performed below this temperature, because analysis of the results then becomes significantly more complicated mathematically.

The temperature 78K often used in experiments was always presumed to be above the transition temperature. Recently, this assumption was justified, in the case of tungsten, by the experiments of Wada et al. (1980) and their interpretation by Forbes and Chibane (1982b). T^c was found to be around 40K.

This value is also in good agreement with some calculations by Kingham (1982).

One should also note that some interesting experimental work, that demonstrates conclusively the existence of a transition region for boron, has recently been presented by Menand and Kingham (1984).

2.10 The definition of evaporation field

We must now discuss the question of how 'evaporation field' is defined.

Several different definitions are in use in field evaporation theory. These definitions are based on the common conception that we should try to quantify when the external field at the high-risk sites is high enough to cause evaporation at a significant rate. The field at which the evaporation rate is considered significant is called the evaporation field.

The concept of a "significant rate of evaporation" has been made quantitative by using three different criteria, that in turn provide definitions of three different types of evaporation fields.

The "zero-Q evaporation field F^e " is defined theoretically by the requirement that the activation energy Q_n (F) as it appears, say in equation (2.21) and (2.24), is zero at that field. This criterion is often used, particularly in the earlier works, e.g. by Mueller (1956), Brandon (1963) and Mueller and Tsong (1971). This field F^e is a species related constant, and is not dependent on temperature. Use of this criterion to define F^e in the literature has probably been because of its mathematical

convenience.

The "critical evaporation field F^c " is defined by the requirement that $k(F^c) = 1\ s^{-1}$. This is called the "unity rate-constant" criterion, and the relevant theory has been discussed by Forbes (1974). This field F^c is particularly useful in single-atom experiments where the evaporation rate-constant is measured directly.

The "onset evaporation field F^o " corresponds to a set value J^o of evaporation flux. In low-temperature field-ion microscope experiments, the criterion that the evaporation flux has a value of 0.01 layer/s is often used to define the 'onset evaporation field'. The onset flux value chosen may be different in different types of experiments; for example, in atom-probe experiments the onset evaporation flux is set to a higher value.

For a particular species, F^c and F^o are more or less the same in value, but F^e is somewhat higher. F^e is, in effect, the value to which F^c and F^o would tend at low temperature if no tunnelling effects occurred. In reality, the evaporation field in the limit of very low temperature is expected to be somewhat less than F^e.

This distinction in principle, between (theoretical) zero-Q evaporation field F^e and the onset evaporation field actually observed in field-ion microscope experiments, is strangely neglected in much of field evaporation literature. It has been a common practice to compare observed field values with zero-Q values calculated from simplified models, and to find relatively good agreement (cf. Tsong 1978). We shall return to this point in chapter (3).

2.11 Field sensitivity and partial energies

2.11.1 Field sensitivity

If the applied voltage on a field ion emitter changes, then the mean field at the high-risk evaporation sites, the evaporation rate-constant and the evaporation flux all vary. Determining the field sensitivity of these last two quantities is the equivalent for field evaporation of determining the slope of a current/voltage characteristic for other emission mechanisms.

It is conventional to use logarithmic arguments in deriving expressions for flux and rate-constant field sensitivities. From equation (2.5a), we may write

$$d\ln(J)/d\ln(F) = d\ln(n_{hr})/d\ln(F) + d\ln(k_{hr})/d\ln(F) \qquad (2.31)$$

Following Forbes (1978b), these quantities are written as total derivatives w.r.t. F (because in the theory there is an indirect dependence of Q on x^p). However, since temperature is held constant, there is also a sense in which these are all partial derivatives. The derivative on the left-hand side of the equation is called the (logarithmic) flux field sensitivity, and is denoted later by s_T.

The quantity $d\ln(k_{hr})/d\ln F$ on the right-hand side is called the (logarithmic) rate-constant field sensitivity.

Experimental measurements of these quantities involve plotting of $\ln(J)$ or $\ln(k_{hr})$ against (V/V^o) or (F/F^o), where V^o is some reference voltage (corresponding approximately to evaporation at a

given flux level J^o or rate-constant level $k_{hr}{}^o$) and F^o is the corresponding onset evaporation field at the high risk sites.

In chapter(3), experimental measurements of field sensitivity will be discussed in detail.

2.11.2 Partial energies

Partial energies are energy-like parameters that are mechanism-independent and can be estimated from the experimental results of various workers. These parameters can also be expressed in terms of the different possible mechanisms of field evaporation. Therefore, partial energies can provide us with a method for comparison between the experimental and theoretical results of field evaporation phenomena.

The following procedure (cf. Forbes 1974) introduces the definitions of partial energies, μ_s.

The equation (2.4) can be written as:

$$k_{hr} = A \exp(-Q_n/k_B T) = \exp(M/k_B T) \qquad (2.32)$$

where: $$M = k_B T \ln(A) - Q_n \qquad (2.33)$$

and (A) is the numerical value of A expressed in seconds. The quantity M is a function of F^c and may be Taylor-expanded about F^c (see 2.10 for definition of F^c), thus:

$$M(F) = M(F^c) + (F-F^c)\, dM/dF + 1/2\, (F-F^c)^2\, d^2M/dF^2 + .. \qquad (2.34)$$

At F^c, $M(F^c) = 0$. Now introduce a new variable, the "fractional

overfield" f, given by:

$$f = (F - F^C)/F^C \tag{2.35}$$

then equation (2.34) becomes:

$$M = \mathcal{M}_1^C f + 1/2\ \mathcal{M}_2^C\ f^2 + \ldots\ldots \tag{2.36}$$

where:

$$\mathcal{M}_s^C = (F^C)^s\ d^sM/dF^s = d^sM/df^s \tag{2.37}$$

These quantities $\mathcal{M}_s^C$ relate to a specific field F^C . It is possible to generalise the definition by using equation (2.32) to obtain:

$$\mathcal{M}_s = (F)^s\ d^sM/dF = k_BT\ \ (F)^s\ d^s\ln k_{hr}/dF^s \tag{2.38}$$

These quantities $\mathcal{M}_s$ are functions of F and T, and $\mathcal{M}_s$ is termed" the s-th partial energy for rate-constant". Now:

$$\mathcal{M}_s^C = \mathcal{M}_s\ (F = F^C) \tag{2.39}$$

By analogy, we may define the "s-th partial energy for flux" by:

$$\lambda_s = k_B\ T\ (F)^s\ d^s\ln(J)/dF^s \tag{2.40}$$

Clearly, from equation(2.31):

$$\lambda_s = k_B T (F)^s \, d^s \ln(n_{hr}) / dF^s + \mu_s \qquad (2.41)$$

It has been universally assumed in past analyses that the field dependence of n_{hr} is negligibly weak, so that we may assume at least that $\mu_1 = \lambda_1$ and $\mu_2 = \lambda_2$, i.e. that experimental measurements of λ_1 and λ_2 give valid experimental estimates of μ_1 and μ_2.

To make theoretical estimates of μ_1 and μ_2 we need to evaluate $d^s M/dF^s$. If we ignore the field dependence in $\ln(A)$, then from equation (2.33) we obtain:

$$\mu_s = -(F)^s \, d^s Q/dF^s \qquad (2.42)$$

With the basic image-hump mechanism, μ_1 and μ_2 are given respectively by:

$$\mu_1 = +1/2(n^3 e^3 F/4\pi\epsilon_0)^{1/2} \qquad (2.43)$$

and

$$\mu_2 = -1/4(n^3 e^3 F/4\pi\epsilon_0)^{1/2} \qquad (2.44)$$

Therefore:

$$\mu_2/\mu_1 = -1/2 \qquad (2.45)$$

With the Gomer mechanisms, the situation is complicated because the total derivative dQ_n/dF is given by:

$$dQ/dF = (\partial Q_n / \partial F)_x^P + (\partial Q_n / \partial x^P)_F \cdot dx^P/dF \qquad (2.46)$$

Most pre-1978 treatments ignored the second part of the right hand-side of equation(2.46), for mathematical convenience.

2.12 Half-width and appearance energies

Consider the situation of energy analysis using a retarding energy analyser.

Since field ionization takes place slightly above the emitter surface, the ions arrive at the retarding electrode with an energy deficit D given by:

$$D = re\,\delta_v \qquad (2.47)$$

where δ_v is the measured voltage deficit between the emitter and retarder, and re is the charge on the ion.

Ions arrive with a spread of energies, but there is a cut-off on the low-energy-deficit side.

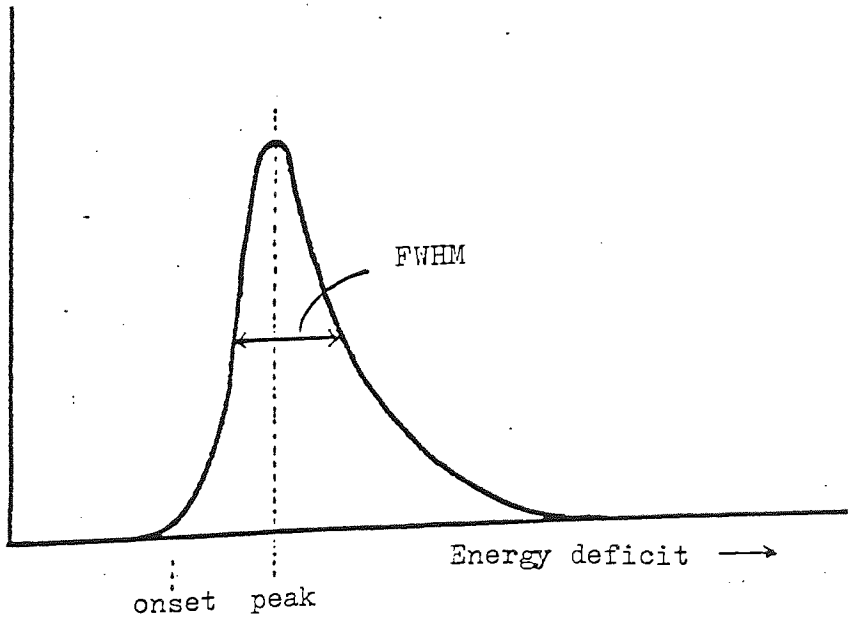

Fig.(2.9) Schematic diagram showing the "onset" and "peak" in an ion energy distribution

According to Ingram and Gomer (1954), the cut-off is caused by the requirement that the electron tunnels into the metal above the Fermi level, and this places the origin of the ion at or above a minimum distance from the surface. Beyond the minimum distance, the ionization rate-constant falls off gradually. Fig.(2.9) roughly shows the energy distribution of a field emitted ion.

Two basic features of the distribution, the absolute position-in-energy of the onset and the FWHM (full width half maximum) of the distribution are of primary interest.

To discuss the former, it is better to work, not with energy deficits, but with the so-called Appearance Energy A defined by:

$$A = D + r.\Phi_c \qquad (2.48)$$

where Φ_c is the local work function of the retarder.

Appearance energy is a property of an individual ion. In the ion-energy distribution, appearance energies at "onset" and "peak" are important in characterising the distribution. For theoretical purposes, however, it is better to work with the so-called "standard appearance energy" A^{st}. This is the appearance energy of an ion that is created by transferring the electrons directly to the emitter Fermi-level, that escapes with zero kinetic energy, and then travels away from the surface without suffering any anomalous energy changes (Forbes 1976a). A^{st} is roughly equal in value to the observed onset appearance energy.

Using a thermodynamic cycle for an ion that is initially bound in charge-state α (partially ionized) and is emitted with a

charge-state n immediately after escape, and arrives at the collector with another charge state r, the standard appearance energy is given (Forbes 1976a) by the equation:

$$A_{\alpha nr}^{st} = \Lambda_{\alpha}^{F} + H_r - Q_{\alpha nr} \qquad (2.49)$$

where Λ_{α}^{F} is the binding energy of the partially ionized atom, H_r is the sum of the first r free-space ionization energies, and $Q_{\alpha nr}$ is the relevant activation energy.

Several other formulae relating to Appearance Energy will be useful later. Clearly, if r = n (i,e. no post-ionization occurs):

$$A_{\alpha nn}^{st} = \Lambda_{\alpha}^{F} + H_n - Q_{\alpha nn} \qquad (2.50)$$

But activation energy depends only on the initial state and escape state, so $Q_{\alpha nn} = Q_{\alpha nr}$, and:

$$A_{\alpha nr}^{st} = A_{\alpha nn}^{st} + (H_r - H_n) \qquad (2.51)$$

An alternative expression can be derived by combining equations (2.50), (2.51), (2.14b) and (2.15), to obtain:

$$A_{\alpha nr}^{st} = (H_r - H_n) + n\phi^{E} - S_n(x^P,F) \qquad (2.52)$$

where x^P is the point of escape for the α - n escape process. Or we may use equation (2.11) (ignoring the small term δ^s), to obtain:

$$A_{\alpha nr}^{st} = H_r - U_n(x^P,F) \qquad (2.53)$$

All these formulae are mechanism independent, but obviously we can substitute specific mechanism dependent formulae for x^p, or $Q_{\alpha nn}$, in order to analyse experimental data.

As regards the FWHM of evaporated ion energy distributions, there seems to be no well-established theory. We return to this issue later.

CHAPTER 3

A REVIEW OF PAST EXPERIMENTAL DATA AND THEIR INTERPRETATION

3.1 Introduction:

As already stated in chapter 1, field evaporation was first observed by Mueller in 1941, and since then the theoretical discussion of field evaporation has been presented in terms of two types of model/mechanism, the Muller type mechanism and the Gomer mechanism. The basic difference between the two mechanisms has been discussed in chapter 2 in some detail.

The Mueller mechanism was first originated (in a somewhat confused manner) by Mueller in 1956, and was then stated more clearly in (Mueller, 1960). The Gomer mechanism was originated at about the same period (Gomer 1959, Gomer and Swanson 1963). Forbes (1981) reminded us that in fact the Gomer mechanism comprises two different mechanisms of field evaporation: 'charge hopping' and 'charge draining'. We have already made a distinction between the two variants of the Gomer mechanism in chapter 2.

In chapter 3, we look at how these two main mechanisms have been used in the literature in the interpretation of various phenomena of field evaporation. In particular, we wish to examine how experimental evidence has been used or might be used in the longstanding attempt to distinguish which of the mechanisms

is operating.

Field evaporation theory has been discussed by various previous workers, and in particular by: Brandon (1964); Ehrlich and Kirk (1968); Mueller and Tsong (1969, 1974); Tsong and Mueller (1970); Tsong (1971); Mckinstry (1972); Vesely and Ehrlich (1973) and Forbes (1974, 1978b).

In this chapter we wish to take these things further, and to give an overview of the whole situation as it developed up to about 1980, when the present work was begun. A few later developments will also be included. A thematic, rather than a strictly historical, approach will be adopted,and we look in turn at: evaporation field values, quasi-thermodynamic relationships, field sensitivity and partial energies, charge state of the evaporated ion, temperature dependence of evaporation field, field dependence of activation energy, appearance energy measurement, energy half-width measurement, and limitations and assumptions of the existing evaporation models in describing the preceding items.

This chapter will show why it was necessary and useful in 1980 to develop classical arguments that would discriminate between the mechanisms, and we will also discuss what is in fact wrong with the existing theories.

3.2 Evaporation field values

The first experimental estimate of evaporation field (for tungsten) was made by Mueller (1956) while he was studying the field desorption of barium and thorium from the tungsten emitter tip of his field ion microscope. The theoretical interpretation

was given in terms of simple image-hump theory (assuming singly charged field evaporation), and it was originally claimed by Mueller that the Schottky effect described the experimental facts well enough to justify using the theory to predict the evaporation fields of other emitter surfaces.

The "zero-activation-energy" (or "zero-Q") definition of evaporation field was first used by Mueller (1960). As already indicated this definition has often been used in determining a theoretical evaporation field F^e because of the convenient mathematics.

The theoretical estimation of F^e usually involves the knowledge of the binding energy Λ^0, ionization energies, and the local work-function of the surface. Both image-hump and charge-exchange formalisms may be used in the calculation of F^e, using the simplified versions of the theories as presented in chapter 2.

Thus, in the basic image-hump formalism, we ignore the F^2-term in equation (2.24) and put Q_n equal to zero to obtain a prediction of F^e for a n-fold charged ion. This gives the result:

$$F^e = (4\pi\varepsilon_0/n^3 e^3).\ K_n^2 \qquad (3.1)$$

where K_n is given by equation (2.25). Equation (3.1) will be known as 'Mueller's formula'.

In his initial estimation of F^e, Mueller (1956) assumed the evaporated ion to be singly charged (n=1). Later, Brandon (1964) still using the Mueller mechanism and basic image-hump theory, estimated F^e for n= 1 to 3 and proposed the criterion that the dominant ion charge immediately after escape (by implication the

observed charge) is that for which the calculated F^e is the lowest, and that the experimental evaporation field corresponds to this lowest predicted value. This assumption is now known as Brandon's criterion. The first four columns of table (3.1) give F^e values for a few specimen calculations using Mueller's formula. (These results are extracted from table 5.2 later).

TABLE (3.1)

Comparison of evaporation fields

	Mueller's formula			Forbes' formula		Charge state	F (obs.)
Element	n=1	n=2	n=3	n = 1	n = 2		V/nm
Mo	56	38	49	48	36	2	43
W	102	56	52	90	53	2	57
Fe	43	34	55	37	33	2	34
Ag	23	44	71	20	42	1	20
Ir	77	44	51	67	42	2	46
Pt	60	44	53	53	42	2	44

The above figures illustrate what is in fact true more generally. For a wide range of metals, when Brandon's criterion is applied, the theoretical values of F^e are very close to the experimental values. This success has sometimes been taken to lend credence to the Mueller model as such. Mueller's original result, and results such as these, were valuable because they confirmed theoretically

that normal field evaporation is a thermally-determined process. In consequence the Muller model has often been completely taken for granted.

There are, however, certain physical objections that can be raised against the Mueller mechanism and the basic image-hump formalism. In particular, the values of x_n^{Sh} predicted from equation (2.23) are too small to be plausible (Brandon 1964; Tsong 1971); and it is by no means clear that any hump could exist at observed evaporation fields if a repulsive contribution is included in the expression for ionic potential energy (Tsong 1971).

For the Gomer mechanism, the activation energy $Q_n(F)$ is a function of both field F and the position x^p of the point of escape. In simple calculations with this model, it is assumed that:

$$x^p = a_0 \qquad (3.1a)$$

where a_0 is the distance of the neutral atom bonding point from the metal's electrical surface (see section 2.6).

Using the $Q_n(F) = 0$ criterion, and equation (2.19) ignoring the F^2-term, we can write:

$$neF^e a_0 = (\Lambda^0 + H_n - n\Phi^E) - n^2 e^2/16\pi\varepsilon_0 a_0 \qquad (3.2)$$

If a_0 is known then F^e can be calculated. In a first approximation this distance a_0 is taken as equal to the metal atom radius (Tsong and Mueller 1970), and use of Brandon's criterion then leads to theoretical evaporation-field values compatible with experimental values, though the comparison shows that it is difficult to predict F with a precision of better than a factor

of about 1.5.

The predictions of evaporation field values using the two models apparently show that both mechanisms have approximately equal success in interpreting the experimental data. The real reason for the approximately equal success of both mechanisms can be simply understood as follows.

In equation (3.2) the image potential term is much smaller than K_n, so we may write for the charge-hopping mechanism:

$$neF^e a_0 = \Lambda^0 + H_n - n\Phi^E \qquad (3.3)$$

With the Mueller mechanism we may apply the $Q_n(F)=0$ criterion to equation(2.21), and ignoring the F^2- term we obtain:

$$neF^e .2x_n^{Sh} = \Lambda^0 + H_n - n\Phi^E \qquad (3.4)$$

It so happens that the values of x_n^{Sh} predicted from equation (2.21) are roughly about half what one might predict for the bonding distance a_0. Hence both mechanisms lead to much the same predictions of evaporation fields, and this predictive ability is in no sense a useful test of evaporation mechanism.

Much later, Forbes (1982b) has derived a new formula for the evaporation field strength F^e on the basis of a more general 'thermodynamic' argument using energetics only. This formula seems to unify the two existing mechanisms of field evaporation, at least as regards evaporation field prediction, by eliminating the physically dubious arguments concerning potential curves that are implicit in image-hump formalisms. In his treatment, making the usual requirement that $Q_n(F) = 0$,the image-potential term is

expressed as some significant fraction of the quantity K_n. This leads ultimately to the result:

$$F_n^e = \sigma_n (16\pi\epsilon_0/n^3e^3) (K_n)^2 \qquad (3.5)$$

where σ_n is a parameter. Forbes recommends taking $\sigma_1 = 0.22$, $\sigma_2 = 0.24$.

The evaporation field values for various exemplary metals (W, Ir, Pt, Fe and Ag) predicted from equation (3.5) are shown in table (3.1) and are in good agreement with the experimental values; in fact the values only differ by between 3% and 20% for the five metals in low temperature field evaporation.

Thus it seems clear that the apparent success of the existing theories in interpreting the experimental field values is simply due to the fact that the models used in the analyses assume that field desorption is thermally activated and obeys the Arrhenius equation. The success of the theories demonstrates that field evaporation is a thermally determined process, and nothing more. The experimental results and their theoretical analysis using the existing models cannot be used to distinguish between different mechanisms of field evaporation.

3.3 Quasi-Thermodynamic relationships

At temperatures near 80 K, field evaporation is considered to be a thermally activated process and in the emission equation the flux J is a function of both field and temperature. Conventionally, the

emission equation in an evaporation theory is expressed in terms of an assumed evaporation mechanism. But Brandon (1966) pointed out that it was possible to derive consistent functional relationships among the variables in the field evaporation phenomenon. Furthermore, it is sometimes helpful to first analyse field evaporation data by a mechanism-independent method.

These mechanism-independent functional relationships amongst field evaporation parameters such as flux, temperature, field, partial energy and activation energy may be regarded as atomic-level kinetic equivalents of thermodynamic equations of state, and are derived as follows.

The emission equation may be written in the form:

$$L = \ln(J) = \ln(n_{hr}) + \ln(A) - Q_n/k_B T \qquad (3.6)$$

L is introduced as the logarithmic evaporation flux.

In equation (3.6), as written, the quantities F and T are the independent variables and L the dependent variable. However, it is equally possible to regard L and T as the independent variables and F as the dependent variable. So we can rewrite equation (3.6) as the functional relationship:

$$F = F(L,T) \qquad (3.7)$$

From the rules for partial differentiation it follows that:

$$(\partial F/\partial T)_L = -(\partial L/\partial T)_F \,/(\partial L/\partial F)_T \qquad (3.8)$$

The first partial energy for flux field-sensitivity is given by:

$$\lambda_1 = k_B T. F(\partial L/\partial F)_T \qquad (3.9)$$

This parameter was discussed in chapter 2, but here needs to be written as a partial derivative. It follows that:

$$(\partial L/\partial F)_T = \lambda_1 /Fk_B T \qquad (3.10)$$

It is also convenient to define a semi-logarithmic field/temperature coefficient s_L by:

$$s_L = (\partial \ln F/\partial T)_L = (1/F)(\partial F/\partial T)_L \qquad (3.11)$$

s_L has the units K^{-1}. In the data analysis of the field-sensitivity measurements it is convenient to express results in terms of λ_1 and s_L.

From equation(3.6), assuming that n_{hr} and A are effectively independent of temperature, we obtain

$$(\partial L/\partial T)_F = Q_n /k_B T^2 \qquad (3.12)$$

From equations (3.8), (3.10) and (3.12) we obtain

$$(\partial F/\partial T)_L = - Q_n F/ \lambda_1 T \qquad (3.13)$$

then by rearranging and using the expression for s_L (eq. 3.11), Q_n may be expressed as

$$Q_n = - s_L \lambda_1 T \qquad (3.14)$$

Alternatively, from the emission equation (2.5b):

$$Q_n = k_B T \ln(n_{hr} A/J) \tag{3.15}$$

Thus in a consistent theory we also have the following relationship:

$$n_{hr} A = J \exp(- s_L \lambda_1 / k_B) \tag{3.16}$$

$$(\partial F/ \partial T)_L = -(k_B F/ \lambda_1) \ln(n_{hr} A/J)_L \tag{3.17}$$

Obviously the quantities s_L, λ_1 and T may be measured.

We can test this theory by estimating Q_n in two different ways as indicated by equation (3.14) and (3.15). Table (3.2) shows values of s_L measured over the temperature range shown, for the onset flux (J^o) listed. For completeness, we have included a number of very early experiments in the table.

The values of λ_1 included in the table (3.2) have been obtained as follows:

With Brandon's data, values of λ_1 can be calculated from his experiments (see Forbes 1974). With the Tsong and Mueller experiment, the value of λ_1 can again be obtained from data in the original paper (Tsong and Mueller 1970). In other cases, λ_1 data have been obtained from a regression analysis of data taken by Tsong (1978b) (see sec. 4.2). The data produced by Tsong and Mueller (1970) are possibly the most reliable because they have in effect measured s_L and λ_1 on the same emitter. Final columns in the table show Q_n derived from equation (3.14) taking T = 78 K and $n_{hr}A$ as derived from equation (3.16). Reliably estimating

uncertainty in these quantities is difficult. In no case, however, can the uncertainty in Q_n be less than 10%, and uncertainty in $n_{hr}A$ be less than an order of magnitude. With the Brandon and Nakamura result the uncertainty in Q_n can approach 30% or more, Mueller's very early measurements have even greater uncertainty.

We now need an independent theoretical estimate of Q_n for comparison with the data in table (3.2). As earlier we assume that at 78K about 10% of the surface atoms are imaged and that of these imaged atoms about 10% are in particularly field-exposed positions: this gives n_{hr} as 0.01 layers. Taking A to have the conventional value 10^{12} s^{-1}, one obtains n_{hr} A as 10^{10} layers/s. At 78K, equation (3.15) then leads to estimates of Q_n lying between 155 meV and 185 meV, for J^o values lying between 1 layer/s and 0.01 layer/s.

The estimates in table 3.2 are broadly compatible with these figures, and the above comparison once again confirms field evaporation is a thermally activated process.

These comparisons, of course, do not help us to discriminate between mechanisms.

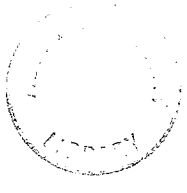

TABLE (3.2)

Experimental values of J, K, s_L, λ_1 and Q_n calculated from equation (3.14) for various species, and of $n_{hr}A$ from equation (3.16)

Species	J layer/s	Temp. range K	s_L $10^{-3}K^{-1}$	λ_1 eV	Q_n meV	$n_{hr}A$ layer/s
Tungsten						
M(1956)	1	21-300	-0.41(a)	1.35± 4%	45	$6\ 10^{2}$
M(1956	1	300-900	-0.36(a)			
N(1966)	0.05	21-79	-0.86± 20%	1.48± 3.5%	100	$1\ 10^{5}$
B(1966)	0.1	62-88	-1.15(a)	2.02± 8%	180	$5\ 10^{10}$
TM(1970)	0.01	77-90	-1.31± 5%	1.63± 10%	165	$6\ 10^{8}$
WKN(1980)	0.1	78	-1.43± 6%	1.45± 3.5%	160	$3\ 10^{9}$
Molybdenum						
N(1966)	0.05	21-79	-1.4± 25%	1.33± 11%	140	$9\ 10^{7}$
B(1966)	0.1	64-88	-0.66(a)	1.6± 25%	80	$2\ 10^{4}$
WKN(1980)	0.1	78	-0.97± 3%	1.31± 11%	100	$3\ 10^{5}$
Platinum						
B(1966)	0.1	63-89	-1.2(a)	1.28± 12%	120	$6\ 10^{6}$
Tantalum						
N(1966)	0.05	21-79	-1.1± 25%			
N(1966)	0.05	21-79	-1.3± 25%			

Footnotes: Brandon (B), Mueller (M), Nakamura (N), Tsong and Mueller (TM), Wada, Konishi and Nakamura (WKN).

(a) Uncertainty large and difficult to estimate.

3.4 Field sensitivity and partial energies

Because the activation energy Q_n appears in the emission equation (2.5b) and the field dependence of Q_n is mechanism dependent, it follows that experimental investigation of the field dependence of J and/or k_{hr} should help to discriminate between mechanisms. Experiments of this type are usually referred to as 'field-sensitivity experiments' or 'evaporation-rate experiments'.

Field dependence of both J and k_{hr} have been directly measured. Two techniques have been used, d.c. field evaporation and pulsed field evaporation. In d.c. field evaporation, the emitter voltage is raised to a certain value, and the times needed for evaporating successive layers are recorded. When sufficent time is allowed for one layer of atoms, the d.c. voltage is stepped up to a new value. The rates measured by d.c. field evaporation usually cover only two orders of magnitude, corresponding to a field strength change of only about 1.5%.

However, the use of high-voltage pulses can extend the rate measurements by several orders of magnitude. Suppose the width of the pulse is t, and it takes N pulses to field evaporate a layer, then the evaporation flux is given by

$$J(F) = 1 \text{ layer}/N.t \qquad (3.18)$$

Rate measurements are usually carried out near temperature 78K or above, where the rate-constant is expected to be determined by thermal activation.

3.4.1 Early experiments

Experimental measurements of field evaporation flux were first carried out by Brandon (1965, 1966) using a d.c. technique. His data analysis was in effect in terms of the field sensitivity s_T discussed in chapter 2, which in this context we define by:

$$s_T = (\partial \ln J / \partial \ln F)_T = F (\partial L / \partial F)_T \qquad (3.19)$$

The subscript T indicates that temperature is held constant. From equation (3.9) we have:

$$\lambda_1 = k_B T s_T \qquad (3.20)$$

Using equation (3.20), Brandon's field-sensitivity results for tungsten, molybdenum and platinum are converted into partial energies(λ_1) and included in table (3.3).

TABLE (3.3)

The first partial energies of W, Mo, Pt

Species	Temperature/K	λ_1/eV
W	62	2.0
	88	2.0
Mo	64	1.7
	88	1.7
Pt	62	1.9
	89	1.9

In Brandon's theoretical analysis, there was no clear conceptual distinction between flux (J) and rate-constant (k_{hr}). But it could be assumed that n_{hr}, the amount of material at high risk of evaporation, was not field dependent. Brandon thought that the existing models of field evaporation worked quite well for the field sensitivity data. We now review the merits of the two models theoretically and compare the results with the experimental values of the partial energies in table (3.3).

With the standard image-hump formalism the activation energy $Q_n(F)$ is given by equation (2.24) namely:

$$Q_n(F) = (\Lambda^0 + H_n - n\phi^E) - (n^3e^3F/4\pi\varepsilon_0)^{1/2} + (1/2)(c_\alpha - c_n) F^2 \quad (3.21)$$

With the approximation indicated in section 2.11, and using equation (2.42), we obtain

$$\lambda_1 = \mu_1 = (1/2)(n^3e^3F/4\pi\varepsilon_0)^{1/2} - \delta c\, F^2 \quad (3.22)$$

where $\delta c = c_\alpha - c_n$

Leaving aside the F^2-term for the time being, consider the case of tungsten field evaporation. Taking n to have the value 2 and F the value 57 V/nm, we get an estimate of λ_1 as about 25eV, which is more than ten times higher than the experimental value of about 2eV as shown in table (3.3). If the values of n is taken as 3 or higher, then the discrepancy is worse. Brandon was aware of the problems in the theoretical calculations.

It would, therefore, seem that without the F^2 term the image-hump mechanism could not account for the field sensitivity data. Although Brandon's estimate of the term was about 15% of the

zero-field binding energy, it seemed that a value for δc in equation (3.22) of about 7 meV $V^{-2}nm^2$ would account for the discrepancy between the theoretical and experimental results. Although it has been thought that c_α makes a major contribution in the expression for $\delta c = c_\alpha - c_n$, no reliable estimates of δc are available since the physical meaning of c_α is not yet clarified.

With the Gomer mechanism and using equation (2.18), without the repulsive effect, we obtain:

$$Q_n(F) = K_n + 1/2(c_\alpha - c_n) F^2 - neFx^p - n^2e^2/16\pi\varepsilon_o x^p \qquad (3.23)$$

and, therefore, λ_1 is given by:

$$\lambda_1 = neFx^p + (dx^p/dF)\{ne F^2 - n^2 e^2 F/16\pi\varepsilon_o (x^p)^2\} - \delta c F^2 \qquad (3.24)$$

In the earlier work the term dx^p/dF was neglected. Accordingly, if we use the first term only and as before, neglect the F^2 term, take n=2 and estimate x^p by half the nearest neighbour distance for W (about 0.14 nm), then the theoretical estimate of λ_1 becomes about 16eV. This value of λ_1 is again too high in comparison with the experimental estimate of 2 ev. Again this discrepancy would be worse if higher values of x^p or n were used in the calculation.

The above discussion shows that the early experiments and data analysis were no help in validating the evaporation mechanisms. The situation stimulated attempts to make more careful field sensitivity measurements.

3.4.2 The Mueller and Tsong (1970) experiments

Combining d.c. and pulse techniques Mueller and Tsong (1970) were able to obtain more detailed data concerning the evaporation flux. They interpreted their results in terms of a Gomer type (charge hopping) mechanism, and our parameters δc and x^p. Because of neglect of the dx^p/dF term in their analysis, the results are not valid, but it does seem that this experiment helped to stimulate a search for independent means of determining c_α and hence δc.

3.4.3 Effect of the imaging gas.

All early rate-measurements were carried out in the presence of the imaging gas, and consequently the effect of this on field evaporation was investigated.

Mueller (1957) found that the evaporation field of tungsten was reduced by increasing the imaging gas pressure, and Nishikawa and Mueller (1964) found that neon reduced the evaporation field much more than helium. They interpreted this as due to collisions between surface atoms and imaging gas atoms carrying a dipole attraction energy.

However, an increase in evaporation flux, at constant field, with increasing gas pressure (10^{-10} Torr to 3.10^{-8} Torr), was observed by Brenner and McKinney (1969) for helium on tungsten at 20K. At such pressure, impact of a gas atom on a given surface atom would be a very rare event, so that this phenomenon cannot be

due to gas impact or to electron bombardment. This suggested that a field-adsorption mechanism might be possible. Tsong (1969) reported experiments showing the effect of adsorption of neon atoms on tungsten.

Later, Taylor (1970) carried out similar experimental measurements on tungsten field evaporation and, in particular, measured evaporation flux as a function of electric field in the presence of inert gases. He concluded that the gas atom impact theory had no direct relevance to the evaporation mechanism and that the adsorption phenomenon played a significant part in the field evaporation process.

Since this work there has been a tendency for rate measurements to be done either in vacuo or in the presence of helium, but in the latter case the presence of helium has generally been ignored in the theory.

3.4.4 Tsong's (1971) experiments

Following the rate measurement experiments by Tsong and Mueller (1970), Tsong (1971) carried out more accurate experiments avoiding any residual chemically active gases to which evaporation is very sensitive. Evaporation fluxes were measured in a UHV system using pulse techniques, and the data were taken at liquid nitrogen temperature with a base field F^o at which J is 10^{-2} layer/sec. Tsong's experimental results are shown in a $\ln\{J(F)/J(F^o)\}$ vs. F/F^o plot (Fig.3.1).

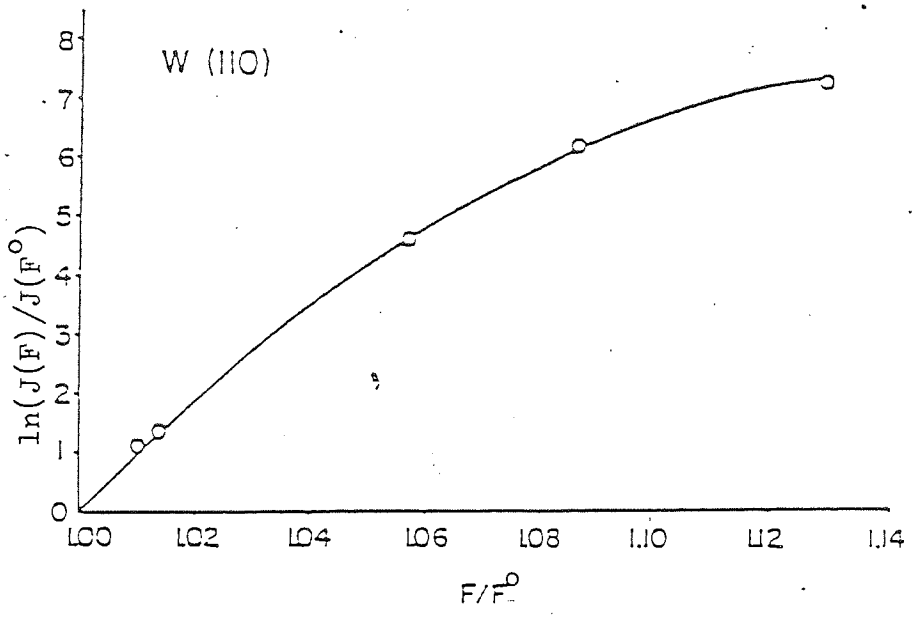

Fig.(3.1) Graph of $\ln(J(F)/J(F^{o}))$ vs. F/F^{o}, Tsong (1971)

At liquid nitrogen temperature, thermal activation is dominant and the evaporation flux is given by the emission equation (2.5b). Using a simple image-hump formalism Tsong expressed $\ln\{J(F)/J(F^{o})\}$ as a power series in F/F^{o} inclusive of the F^{2}-term; assuming the tungsten ion to be triply charged for F =57 V/nm, the theoretical curves were compared with the experimental ones. The discrepancy between the theoretical and experimental curves could not be improved by optimising the rate of evaporation by using higher ionisation states.

In the seventies it was difficult to analyse the field evaporation data using the Gomer mechanism. However, Tsong treated the experimental data analytically by making approximations in the emission equation, and from a straight line plot of $\ln\{J(F)/J(F^{o})\}/\ (F/F^{o}-1)$ vs. F/F^{o} he made estimates of δc and of a complex parameter relating to the intersection distance, the slope of the ionic curve, the field F^{o}, and a hypothetical linear

dependence of bonding energy on field. The value of δc obtained was "4.6 A^3" (3.2 meV V^{-2} nm^2).

Tsong (1971) also made direct measurements of the evaporation rate-constant for adsorbed tungsten atoms, but he analysed these ignoring the dx^p/dF term and there was some confusion over the validity of his statistical analysis (Forbes, private communication).

Vesely and Ehrlich (1973) reanalysed Tsong's results by fitting the rate-constant data using regression procedures and series expansions (for Q in terms of F) associated with both the standard image-hump formalism and the Gomer (charge-hopping) mechanism. The best fit to the data was given by the image-hump formalism, with n=2. Their finding thus contradicted the then current view that the escape probably occured via the Gomer mechanism, and was also apparently incompatible with observed evaporation charge states.

Patel and Forbes (Forbes 1974) developed a rate-sensitivity analysis that is independent of the assumed evaporation model and is directly related to the coefficients in a certain Taylor expansion series. Tsong's data were converted to be functions of the " fractional overfield " as defined in section (2.11.2). The first and second partial energies μ_1 and μ_2 were then derived from a statistical analysis using regression procedures, described in detail by Patel (1974).

Partial-energy data for tungsten had now been estimated from Brandon's (1966), Taylor's (1970) and Tsong's (1971) evaporation rate results. We here regard these all as estimates of λ_1 and λ_2, but they could equally well be regarded as estimates of μ_1 and μ_2.

TABLE (3.4)

Estimated values of λ_1 and λ_2 for W

Data Source	Temp./K	λ_1 /ev	λ_2 /ev
Brandon (1966)	62	2.0	
	88	2.0	
Taylor (1970)	65	2.0	
	80	2.3	
	90	2.6	
Tsong (1971)	78	1.4	-12
	78	1.3	- 9

The above partial energy data were then used in further analysis relating to the two proposed evaporation mechanisms. Forbes and Patel's (1974) conclusion was that the mechanisms could not be distinguished by the field sensitivity data and that neither model seemed particularly plausible if the escape charge-state were taken as 3+ or higher.

3.4.5 "Polarisability" experiments

As we saw earlier, one explanation for the discrepancy between experimental estimates of λ_1 and values predicted from simple theory lay in the assumption of high value for δc. In the early seventies, there were various attempts to get independent experimental estimates of c_α, beginning with the work of Tsong and Kellogg (1972). These attempts are discussed in Forbes and

Chibane (1982) who argue that in nearly all cases the experimental data have not been validly interpreted to give estimates of our c_α. In practice, the importance of this search for independent estimates of c_α diminished somewhat when it was realised that a better explanation of the discrepancy lay in the omission of the dx^p/dF term, (as we shall now see).

3.4.6 The Forbes (1978) analysis.

Until 1978, the term dx^p/dF in the dQ/dF expression for the Gomer mechanism was not taken into serious consideration. Although McKinstry (1972) pointed out the possible error involved, it remained a mathematical oversight in the literature. Forbes (1978), however, circumvented the issue by developing an alternative treatment to derive partial-energy expressions. The bound atom is assumed to be vibrating in a parabolic potential energy well with force-constant k and the activation energy is given by:

$$Q_n = (1/2)\, k\, r^2 \qquad (3.25)$$

where r is the distance of the escape point from the well minimum. His work leads to the expressions:

$$\mu_1 = k r x^p = 2Q_p (x^p/r) \qquad (3.26)$$

$$\mu_2 = -\mu_1 (1+x^p/r) = -\mu_1 (1 + \mu_1/2Q_n) \qquad (3.27)$$

$$\mu_2/\mu_1 = -(1 + \mu_1/2Q_n) \qquad (3.28)$$

Now using the estimate of Q_n as about 0.2 eV at 80K and μ_1 as 2 eV, we obtain for tungsten the semi-theoretical estimate: $\mu_2/\mu_1 = -6$

which is close to the experimental value of about -5. The analysis is therefore a strong indicator that the Gomer mechanism may be operative in low temperature field evaporation. The analysis is also independent of the assumed escape charge state of the ion.

Simultaneously with this, Tsong (1978b) again carried out field sensitivity measurements for a variety of materials (Mo, Ru, Hf, W, Ir, Pt) and analysed the data with a theory of the Gomer mechanism that neglects the dx^p/dF term. His analysis was thus incomplete.

So, in 1980 when the present work began, the situation as regards field sensitivities seemed to show that the Gomer mechanism was the more likely mechanism for tungsten field evaporation. Although there was some support for the Mueller mechanism, there was also doubt over how well the mechanism worked. More data, concerning the field sensitivity of field evaporation flux for other materials, had been published; but these were incompletely analysed. It was, therefore, an obvious task for the author to re-examine the consistency of the field sensitivity data with the conventional theories of the field evaporation mechanism, and if possible to discriminate decisively against one escape mechanism. This is the task of chapter 4.

3.5 Charge state of the evaporated ion

As already seen, the theoretical prediction of evaporation field is dependent on the charge state of an evaporated ion at the onset of evaporation. In early evaporation experiments with field-ion microscopes, the charge state of ions field evaporated from the emitter tip could not be measured. Therefore, evaporation field values had to be calculated using assumed values for the charge state.

Mueller (1956, 1960) considered the ions to be singly charged and carried out the theoretical analysis accordingly. Brandon then introduced his criterion (see section 3.2). As already indicated, Brandon (1964) using the basic image-hump formalism, and later Mueller and Tsong using a curve intersection formalism, predicted that for most transition metals the evaporation charge state at escape would be 2+.

With the development of mass spectrometry, experimental measurements of evaporation charge state became possible. Barofsky and Mueller (1969) made a qualitative study of the field evaporation properties of Be, Fe, Ni, Cu and Zn at liquid hydrogen temperature using a mass spectrometer whose ion source was the tip assembly of a field-ion microscope. The ions detected were Be^{+++}, Fe^{++}, Cu^{+}, Cu^{++}, Zn^{+} and Zn^{++}, and the observed charge states were in good agreement with Brandon's predictions from the basic image hump model.

Using the atom-probe field-ion microscope, Mueller, Panitz and

McLane (1968) discovered that refractory metals could often evaporate in charge states higher than 2+. Brenner and McKinney (1968) confirmed these findings by observing tungsten to evaporate in charge states of 3+ and 4+. Later, Mueller and Krishnaswamy (1976) found, for tungsten, that the charge state could be as high as 6+. Tsong (1978) has tabulated some observed charge states of various ion species as observed in atom probe experiments.

With some materials, if an imaging gas were present during evaporation, then the evaporation product could be a complex between the metal and a field adsorbed gas atom. For example in the presence of hydrogen Be, Cu, Fe, Ni exhibit hydrides, and in the presence of helium, W can form $(WHe)^{3+}$. A list of observed complexes has been compiled by Mueller and Tsong (1974).

The atom probe experimental results thus disagree with Brandon's criterion for the predicted values of the charge states. These findings seem to have caused theoretical uncertainty for much of the seventies, until the idea of " post-ionization " became accepted, with the implication that the observed charge on an evaporated ion is in most cases determined by the occurrence of post-ionization after escape.

Mueller and Tsong (1974) first raised the possibility that field evaporation was a two-stage process: first escape, which would then be followed by one or more post-ionization events as the energy levels of lower-lying orbitals in the departing ion came up above the Fermi-level. The idea of post-ionization in field ion emission was not in itself new, having been introduced by Goldenfeld et al. (1974) in connection with multiply-ionized states of organic molecules.

The experimental fact is that charge states upto 6+ are

observed. But the theoretical idea that 3+, 4+, or 6+ ions would be formed in a single-stage process is difficult or impossible to accept. An obvious possibility is that evaporated ions undergo post-ionization. Two theoretical investigations were soon made into the possibility of post-ionization. The theoretical calculation by Taylor (1970) on the field evaporation of tungsten, and that by Chambers et al. (1970) on molybdenum, both seemed to show that post-ionization was highly improbable for these two species. So a problem existed.

The first significant clue to the solution came from the work of Ernst (1979) and Ernst and Block (1980) on the field evaporation of rhodium. By combining a magnetic sector mass spectrometer with a retarding-potential energy analyser and sensitive digital ion detection techniques, Ernst was able to separate the observed Rh^{+}, Rh^{++} species and measure their evaporation characteristics separately. The field dependence of the relative abundance of the two species was also determined.

The experiment also involved measurement of activation energies of both Rh^{+} and Rh^{++} ions as a function of evaporation field. It was observed that, within experimental error, the Rh+ and Rh^{++} ions had similar activation energies at all evaporation fields. The result strongly suggested that in all cases evaporation occurs into a singly-charged state and that, for a proportion of Rh^{+} ions, a second stage of ionization is a subsequent event. Ernst confirmed this possibility by a calculation of the expected relative abundance of Rh^{+} and Rh^{++} ions using a one-dimensional model to predict ionization probability. The theoretical curve fits the experimental one within the limits of experimental error.

Our understanding of post-ionization has now been much improved by the work of Kingham and colleagues.

Haydock and Kingham (1980) initially criticised Ernst's use of an one-dimensional model for prediction of ionization rate-constant. So they developed an improved method of calculating the field-ionization rate constant using a three-dimensional version of accepted WKB methods. This three-dimensional model calculation was then applied to the field ionization of metal ions.

The three dimensional numerical calculation of Haydock and Kingham was based on a simple surface model. Ernst and Jentsch (1982) subsequently pointed out that the calculation was not self-consistent, and carried out three-dimensional numerical calculations based on a more realistic surface barrier model. Kingham has subsequently modified his theoretical treatment and carried out post-ionization calculations for a large number of materials.

In general terms, the results of Kingham and colleagues have enhanced the acceptance of the likelihood of post-ionization. They indicate that a sequence of post-ionization events is possible and that the mean observed charge-state should increase systematically with field strength. Kingham (1982b) has reassessed all previous experimental work and finds it generally compatible with the idea of post-ionization.

Post-ionization would also explain certain results of 'imaging atom-probe experiments'. The application of this instrument to the field evaporation of a number of elements (W, Ir, Al, Mo, Ta, Fe etc.) shows that the ions of higher charge-states come from certain areas of the end form, and the general observation seems

to be that high evaporation charge-state correlates with high-field regions of the endform.

Other work supporting post-ionization has been carried out by Kellogg (1982), Andren et al. (1984) and Menand and Kingham (1984).

From the evidence it is absolutely clear that in field evaporation experiments post-ionization happens, but it is not always clear whether the initial charge-state is 1+ or 2+. It is most unlikely that the initial charge state would be above 2+.

This result, that the escape charge state is 1+ or 2+, is important in the context of later work in this thesis. We shall be developing a mathematical model that demonstrates the inapplicability of the Mueller mechanism, on the grounds that the field F_n^{HD} at which the hump disappears is significantly less than observed evaporation fields. The arguments are convincing if the escape charge state is 1+ or 2+, but becomes less convincing for 3+ or higher charge states because the corresponding values are higher. Knowledge that the escape charge state is (may be) less than the observed charge state is thus vital to our arguments.

3.6 Temperature dependence of evaporation field, and evaporation regimes

In principle, analysis of the experimental evaporation field vs. temperature data (using the theoretical F-T variation as given by the existing field evaporation theories) might distinguish between models.

As already indicated, Q_n is related to T by equation (3.15), namely:

$$Q_n = k_B T \ln(n_{hr} A/J) \qquad (3.29)$$

This formula is, of course, valid only over a certain temperature range. As indicated earlier, it breaks down at low temperature, (due to ion tunnelling effects). It will also break down at sufficiently high temperatures (due to the onset of surface diffusion, or possibly for other reasons- see Forbes and Chibane (1982b).

Within the range of validity, if measurements are taken at constant flux J^o, and if there is no F or T dependence in the flux pre-exponential $n_{hr}A$, then:

$$Q_n = \text{const.}\ k_B T \qquad (3.30)$$

where the value of the constant depends on the chosen value of J.

The different mechanisms provide different Q-F relationships, so using equation (3.30) it is possible to obtain mechanism dependent F-T relationships.

For the Mueller mechanism, using the basic image-hump formalism, the evaporation field at onset F^o could be written using equation (2.24), without the F^2-term, as:

$$F^{o\ 1/2} = (4\pi\xi_o/n^3\ e^3)^{1/2}\ (\Lambda^0 + H_n - n\Phi^E - \text{const.}k_B\ T) \qquad (3.31)$$

where the symbols have their usual meanings.

In the early days of the subject, Gomer (1959) and Mueller

(1960) used T-F data to discuss the field desorption of barium and thorium from tungsten substrates: both found that for the field desorption of thorium from tungsten a linear relationship existed in the plot of $(F^o)^{1/2}$ vs. T, where F^o is the measured (onset) desorption field. Their findings are in rough agreement with the basic image-hump formalism.

Nakamura and Kuroda (1969) carried out measurements of the temperature dependence of evaporation field ranging from 20K to 300K for tungsten, molybdenum and tantalum. For the temperature range between 180K to 300K, their findings were broadly similar to Mueller and Gomer's findings, in that evaporation field decreased with the nearly square of the emitter temperature.

However, in the 1980's it is clear that the basic image-hump formalism is unsatisfactory and that the inclusion of the repulsive ion-surface interaction term in the ionic potential energy expression makes it more difficult to derive a satisfactory analytical approximation for Q_n as a function of F (and correspondingly F^o as a function of T). At any rate, none existed when this work was begun.

Also in 1980, when this work began, there were no satisfactory analytic theories of the Gomer mechanism that could be used to discuss the temperature dependence of evaporation field. But since that time the theory has been developed. This will be discussed in chapter 6.

3.7 Field dependence of activation energy

The formula for field dependence of activation energy is usually dependent both on the postulated mechanism of field evaporation

and on the mathematical formalism that is used to describe the mechanism. In principle, therefore, by fitting the available experimental data to the mechanism-dependent field dependency of activation energy formula, it is possible to discriminate between mechanisms of field evaporation. But, in the literature, only a few workers used this method to gather support for the competing field-evaporation theories because of the difficulties in experimental determination of Q_n.

However, in the previous section, we have pointed out that, for a certain range of temperatures field evaporation is a thermally activated process obeying the emission equation. Therefore, a semi-experimental value of Q_n may be determined from the slope of the Arrhenius plot of ln(J) versus 1/T at a given field, using equation (3.6). Such measurements, however, were for many years not very reliable. It was only when direct ion counting techniques were developed that useful 'measurements' of Q_n became available.

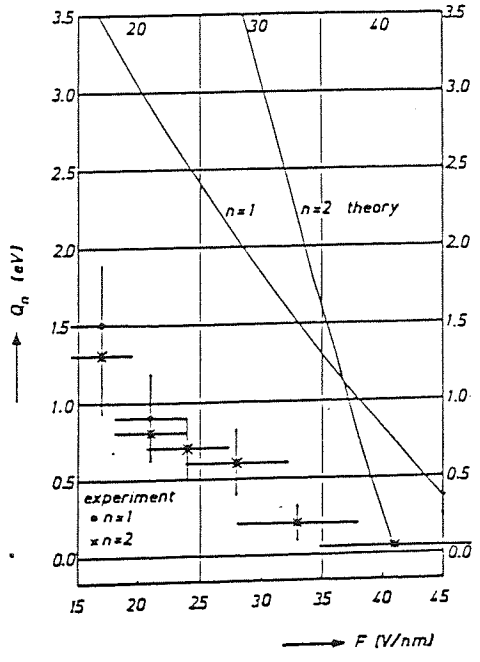

Fig. (3.2) Field dependence of activation energy for rhodium ions

Ernst (1979) used the direct ion counting technique to obtain experimental data on the field dependence of activation energy of rhodium ions. He drew two important conclusions: that activation energies of singly and doubly charged rhodium ions are the same; and that the field dependence of activation energy does not comply with (the basic image-hump analysis of) the Mueller mechanism. Ernst's results are shown in Fig. (3.2). At that time, Ernst thought that his results demonstrated the non-applicability of the Mueller mechanism to rhodium field evaporation. However, because the basic image-hump formalism omits the repulsive interaction term, this conclusion is not valid.

Ernst's rhodium results have been further analysed by other workers after 1980. We shall extend this discussion in chapter 6.

3.8 Appearance energy measurement

In chapter 2, we have introduced the concept of appearance energy. If field evaporation is a thermally activated process then the standard appearance energy is given by equation (2.48) namely:

$$A_{\alpha nr}^{st} = \Lambda^{F} - H_{r} + Q_{\alpha nr} \qquad (3.32)$$

Equation (3.32) can be used to compare the experimentally determined appearance energies with their theoretical values. The values of the parameters on the right hand side of the equation are approximately known, so $A_{\alpha nr}^{st}$ can be predicted. Therefore, if the experimental onset appearance energy agrees, then this will constitute yet another indication that field evaporation is a

thermally determined process. Ernst et al.(1979) made measurements of onset appearance energies of Cu, Be and Ni ions, and for each species a satisfactory comparison between the theory and experiment was found.

Since $Q_{\alpha nr}$ in equation (3.32) is mechanism dependent, measurements of appearance energy might also in principle be used to discriminate between evaporation mechanisms. In practice, in 1980, only the basic image-hump formalism could be treated in this way. Taking equation (2.52), using just the electrostatic and image-potential terms in S_n (x^p,F), and using equation (2.23), we obtain:

$$A_{\alpha nr}{}^{st} = H_r - H_n + n\phi^E + (n^3 e^3 F/4\pi\varepsilon_0)^{1/2} \qquad (3.33)$$

If it is assumed that no post-ionization occurs then r=n, and the above equation becomes:

$$A_{\alpha nn}{}^{st} = n\phi^E + (n^3 e^3 F/4\pi\varepsilon_0)^{1/2} \qquad (3.34)$$

Ernst (1979) plotted appearance energy data as a function of field for Rh^+ and Rh^{++} ions and compared the result with a theoretical plot using equation (3.33). Fig.(3.3) shows the comparison.

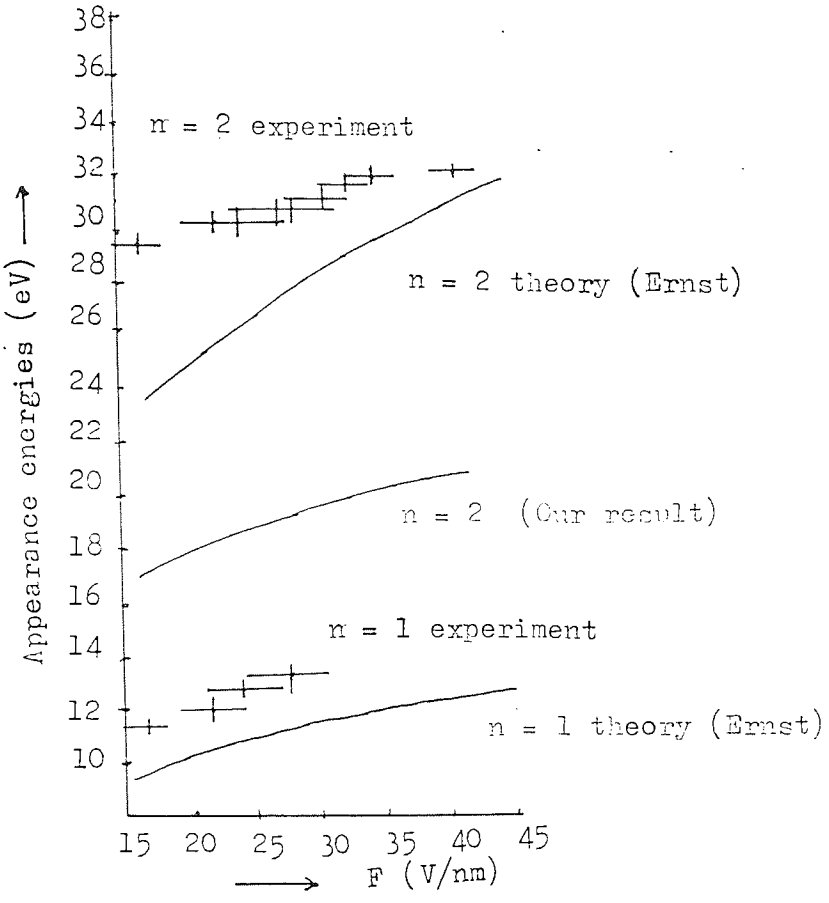

Fig. (3.3) Appearance energy variation with field, Ernst (1979).

It seems from the diagram that the basic image-hump theory does not fit the appearance energy experiment well.

However, there was an omission in Ernst's work. Although his activation energy measurements confirmed post-ionization, he did not take this into account when calculating the appearance energy for Rh^{++} ions using equation (3.34). In reality equation (3.33) should have been used. We have thus inserted the (n=1, r=2) curve onto the diagram. Again, the theoretical plot does not fit the experiments well.

However, as in section (3.7), it is impossible to draw any general conclusion from this because the basic image-hump

formalism is not a complete theory of the Mueller mechanism. (Also, of course, in 1980 the theory of the Gomer mechanism was not sufficiently developed to formulate a valid expression for $A_{\alpha nr}^{st}$ in terms of field).

3.9 FWHM measurements.

In principle, the FWHM of the observed energy distribution of the field evaporated ions is capable of giving information about the mechanism of emission. However, in 1980 there were relatively few experimental measurements of half-widths.

The FWHM of the Be, Co and Ni ions may be measured from the relevant experimental data obtained by Ernst et al.(1979), and typical FWHM values for these species are of order 2eV.

Moreover, in the pre-1980 literature, there had been no satisfactory discussion on the application of theory of field evaporation to FWHM Measurement, so such measurements seemed unhelpful as a means of discriminating between escape mechanisms.

3.10 Some limitations and assumptions of existing theories

In the preceding sections we have seen that the assumed escape mechanism determines the theoretically predicted values of numerous field evaporation parameters.

Although the experiments suggest that low-temperature refractory metal field evaporation is a two-stage process (escape followed by post-ionization), in 1980 the theories of field

evaporation were not developed enough to discriminate definitively between the different escape mechanisms. In part, as we shall see in later chapters, this is due to mathematical oversights in the analysis of the various mechanisms. But there is also a more fundamental difficulty with the type of theory discussed here, which we need to consider.

The basic physics of the interaction between an external ion and a metal surface is assumed in field evaporation theory to be contained in equation (2.12), which sets out the mathematical representations of the various potential-energy contributions. But, even in a classical analysis, it is by no means clear that these mathematical expressions are strictly correct, and we need to look at them in more detail.

3.10.1 The electrostatic term

The definition of each potential energy term in chapter (2) is in fact made in the context of flat surfaces. In the literature, in discussing the electrostatic potential energy term, two flat-surface models are considered: a perfect "smooth-flat" surface and an "atomically-flat" surface.

In both these models, the electric field is always considered uniform and constant at sufficient distance from the surface. This is what we introduce as the "external field" and denote by F. Correspondingly, the electrostatic potential energy of an ion of charge (ne) at a distance x is given by -neFx, where the distance x is said to be measured from the model's electrical surface, and the electrostatic potential is taken as zero inside the metal. With the "smooth-flat" models, the nucleus is always in the region

of uniform field. But with the "atomically-flat" models, there are field variations close to the surface, and with this model, the ion cannot in fact be in an uniform electric field. Thus, we need to examine the problem of local field variation above the model surface.

The source of the local field variation is the local crystallographic structure of the plane in question. The problem of field variation has never been examined in detail, but Wafi (1981) attempted to take this problem on board using an array of monopoles and dipoles to represent the W(111) surface (with a distant array of negative charges for electrostatic self-consistency). Fields and potentials were calculated by Wafi for two cases:

(1) above a surface atom;

(2) above a point midway between two surface atoms.

The field variation as a function of distance R_z , is shown in Fig. (3.4), for two values of surface atom polarisability. The above-atom field approaches infinity as the plane of the surface nuclei is approached, whereas the between-atom field has in this plane a finite value. At large distances, both curves converge to the external field. Wafi suggests that the size of these field variations across the surface will depend on the crystallographic structure of the array but mainly on the area per lattice point of the array.

We give some indication of the size of local field variations at distances likely to be of interest in field evaporation.

For a hypothetical "field-adsorbed" W atom on the W(111) plane at the above-atom position, the distance R_z would be $2\rho_0 = 0.274$ nm from the plane of the nuclei, where ρ_0 is the neutral W

radius (0.137 nm). It can be seen from Fig (3.4) that at this position the local field has increased by nearly 10% from the external field value.

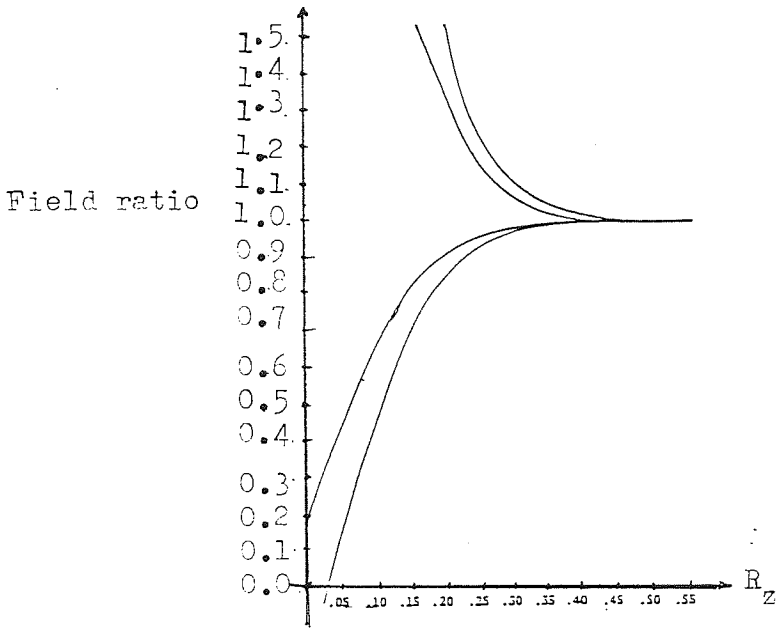

Fig. (3.4) Field variation as a function of distance R_z

For the "field-adsorbed" W atom on the W(111) plane but above the between-atom position (i.e. between closest neighbours) and in contact with the underlying atoms, the nucleus would be at R_z = 0.16 nm from the plane of the nuclei. At this position, the local field is less than the external field value by about 15%. If the atom is adsorbed on the W(111) plane in the "symmetrical" position, so that it is in contact with three underlying atoms, then its nucleus would be at a distance R of approximately 0.09 nm. The corresponding predicted difference between the external field and the local field would be significantly higher than 15%, but unfortunately Wafi did not carry out calculations for this case.

3.10.2 Work-function related effects.

So far, our discussion has been concerned with the atomically flat model and effects resulting from the presence of an applied field. However, even in the absence of an applied field, other sources of local field variations exist , originating from the "smoothing" and "spreading" of electron clouds across the surface. These were discussed by Smoluchowski (1941), when he was attempting to account for the surface double layer. These are short range efects and give rise to " surface fields".

Each double layer is characterised by its own electric dipole moment (per unit area), and differences in work-function from one plane to another are attributed to different moments. On a real emitter, between two adjacent planes there are local fields due to these different work-functions, and their effects can extend well away from the surface. These fields are called "patch fields". Normally, the theoretical models of field evaporation do not consider these effects at all.

3.10.3 Tip Geometry effects.

In a real field-ion emitter, different atomic planes are exposed to the external applied field whose average value is calculated over the entire cap using the applied voltage and assuming some hemispherical or paraboloidal shape for the emitter endform. However, the field normally has different average values over different areas of an emitter endform. These variations in average external field are of "macroscopic" origin and they depend on the cone angle of the shank, the angular distance from the apex, the

local radius of curvature, the degree of protrusion and the size of the plane from which evaporation is occurring. The field variation due to these factors is of the order of 10% to 20%. The literature, however, usually ignores this variation. These macroscopic fields fall off very slowly with distance away from the surface, and thus negligibly affect the linear approximation of the neFx term.

There may also be field variations over steps at the edges of atomic planes, and at kink sites. Birdseye (1972) has investigated these variations in the context of a classical conductor model and found that the variations effectively vanished at about 1Å away from the step edges.

Field evaporation theories should in principle take into account the effects of all these types of field variation. There is, in particular, a difficulty associated with the process of field calibration. Thus, what Sakurai and Mueller (1973) measured was the external field somewhat above the atom instead of the "mean field as experienced by the ion during the evaporation process". The "mean field", as we call it, may involve various of the effects that we have discussed above and is likely to be somewhat different from the external field. The assumption of a linear form for the potential variation with distance may also not be particularly good; however, we will continue with this approximation in the following chapters.

3.10.4 The image-potential term

The correlation interaction of an ion is usually taken as the classical image-potential $-n^2 e^2 / 16\pi\varepsilon_0 x$, where (as before) x is distance measured from the electrical surface. According to Lang and Kohn (1973), this form is correct in the limit of large distance from the surface. However, very near the surface this approximation is expected to break down as shown by Smith et al.(1973) for hydrogen chemisorption on metals. These authors showed that for a proton, at a distance less than 1Å from the surface, the interaction energy began to deviate significantly from the image potential approximation. Therefore, in the Mueller model of field evaporation , at the Schottky distance (about 0.1 nm) from the surface, the image potential term may not be applicable.

For most metals, however, the atomic radius is greater than 0.1 nm. Therefore, according to the findings of Smith et al. the classical image-potential term in metal field evaporation may be adequately valid, at least as a first approximation.

3.10.5 The repulsive term

As we have already pointed out, the main objection to the simple image-hump formalisms has been the neglect of any repulsive term that may be important at very small distances from the metal's surface. Thus we have developed in later chapters an extended model that includes a repulsive ion-surface interaction term. In

our work, we have assumed the form G/x^t for the repulsive ion-surface interaction term, where G and t are adjustable constants and x is measured from the metal's electrical surface.

Alternatively, the repulsive term could be given in an exponential form as is given in the Buckingham potential.

This form is certainly an approximation and is used because of its mathematical convenience. Alternatives, such as a repulsive exponential form, certainly exist. It is also possible for the repulsive term to be expressed as a sum of pairwise interactions, summed over all the surface atoms (though this procedure may not be valid at a metal surface).

We return to the question of the validity of the G/x^t form later in the thesis.

3.10.6 The F^2 - energy term in the atomic bonding potential.

In chapter(2), we have discussed the form $1/2\ c_\alpha F^2$ of the F^2-energy term for a surface atom in its bonding state, and the meaning of the coefficient c_α. Field evaporation theory normally assumes the surface atom to be in a constant field, usually taken to be the external field. But for reasons discussed earlier, such atoms are affected by various local field variations. Therefore, we expect the coefficient c_α as defined by equation (2.6) to vary from site to site. In practice, since realistic models of a charged-surface do not exist , we use the form $1/2\ c_\alpha F^2$ in our numerical work, and c_α is taken as constant.

Similar assumptions are made in respect of the ionic term, $1/2\ c_n F^2$.

These difficulties are, of course, additional to those

resulting from the partial ionization of surface atoms, and the possible variations of bonding position with field, which were mentioned in section 2.4.

3.10.7 Topology of the escape path

Existing field evaporation theories assume that a field evaporated ion escapes at right angles to the emitter surface. This one-dimensional model is used for simplicity and mathematical convenience. However, it is not impossible that the nucleus of the evaporated ion may move sideways prior to evaporation. This possibility has been discussed by Waugh et al. (1976). Fig.(3.5) depicts the situation.

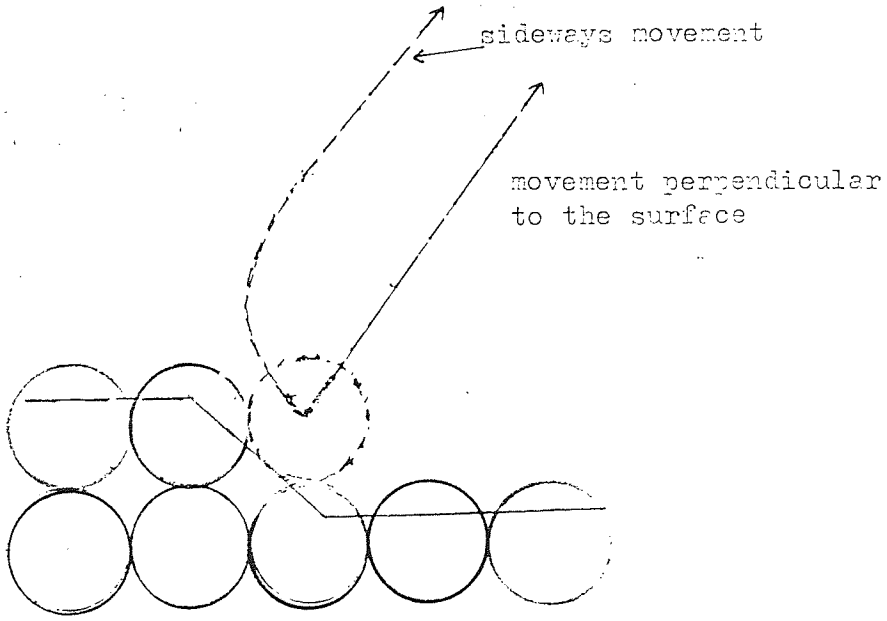

Fig. (3.5) Toplogy of the escape path

A kink-site atom on a low-index plane tends to move to a position more exposed to the field than its own lattice site. Waugh et al. (1976), therefore, suggest that all atoms are likely to move on the specimen surface before evaporation, rather than evaporate perpendicularly from their original sites. These drifting atoms interact with their neighbours and assume a

resultant motion towards the position of higher field.

There is some evidence from imaging atom-probe experiments to suggest that sideways motion before evaporation does occur (cf. Waugh et al. 1976). If sideways movement of atoms takes place then it gives rise to the question of where ionization and escape are taking place, whether on the "lateral" or "perpendicular" portions of the path. Briefly, it seems that the evaporation theories should work adequately if escape takes place on the perpendicular part of the path. We shall return to this question later.

3.11 Assessment and conclusion.

In this chapter, we have been looking at various field evaporation parameters and their experimental and theoretical estimates, in order to get a feel for how field evaporation of ions occurs, to what extent the existing field evaporation theories can interpret the available experimental data and whether the available information can discriminate between evaporation mechanisms. The following is the assessment of our findings about the field evaporation theories and their relevance to the experimental data, as they existed up to 1980.

1. The calculated values of F_n^e by both the Mueller mechanism and Gomer mechanisms are apparently in good agreement with the experimental values of F_n^e, but the comparison really signifies only that field evaporation is a thermally activated process.

2. The Q_n-values independently estimated from measurements

and quasi-thermodynamic relations are found to be in good agreement with the Q_n-values calculated more directly using the Arrhenius type emission equation (2.5b). This supports the finding that field evaporation is thermally activated.

3. Conversion of field sensitivity data into partial energies and subsequent analysis on the basis of the two main types of existing field evaporation mechanism, seems to show that the Gomer mechanism may be a likely mechanism for field evaporation of refractory metals. Our analysis also show some support for the Mueller mechanism. Up to 1980 there had been no conclusive arguments that would fully support (or discard) either of the mechanisms. Also until 1978, many papers contained an error in the mathematics of the Gomer mechanism. There is, however, a significant amount of field-sensitivity data available.

4. In field evaporation, it is unlikely that observed higher charge state ions would be formed in a single stage process. The literature presents strong evidence that ions first escape with charges +1 or +2 and then post-ionize into higher charge states.

5. The variation of evaporation field with temperature should be mechanism dependent, therefore relevant results might be used to distinguish between mechanisms. However, explicit expressions for Q_n in terms of F are needed to do the theoretical analysis and these were not available in 1980.

6. Since the form of the relationship between activation energy Q_n and field F is dependent on the postulated escape mechanisms, measurements of Q_n could be used to discriminate between mechanisms. But because of the difficulties both in experimental determination of Q_n and in deriving explicit Q_n-formulae it had not been possible in 1980 to use this method

effectively.

7. Appearance energy (A)-values calculated using thermodynamic data can be compared with their experimental values. This again shows that field evaporation is a thermally activated process.

However, it is also possible in principle to derive mechanism dependent appearance energy expressions for A, in terms of F, so the theoretical A-F variation might be compared with the experimental A-F variation to discriminate between mechanisms. But in 1980 the theory was incomplete.

8. So far, FWHM-measurements have not been useful in discriminating between mechanisms because no mechanism dependent theoretical expressions for FWHM have been used in the literature.

So, to summarise, by 1980 we knew that field evaporation was thermally activated, and that post-ionization occured, but there was little in the way of decisive argument about the nature of the escape mechanisms and there were some obvious weaknesses in the theory. We thus need to develop necessay theoretical formulae, develop appropriate tests, and make use of recent experimental data to discriminate between mechanisms.

It seemed that tests based on field-sensitivity data and partial energies, evaporation field variation with temperature, activation energy variation with temperature, appearance energy variation with temperature, and FWHM-measurements might potentially discriminate between mechanisms. The field-sensitivity data seemed most plentiful and in the following chapter, we will investigate the most recent field senstivity data (Tsong 1978b and Ernst, 1979). This leads naturally in chapter 5 to a more purely theoretical assessment of the plausibility of the Mueller

mechanism.

It seemed more difficult to use other types of test, namely F-T variation, Q-F variation, A-F variation and FWHM, due to lack of reliable data and appropriate mechanism-dependent theoretical formulae. But later we will derive necessary theoretical expressions so that we can make use of recently available experimental data to develop additional tests.

A further conclusion from this assessment is, of course, that the whole detailed analysis of field evaporation theory was in 1980 based on certain underlying assumptions - namely the "flat-surface" approximation and the validity of the classical potential energy expressions. We continue with these assumptions for the time being, but will go some way towards investigating their validity in later chapters.

CHAPTER 4

FLUX - FIELD SENSITIVITY DATA AND THE MUELLER MECHANISM

4.1 Introduction

In 1978 Tsong (1978b) reported some field sensitivity data for six refractory metals: Mo, Ru, Hf, W, Ir and Pt. The data are in the form of a plot of $\lg(J/J^{o})$ against F/F^{o}, where the symbols have their usual meanings, and J^{o} is a flux of 0.01 layers/sec. Tsong's data were reanalysed in relation to the existing field evaporation mechanisms in a paper by Forbes, Biswas and Chibane (1982). The report suggested that the Mueller mechanism was not compatible with the field sensitivity data. However, it was subsequently found that the error limits on the derived values of some parameters involved were unreliable.

In this chapter, we present a revised analysis of the data and also include some further tests on field sensitivity for the same materials, using the "extended image-hump formalism".

In this context, we would like to remind the reader of the terminology that we have used to describe the types of image-hump formalism. As mentioned in chapter 2, we are dealing with three types of image-hump formalism- "basic", "standard" and "extended". In all cases the electrostatic term is included in the ion potential energy expression. Inclusion of this and just the image-potential term constitutes the "basic" formalism, whereas with the further addition of the F^{2}-term, we obtain the "standard"

formalism. The "basic" and the "standard" formalisms together are known as the "simple" formalisms, and the additional inclusion of a repulsive term in the ion-potential energy constitutes the "extended" formalism.

The structure of the chapter is as follows. First we convert the Tsong (1978b) flux-field sensitivity data into partial-energies, and then we study the consistency of the partial energy values with the simple formalisms (the basic and standard formalisms). Also, from the partial-energy values we derive the evaporation fields for the six metals, using the "standard" formalism, and compare these with the field values observed by Tsong (1978b).

Following the above work, we derive partial-energy expressions using the "extended" formalism, and again calculate evaporation field-values for the six metals, to compare with the observed evaporation fields.

Finally, we use Ernst's (1979) rhodium data for the field dependence of activation energy to calculate the first partial energy of the Rh^+ ion, and then look at its compatibility with image-hump theory using the a general formalism where no specific forms of image-potential and repulsive terms are used in the ion-potential energy expression.

4.2 Conversion of Tsong (1978b) data into partial energies.

Tsong's (1978b) flux-field sensitivity data for tungsten are shown in Fig.(4.1) in the form of a $\lg(J/J^o)$ vs. F/F^o plot. Tsong expanded his flux term in the form:

$$\lg(J/J^{o}) = a_0 + a_1 (F/F^{o}) + a_2 (F/F^{o})^2 + \ldots . \qquad (4.1)$$

and obtained a_1 , a_2 etc. as best fit coefficients to experimental data.

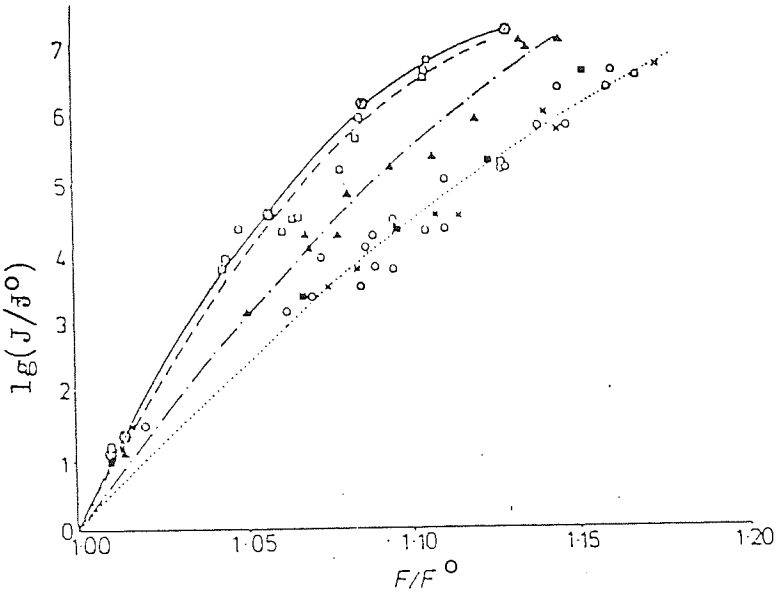

▨ W(110); □ Mo(110); ▲ Hf(10$\bar{1}$0); ■ Ru(11$\bar{2}$1); ○ Ir(100); × Pt(100).

Fig. (4.1) The field dependence of the field evaporation rate of tungsten, molybdenum, hafnium, ruthenium, iridium and platinum ($J^{o} = 10^{-2}$). The Ru, Ir, and Pt data fit into the same dotted curve.

However, for our analysis it is better to adopt a chapter 2 type approach, and write:

$$\ln(J/J^{o}) = (\lambda_1/k_B T)g + 1/2(\lambda_2/k_B T)\, g^2 + . \qquad (4.2)$$

where $g = (F - F^{o})/F^{o}$, and the coefficients λ_s are defined as:

$$\lambda_s = k_B\, T.\, F^{s} \left(d^{s} \ln J/dF^{s}\right)\Big|_{J = J^{o}} \qquad (4.3)$$

In the original paper, Forbes et al. (1982) deduced λ-values (and error limits for these) from Tsong's published a-values. Subsequently, however, we have carried out a direct regression of $\ln(J/J^{o})$ vs. g, with the results shown in table (4.1). (The results shown contain a small correction to allow for the fact that the regressed curves do not pass through the origin of g. A correction procedure due to Forbes has been used.)

Overall, this analysis gave noticeably different values for some of the parameters calculated, as may be seen by comparing table (4.1) with table 2 in Forbes et al. 1982. (It should be noted that we have chosen to present results here as values of λ_1, λ_2, rather than as estimates of μ_1 and μ_2.)

Because of the differences, it is necessary to look again at the compatibility of the results with the image-hump formalisms.

TABLE (4.1)

Experimental partial energies λ_1 and λ_2 and their ratios, derived from regression of Tsong's (1978b) original data.

Species	λ_1/eV	λ_2/eV	λ_2 / λ_1
Mo(110)	1.39± 0.13	-8.2± 2.2	-5.9± 2.1
Ru(1121)	0.76± 0.11	-1.5± 1.5	-1.97± 2.8
Hf(1010)	1.05± 0.18	-3.6± 2.2	-3.43± 2.7
W(110)	1.55± 0.05	-10.3± 0.7	-6.65± 0.7
Ir(100)	0.73± 0.08	-1.6± 0.8	-2.91± 1.3
Pt(100)	0.71± 0.10	-1.5± 1.1	-2.11± 1.8

4.3 Comparison with theory - introduction.

It follows from the arguments in chapter 2 that, if field dependence in $\ln(n_{hr})$ and $\ln(A)$ may be neglected, then:

$$\lambda_s = M_s = -(F)^s . d^s Q_n / dF^s \qquad (4.4)$$

We shall assume here that neglect of field dependence in $\ln(n_{hr}A)$ is justified, and hence will regard the expressions obtained by evaluating the derivatives of Q_n w.r.t. F as estimates of λ_s-values. Since the λ-expressions depend on precisely which expression for Q_n is used, i.e. precisely which formalism, we look at the various formalisms in turn.

4.4 Comparison with simple formalisms

4.4.1 The basic image-hump formalism

As shown in equation (2.45), according to the basic image-hump formalism:

$$\lambda_2 / \lambda_1 = M_2 / M_1 = -1/2.$$

Table (4.1) shows that experimental values of this ratio lie between -2 and -6.7. It can be seen that for Mo and W the experimental values of λ_2/λ_1 are unlikely to be compatible with the theoretically predicted values using BIH, but for Ru, Hf, Ir

and Pt, the error limits are very large, so no conclusion is possible.

Since the BIH formalism does not include the F^2-term the predicted theoretical value of λ_2/λ_1 is independent of species and of charge state at escape. Because the tabulated values of λ_2/λ_1 for the six species have been calculated directly from the experimental results, we can consider these as independent estimates of λ_2/λ_1. The average experimental value is -3.7 ± 0.8. It is obvious that this average value is not in agreement with the BIH predicted ratio.

4.4.2 The standard image-hump formalism - energy expressions.

The standard image-hump formalism includes the F^2-term. Correspondingly, equation (3.21) gives an expression for the activation energy, namely:

$$Q_n(F) = K_n - (n^3e^3.F/4\pi\varepsilon_0)^{1/2} + (1/2)(c_\alpha - c_n)F^2 \qquad (4.5)$$

where the symbols have their usual meanings. Using the expressions for partial energies given by equation (4.4), we can show that:

$$\lambda_1 = 1/2(n^3e^3/4\pi\varepsilon_0)^{1/2}(F^o)^{1/2} - (c_\alpha - c_n)(F^o)^2 \qquad (4.6)$$

and $$\lambda_2 = -(1/4)(n^3e^3/4\pi\varepsilon_0)^{1/2}(F^o)^{1/2} - (c_\alpha - c_n)(F^o)^2 \qquad (4.7)$$

From equations (4.6) and (4.7) we obtain:

$$(n^3e^3 F^o/4\pi\varepsilon_0)^{1/2} = (4/3)(\lambda_1 - \lambda_2) \qquad (4.8)$$

and $1/2(c_{\alpha} - c_n)F^2 = (-1/6)(\lambda_1 + 2\lambda_2)$ (4.9)

Substituting equations (4.8) and (4.9) into equation (4.5) we obtain:

$$K_n - Q_n(F) = (3/2)\lambda_1 - \lambda_2 \quad (4.10)$$

where K_m is given by equation (2.17), namely:

$$K_n = \Lambda^0 + H_n - n\Phi^E \quad (4.11)$$

TABLE (4.2)

$K_n - Q_n(F^o)$ values for Mo, Ru, Hf, W, Ir, and Pt.

Species	Φ^E/eV	$[(3/2)\lambda_1 - \lambda_2]$/eV	σ/eV	$[K_n - Q_n(F^o)]$/eV		Δ/σ
				n=1	n=2	n=1
Mo(110)	5.12	10.3	2.4	9.5	21.5	0.3
Ru(1121)	4.86	2.6	1.7	9.3	21.6	4.0
Hf(1010)	3.65	5.2	2.5	9.7	21.1	1.8
W(110)	5.14	12.6	0.8	11.9	25.4	0.9
Ir(100)	5.27	2.7	0.9	10.5	22.2	8.7
Pt(100)	5.84	2.6	1.2	9.4	22.6	5.7

Now, the value of $(3/2)\lambda_1 - \lambda_2$) can be derived from the experimental values of λ_1 and λ_2 , and can then be compared with the value of the expression $\{K_n - Q_n(F^o)\}$. $Q_n(F^o)$ is set to 0.2eV, and values of Φ^E have been taken from J.C.Riviere (1969) and Knor (1977), whilst values of Λ^0 and ionization energies I_n have been taken from Tsong (1978b). Table (4.2) shows the values of $K_n - Q_n(F^o)$ for the six metals, λ_1 and λ_2 can be used to compare with the corresponding values of the r.h.s of equation (4.10).

The r.h.s. of equation (4.10) was calculated using table (4.1) for each species and was compared with the l.h.s. as given by the table above. Δ denotes the difference between the l.h.s and r.h.s of equation (4.10) for n=1, and σ is the standard deviation for $(3/2)\lambda_1 - \lambda_2$ calculated by the "propagation formula"

It can be observed that for n = 2 there is no consistency between the l.h.s. and r.h.s. of equation (4.10) for any species. In the n = 1 case, there is no consistency for each of the species Ru, Ir, and Pt. For Hf the situation is indecisive. Surprisingly, however, there seems good agreement between the two sides of equation (4.10) for W and Mo.

4.4.3 Standard image-hump formalisms - field comparisons.

A second consistency test can be based on equation (4.8). This can be used to deduce a predicted evaporation field value from the experimental data concerning each of the six species, for different values of n.

The derived evaporation field values can then be compared with

the observed field values obtained experimentally by Tsong (1978). Table (4.3) shows the comparison between two field values for each species.

TABLE (4.3)

Derived evaporation fields F using the data from table (4.1) for n=1, 2. The r.h.s of equation (4.8) is denoted by K´. The last column gives the experimental evaporation fields F^{obs} (cf. Tsong 1978) at liquid nitrogen temperature.

Species	K´/eV	F_1^e (V/nm)	F_2^e (V/nm)	F^{obs}(V/nm)
Mo	12.8± 3.1	113.5± 55.0	14.2± 6.9	46
Ru	3.0± 2.1	6.3± 9.0	0.8± 1.1	42
Hf	6.2± 3.2	26.7± 27.2	3.3± 3.4	40
W	15.8± 1.0	173.4± 21.7	21.7± 2.7	55
Ir	3.1± 1.2	6.7± 5.0	0.8± 0.6	52
Pt	2.95± 1.6	6.0± 6.6	0.75± 0.8	48

(The error limits have been calculated using the propagation formula)

Again, it can be observed from table (4.3) that, for n=2, derived

evaporation field values and observed fields are not in agreement. In the n=1 case, for Ru, Ir and Pt we may conclude that derived and observed field values are not compatible in spite of error limits that are large in comparison with the derived value, and for W the incompatibility is evident. However, for Mo and Hf no conclusion is possible, when the error limits are taken into account.

4.4.4 Conclusion.

The general impression to be drawn from these tests is one of inconsistency. We therefore conclude that, in general, the simple image-hump formalisms cannot account for the experimental values of partial energies. Hence, it follows that either the Mueller mechanism is not operating, or that these simple image-hump formalisms do not properly represent the Mueller mechanism, or both.

If we assume that the simple image-hump formalisms do not properly represent the Mueller mechanism, then we have to find a remedy for the supposed invalidity of the simple formalisms.

4.5 An Extended image-hump formalism.

The analyses in the previous section have been carried out without including any term relating to the repulsive ion-metal interaction term that must be physically present. The standard image-hump formalism can be extended to include the repulsive term and then be used to investigate the compatibility of the theory with the experimental data.

4.5.1. Theoretical analysis.

In an extended formalism, the potential energy of an n-fold ion at a distance x from the emitter's electrical surface is given in the full form (cf. equation 2.11):

$$U_n(x, F) = (H_n - n\phi^E) - neF^o x - n^2e^2/16\pi\varepsilon_o x + G/x^t - (1/2)\, c_n F^2 \qquad (4.12)$$

where the symbols have their usual meanings.

For notational simplicity we here denote the distance of the Schottky hump from the emitter's electrical surface by R. This distance R is associated with the condition (cf. equation 2.20):

$$\partial U_n / \partial x \Big|_R = - neFR + n^2 e^2/16\pi\varepsilon_o R^2 + tG/R^{(t+1)} = 0 \qquad (4.13)$$

For a given value of F, there can be two solutions for R: the Schottky-hump position corresponds to the larger of these. Then for an atom, the field-evaporation activation energy at position R is given by:

$$Q_n(F) = (\Lambda^0 + H_n - n\phi^E) - neFR - n^2e^2/16\pi\varepsilon_o R + G/R^t + (1/2)(c_\alpha - c_n)F^2 \qquad (4.14)$$

As in equation (2.38), the partial energies λ_1 and λ_2 are given approximately by:

$$\lambda_1 = -F\, dQ/dF$$
$$\lambda_2 = -F^2\, d^2Q/dF^2 \qquad (4.15)$$

Now from equation (4.14) we obtain:

$$dQ/dF = -neR + dR/dF \left(- neF + n^2e^2/16\pi\varepsilon_0 R^2 - tG/R^t \right) + (c_\alpha - c_n)F \qquad (4.16)$$

However, the term in brackets in equation (4.16) vanishes, due the condition given by equation (4.13); thus we obtain:

$$dQ/dF = - neR + (c_\alpha - c_n)F \qquad (4.17)$$

$$d^2Q/dF^2 = -nedR/dF + (c_\alpha - c_n) \qquad (4.18)$$

Hence

$$\lambda_1 = neFR - (c_\alpha - c_n)F^2 \qquad (4.19)$$

Equation (4.13) defines the relationship between R and F; it follows that:

$$dR/dF = neR^2/ \{(t - 1)n^2e^2/16\pi\varepsilon_0 R - (t + 1)\ neFR \} \qquad (4.20)$$

By using equations (4.15)., (4.18) and (4.20), we obtain:

$$\lambda_2 = - (neFR)^2/\{(t + 1)neFR - (t - 1)n^2e^2/16\pi\varepsilon_0 R\} - (c_\alpha - c_n)F^2 \qquad (4.21)$$

Finally, using equations (4.13) and (4.14) and eliminating the repulsive term, we obtain:

$$(\Lambda^0 + H_n - n\phi^E) - Q = (t+1)/(t)\ neFR + \{(t-1)/t\}\ n^2e^2/16\pi\varepsilon_0 R - (1/2)(c_\alpha - c_n)F^2 \qquad (4.22).$$

In equations (4.19), (4.21) and (4.22), the left hand sides involve parameters whose values are either known independently, or are given from field sensitivity experiments. The right hand sides of the equations contain three "unknown" terms - electrostatic (v), correlation (w) and F^2-term (p), given by:

$$v=neFR \qquad (4.23)$$

$$w=n^2e^2/16\pi\varepsilon_0 R \qquad (4.24)$$

$$p=1/2(c_\alpha - c_n)F^2 \qquad (4.25)$$

If parameters B and C are defined by the equations:

$$B=\lambda_1 - \lambda_2 \qquad (4.26)$$

$$C=\{\Lambda^0 + H_n - n\phi^E - Q_n(F)\} - \lambda_1 \qquad (4.27)$$

then the quadratic equation for v is given by:

$$(3t+6)v^2-(tC+(3t+4)B)v+tBC=0 \qquad (4.28)$$

B and C are "known", and t can be assumed, so v can be obtained.

For a real solution of this equation we obtain w,R, and F from:

$$w=\{tC-(t+2)v\}/2(t-1) \tag{4.29}$$

$$R=(n^2e^2/16\pi\varepsilon_0)\ w^{-1} \tag{4.30}$$

$$F=(16\pi\varepsilon_0/n^3e^3)vw \tag{4.31}$$

Equation (4.28) will have either no real solution or two real solutions. If the former then the implication is that no Schottky hump exists, and hence the data are incompatible with the Mueller mechanism. If the latter then two sets of numerical values will be obtained from equations (4.30) and (4.31); R and F are a set corresponding to the larger value of R. (The other set corresponds mathematically to the alignment of the bottom of the ionic potential well, and has no physical significance here.)

For a real set of F and R, we may obtain a value for (tG) from equation(4.13). Then the ionic bonding distance a_n can be obtained from the equation:

$$dU_n/dx\ \Big|_{x\,=\,a_n}=(n^2e^2/16\pi\varepsilon_0a_n^{\,2})-\{tG/a_n^{\,(t+1)}\}=0 \tag{4.32}$$

From which it follows that:

$$a_n\ =\ (16\pi\varepsilon_0tG\ /\ n^2e^2)^{\{1/(t-1)\}} \tag{4.33}$$

It should be noted that the validity of the whole analysis depends on the field dependence of binding energy being as given by equation (2.7).

4.5.2 Comparison between derived and observed evaporation fields.

In this section, we shall use Tsong's field sensitivity data converted to partial energies to derive numerical values of the Schottky distance (R), the ionic bonding distance (a_n) and the evaporation fields via the above formalism, and compare the derived evaporation field values, for the six species, with the observed ones as given in Table (4.1).

Using λ_1 and λ_2 values from table (4.1) the values of F, R and a_n for the six species, Mo, Ru, Hf, W, Ir and Pt have been calculated from equations (4.30), (4.31) and (4.32). The charge states used are n= 1,2 and 3, and for each charge state the t-values used are 6, 9, 12 and 15. For each charge state and t-value the calculations have been carried out for all four combinations of the partial energy values, namely: $\mu_1 \pm \sigma(\mu_1)$, $\mu_2 \pm \sigma(\mu_2)$,(where $\sigma(\mu_1)$ and $\sigma(\mu_2)$ are the relevant standard deviations), as well as for the combination μ_1, μ_2 . In all cases $Q_n(F)$ has been taken as 0.2 eV.

The results are summarised in table (4.4). In the columns giving the derived values of F^o, R and a_n, the first figure corresponds to taking t=12 and the partial energies equal to the best estimates, and the figures in brackets indicate the range of results, derived from all combinations of parameter values.

TABLE (4.4)

R, F and a_n values, as derived using the extended image-hump formalism.

Species	F^{o}(V/nm)	R (pm)	a_n(pm)	F (V/nm) Observed	ρ_o(pm)
Mo^{+}	-	-	-	43	136
Mo^{++}	-	-	-	43	136
Mo^{+++}	80 (73-81)	100 (87-101)	88 (75-91)	43	136
Ru^{+}	89 (85-92)	54 (49-56)	48 (41-50)	42	133
Ru^{++}	64 (60-65)	93 (83-94)	81 (69-83)	42	133
Ru^{+++}	86 (82-87)	98 (89-100)	85 (73-88)	42	133
Hf^{+}	-	-	-	40	157
Hf^{++}	59 (58-60)	94 (86-98)	84 (71-87)	40	157
Hf^{+++}	69 (65-70)	109 (98-111)	96 (82-99)	40	157

TABLE (4.4) Continued

R, F and a_n values, as derived using the extended image-hump formalism.

Species	F^o (V/nm)	R (pm)	a_n (pm)	F (V/nm)	ρ_o (pm)
				Observed	
W^+	160 (146-164)	65 (63-72)	64 (40-72)	57	137
W^{++}	-	-	-	57	137
W^{+++}	81 (73-83)	98 (85-101)	87 (74-90)	57	137
Ir^+	117 (113-118)	47 (43-49)	42 (36-43)	46	135
Ir^{++}	68 (64-70)	90 (81-92)	78 (67-81)	46	135
Ir^{+++}	80 (77-82)	102 (92-104)	88 (76-92)	46	135
Pt^+	91 (87-95)	54 (49-56)	47 (40-49)	44	139
Pt^{++}	71 (67-72)	88 (79-90)	77 (66-79)	44	139
Pt^{+++}	86 (82-87)	98 (89-101)	86 (73-89)	44	139

These results may be compared with the "observed" evaporation fields as given by Tsong (1978b) and listed in table (4.3), and the neutral-atom radius ρ_0. In no case is there compatibility between the derived values (using the extended image-hump formalism) and the observed field-value and known ρ_0-value, even when allowance is made for a 20% error in F^o and for the expectation that a_n may be slightly less than ρ_0.

4.6 A more general image-hump formalism.

In the previous analyses, specific algebraic forms were used for all elements of the ion-potential energy. It is also possible to derive an expression for λ_1 by using a version of the extended formalism where the repulsive and attractive ion interaction terms are not given any specific mathematical forms, and in this case, we shall describe the formalism as the "general image-hump formalism". In appropriate cases, where relevant experimental data exist (as they do for Rh^+), theoretical/experimental comparison can take place.

4.6.1 Theoretical analysis.

In the general image-hump formalism let $U_n(x,0)$ be the ionic potential energy, in zero field, that contains the repulsive and attractive ion interaction terms; let $U_n(x, F)$ be the same in field F and R be the distance of Schottky hump from metal's electrical surface. Then $U_n(x, F)$ is given by:

$$U_n(x,F) = U_n(x,0) - neFx - (1/2)c_n F^2 \qquad (4.34)$$

At the Schottky hump, $\{dU_n(x,F)/dx\}\Big|_R = 0$. i.e.

$$\{dU_n(x,0)/dx - neF\}\Big|_R = 0 \qquad (4.35)$$

Now by definition, the activation energy is given by:

$$Q_n = U_n(R, F) + \Lambda^0 + (\tfrac{1}{2})\, c_\alpha F^2 \qquad (4.36)$$

Therefore:

$$dQ_n/dF = (\partial Q_n/\partial F)_R + (\partial Q_n/\partial R)_F \cdot dR/dF$$

$$= - neR + (c_\alpha - c_n)F + (dU_n(R,0)/dR - neF)\, dR/dF \qquad (4.37)$$

$$\text{But } dU_n(R,0)/dR = dU_n(x,0)/dx\Big|_R \qquad (4.38)$$

Therefore, using equation (4.35):

$$dQ_n/dF = -neR + (c_\alpha - c_n)F \qquad (4.39)$$

and

$$\lambda_1 = -F\, dQ_n/dF = + neFR - (c_\alpha - c_n)F^2 \qquad (4.40)$$

It can be seen from equation (4.40) that the first partial energy expression is independent of $U_n(x,0)$ terms, and that this equation or equation (4.39) is a new form of self-consistency test.

4.6.2 Application to data for rhodium ions (Rh^+).

Use of equation (4.39) requires that we have a reliable independent estimate of the F^2-term. The only material for which this is true is rhodium.

Ernst's (1979) activation energy data for rhodium have been shown in Fig. (3.2). From this, at F = 30 V/nm , the value of $dQ_n/dF = -0.08 \pm 0.01$ eV.nm/V.

So the F-term in equation (4.39) is 0.027 ± 0.009 eV V^{-1}nm. Ernst has determined R to be 0.21 ± 0.05 nm (see Forbes et al. 1984). It follows that the r.h.s. of equation (4.39) is equal to 0.17 ± 0.05 eV V^{-1}nm.

The agreement between the two sides is poor, but the difference is not infact statistically significant. Clearly, this method requires us to have an accurate independent estimate of R which is difficult to achieve.

4.7 Discussion

From the comparisons that have been made above, we may conclude with reasonable confidence that Tsong's (1978b) data concerning evaporation-flux field sensitivity are compatible neither with the conventional image-hump formalisms (both BIH and SIH) used to analyse the Mueller mechanism of field evaporation, nor with the extended image-hump formalism developed here.

This result has been proved only in the six cases for which data have been available. However, from this result we may presume that these image-hump formalisms are not generally appropriate for metal field evaporation.

The inability of simple image-hump formalisms (BIH & SIH) to explain field sensitivity data suggests that the use of such formalisms to predict evaporation fields by setting the activation energy (cf. equation (2.24)) to zero is inappropriate, although at times this procedure leads to reasonable agreement with experiment. (But evaporation fields can be of course predicted from energetics alone; see Forbes 1982a).

We have already seen that the simple image-hump formalisms are manifestly incomplete, for they do not include any term relating to the repulsive ion-metal interaction that must physically be present. To avoid this inconsistency we included a repulsive term; but the corresponding results still tend to show that the field sensitivity data are incompatible with the Mueller mechanism.

It might of course be argued that the inconsistencies result from the neglect of field dependence in the pre-exponential and/or by not taking a more sophisticated approach to the calculation of the correlation interaction. There is infact, some recent evidence, provided by Kellogg (1984), that field dependence in $n_{hr}A$ exists for tungsten at evaporation fields below 50V/nm.

However, rather than explore these difficulties here we defer discussion until chapter 5 on the grounds that chapter 5 discusses forms of test in which the difficulty concerning the possible field dependency in $n_{hr}A$ does not arise.

Let us now summarise the position. In this chapter we have used experimental data and classical theoretical analysis to demonstrate that none of the conventional classical image-hump formalisms can provide a generally consistent interpretation of the experimental data. Behind all this analysis, however, has usually been the implicit assumption that a Schottky image-hump

exists in the ion potential energy curve; which may not be true. It is also the case that field-sensitivity measurements are difficult to make, and the resulting partial-energy values are of limited accuracy, so there is often some degree of uncertainity in individual cases. It thus seemed useful to look more closely at the question of whether the image-hump actually exists. This is the theme of chapter 5.

CHAPTER 5

EVAPORATION FIELDS AND THE EXTENDED IMAGE-HUMP FORMALISM.

5.1 Introduction.

Quite apart from the inconsistencies already demonstrated, there are two main objections regarding the simple image-hump formalisms:

1. The distance of the Schottky hump from the electrical surface, as calculated by the simple formalisms using observed evaporation fields, is too small to be plausible (only about 0.12 nm for tungsten).

2. If repulsive forces between ion-core electrons and the metal's substrate electrons were taken into account, then it would be doubtful if any Schottky hump actually exists in the ion potential energy curve (eg. Brandon 1964).

In this chapter, we put actual numbers onto the second of the above objections. By choosing the mathematical form as given in section (2.5) for the repulsive potential, it is possible to make numerical estimates for the field F_n^{HD} at which the Schottky hump disappears. The values of this field F_n^{HD} can then be compared with: (a) the evaporation fields as predicted by the simple image-hump formalisms; and (b) the observed evaporation fields.

This should provide a test, firstly of the theoretical self-consistency of the simple formalisms, secondly of the plausibility of the Mueller mechanism as the physical process by

which field evaporation might occur.

5.2 Theoretical analysis.

5.2.1 The simple formalisms.

For comparison purposes, we first need to look again at the conventional formalisms. As before, we use a zero-Q definition of evaporation field F_n^e for an n-fold charged ion. In the basic formalism, F_n^e is given by Mueller's formula, equation (3.1), namely:

$$F_n^e = (4\pi\varepsilon_0/n^3e^3)(\Lambda^0 + H_n - n\phi^E)^2 \qquad (5.1)$$

In the standard formalism we include the F^2-term and use expression (2.24) for $Q_n(F)$; this means that a self-consistent solution must be found to the equation:

$$(\Lambda^0 + H_n - n\phi^E) = (n^3e^3 . F_n^e /4\pi\varepsilon_0)^{1/2} - (1/2)(c_\alpha - c_n)(F_n^e)^2 \qquad (5.2)$$

As long as the F^2-term is sufficiently small, this equation has a solution that leads to a value of F_n^e somewhat greater than would be obtained from equation(5.1).

Various authors, including Tsong (1978a), have tabulated F_n^e for various metals using one or other of the equations. Our results for the calculation of F_n^e, for a number of metals, using equation (5.1), are tabulated in table (5.2); table (5.1) shows the basic parameters that are used in the calculation.

TABLE (5.1)

The values of Λ^0, ϕ^E, I_1, I_2, I_3, H_1, H_2 , H_3, where values of zero-field binding energy Λ^0, local work-function ϕ^E, ionization energy I_n, and the quantiity $H_n = \sum_{r=1}^{n} I_r$, n=1, 2, 3

Species	Λ^0	ϕ^E	I_1	I_2	I_3	H_1	H_2	H_3
	eV	eV	eV	eV	eV	eV	eV	eV
W	8.67	4.52	7.98	17.70	24.00	7.98	25.68	49.68
Ta	8.089	4.2	7.89	16.00	22.00	7.89	23.89	45.89
Re	8.10	5.1	7.88	17.00	26.00	7.88	24.88	50.88
Ir	6.50	5.00	9.00	17.00	27.00	9.00	26.00	53.00
Hf	6.35	3.50	7.00	15.00	23.3	7.00	22.00	45.30
Mo	6.15	4.30	7.10	16.15	27.13	7.10	23.25	50.38
Pt	5.62	5.32	9.00	18.56	28.00	9.00	27.56	55.56
Ru	5.52	4.52	7.36	16.76	28.47	7.36	24.12	52.58
Au	3.78	4.30	9.23	20.50	30.00	9.23	29.73	59.73

TABLE (5.1) Continued

Species	Λ^0 eV	Φ^E eV	I_1 eV	I_2 eV	I_3 eV	H_1 eV	H_2 eV	H_3 eV
Si	4.90	4.80	8.15	16.34	33.46	8.15	24.49	57.95
Rh	5.77	4.80	7.46	18.07	31.05	7.46	25.53	56.58
Co	4.40	4.40	7.86	17.05	33.49	7.86	24.91	58.10
Fe	4.13	4.17	7.87	16.18	30.64	7.87	24.05	54.69
Ti	4.85	4.17	6.82	13.57	27.47	6.82	20.39	47.86
Ni	4.36	5.01	7.63	18.15	35.16	7.63	25.78	60.94
Ge	3.47	4.80	7.88	15.93	34.21	7.88	23.81	58.02
La	4.49	3.30	5.58	11.06	19.17	5.58	16.64	35.81
Cu	3.50	4.55	7.72	20.29	36.83	7.72	28.01	64.81
Cr	4.16	4.45	6.76	16.49	30.95	6.76	23.25	54.20
Sn	3.17	4.39	7.34	14.63	30.49	7.34	21.97	52.46
Ag	2.90	4.70	7.57	21.48	34.82	7.57	29.05	63.87
Al	3.30	4.20	5.98	18.82	28.44	5.98	24.80	53.24
Ga	2.78	4.10	5.999	20.610	30.710	5.999	26.509	57.219
Os	6.95	4.55	8,70	17.00	25.00	8.70	25.70	50.70
Cs	0.691	2.14	3.894	25.100	35.00	3.894	28.994	63.994

TABLE (5.2)

The values of K_n and F_n^e, where n=1, 2, 3; $F_n^e = (4\pi\varepsilon_0/n^3e^3)(K_n)^2$, and $K_n = \Lambda^0 + H_n - n\phi^E$. K_n is in eV, and F_n^e is in V/nm.

Species	K_1	K_2	K_3	F_1^e	F_2^e	F_3^e	F^o (obs.)	Ref.
W	12.13	25.31	44.79	102.11	55.57	51.51	57	T78a
Ta	11.78	23.58	41.38	96.00	48.00	44.00	43	N66
Re	10.88	22.78	43.68	82.00	45.00	49.00	45	N66
Ir	10.50	22.50	44.50	76.51	43.92	50.90	46	N66
Hf	9.85	21.25	41.05	67.00	39.00	43.00	40	T78b
Mo	8.95	20.80	43.63	55.57	37.53	48.93	43	N66
Pt	9.30	22.54	45.22	60.02	44.07	52.56	44	N66
Ru	8.36	20.60	44.54	48.50	36.81	50.99	42	T78b
Au	8.70	24.90	50.60	53.00	54.00	66.00	35	T78a
Si	8.25	19.79	48.45	47.24	33.98	60.34	10	BF63
Rh	8.43	21.70	47.95	49.32	40.85	59.10	41	N66
Co	7.86	20.51	49.30	42.88	36.49	62.47	35	N66

TABLE (5.2) Continued

Species	K_1	K_2	K_3	F_1^e	F_2^e	F_3^e	F^o (obs.)	Ref.
Fe	7.83	19.84	46.31	42.55	34.15	55.12	34	N66
Ti	7.50	16.90	40.20	39.04	24.78	41.54	25	T78a
Ni	6.98	20.12	50.27	33.51	35.12	64.96	35	T78a
Ge	7.05	18.18	47.59	34.49	28.67	58.21	20	EB75
La	6.97	14.73	30.60	34.00	19.00	24.00	-	-
Cu	6.67	22.41	54.66	30.88	43.57	76.80	24	N66
Cr	6.47	18.51	45.01	29.05	29.72	52.07	-	-
Sn	6.12	16.36	42.46	25.99	23.22	46.34	21	WKN80
Ag	5.77	22.55	52.67	23.11	44.11	71.31	20	N66
Al	5.08	19.70	43.94	17.91	33.67	49.63	27	BWTMS77
Ga	4.679	21.089	47.699	15.00	39.00	59.00	15	WKN80
Os	11.10	23.5	44.00	85.51	48.11	49.76	-	-

According to Brandon's criterion, it is assumed that the evaporation field is the smallest of these calculated for different values of n. Table (5.2) also shows the comparison between the observed evaporation fields (collated from sources as shown by the abbreviated references) and the calculated evaporation fields. As noted in chapter 3, the calculated fields agree with observed evporation fields to within a factor of 1.5, or often better; the agreement has sometimes been held to justify the simple formalisms.

As already stated, there is a serious objection to the simple formalisms, namely the neglect of the repulsive term. In reality, the shape of the ion potential energy curve, as a function of field, is shown in Figs. (5.1).

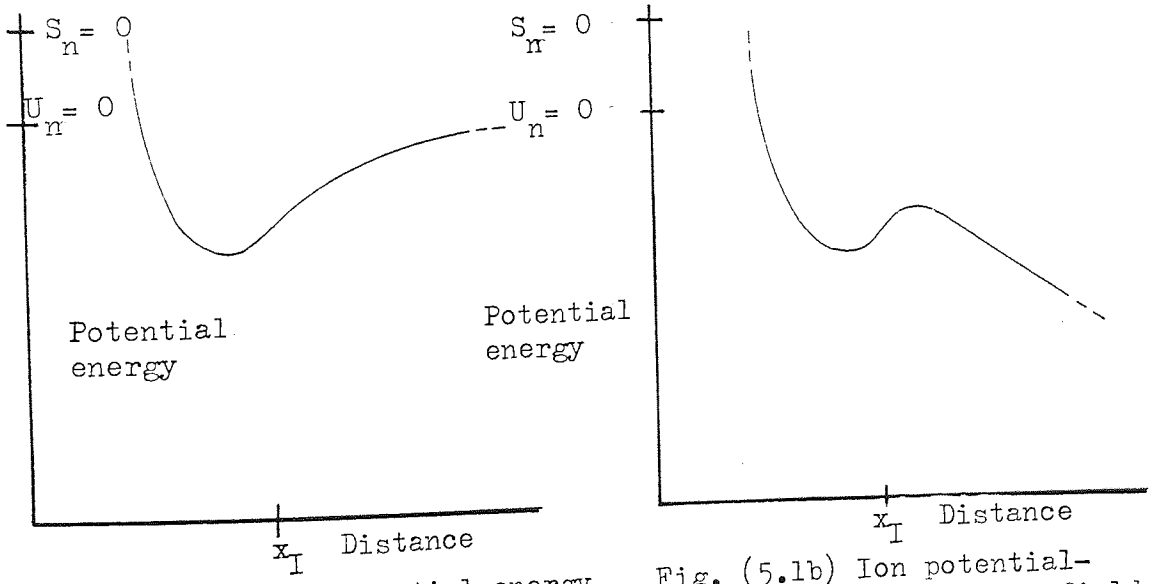

Fig. (5.1a) Ion potential-energy curve at zero field

Fig. (5.1b) Ion potential-energy curve at low fields where a hump exists

Figs. (5.1) $S_n(x,F)$ and $U_n(x,F)$ as functions of field.

At zero field, the shape is that of an ionic bonding potential (Fig. 5.1a). At low fields, a Schottky hump develops (Fig.5.1b). As field increases there comes a critical situation, at some field F_n^{HD} (Fig.5.1c) at which the hump "just disappears", where the curve is flat at the point of inflexion. Above the critical field (Fig.5.1d), there is no hump at all in this curve.

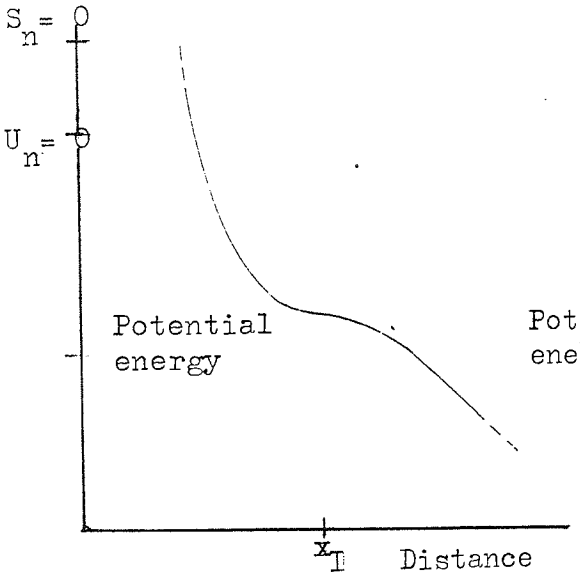

Fig. (5.1c) Ion potential-energy curve at a higher field where the hump has just disappeared

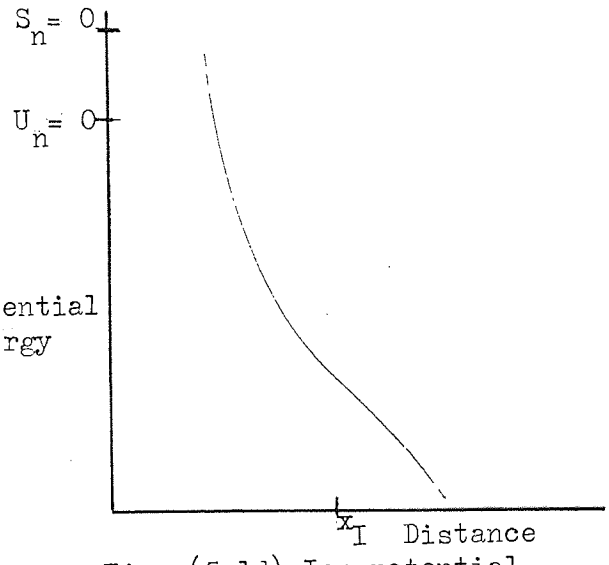

Fig. (5.1d) Ion potential-energy curve at a much higher field where no hump exists

The 'full' classical expression for the 'variable' part of the ion potential energy is given by equation (2.12), namely:

$$S_n(x,F) = - neFx - n^2e^2/16\pi\varepsilon_0 x - (1/2)c_n F^2 + G/x^t \qquad (5.3)$$

If there is no Schottky hump in the potential curve as given by this equation, then it is not mathematically legitimate to apply the hump-disappearance condition (equation 2.20), namely:

$$dS_n/dx \Big|_{x_n^{Sh}} = 0 \qquad (5.4)$$

to the abbreviated version of equation(5.3), namely:

$$S_n(x,F) = -neFx - n^2e^2/16\pi\varepsilon_0 x - (1/2)\alpha_n F^2 \qquad (5.5)$$

in which the repulsive term does not appear.

At high fields, above F_n^{HD}, $S_n(x,F)$ as given by equation (5.5) is unphysical, and the maximum in it is a mathematical artefact. Consequently, it is unphysical to put the level of this artefact maxiumum equal to the bonding-state level, as the simple formalisms do.

5.2.2 The extended formalism.

In the extended formalism, in the absence of a field, the standard potential energy of an n-fold ion is given by:

$$U_n(x,0) = (H_n - n\phi^E) - \sigma/x + G/x^t \qquad (5.6)$$

where $\sigma = n^2e^2/16\pi\varepsilon_0$

The potential has the shape as in Fig. (5.1a). If the potential minimum is at distance a_n from the metal's electrical surface, then:

$$\partial U_n(x,0)/\partial x \Big|_{x = a_m} = \sigma/a_n^2 - tG/a_n^{t+1} = 0 \qquad (5.7)$$

$$G = (\sigma/t)\ a_n^{t-1} \tag{5.8}$$

The point of inflexion x_I , measured from the metal's electrical surface, is given by the condition:

$$\partial^2 U_n(x,0)/\partial x^2 \Big|_{x_I} = 0 \tag{5.9}$$

If we substitute equation (5.8) in equation (5.6), then at the point of inflexion at a distance x_I from the metal's electrical surface we obtain:

$$\partial^2 U_n(x)\ /\partial x^2 = \sigma\{(t+1)a_n^{(t-1)}/x_I^{(t+2)} - (2/x_I^3)\} = 0 \tag{5.10}$$

therefore,

$$x_I = \{(t+1)/2\}^{1/(t-1)} \cdot a_n \tag{5.11}$$

$$\text{Let} \quad \gamma = \{(t+1)/2\}^{1/(t-1)} \tag{5.12}$$

$$\text{then} \quad x_I = \gamma . a_n \tag{5.13}$$

Note that the value of γ depends only on the exponent assumed for the repulsive power law, and not on the charge number n, nor the field F.

Using equations (2.13) and (5.8), in the presence of a field F, we obtain the ion potential energy as:

$$U_n(x,F) = (H_n - n\phi E) - neFx + \sigma\{(a_n^{(t-1)}/tx^t - (1/x)\} \tag{5.14}$$

At the hump disappearance field F_n^{HD}, the potential curve becomes horizontal at the point of inflexion, so:

$$\partial U_n/\partial x \Big|_{x_I} = \sigma[-\{a_n^{(t-1)}\}/x_I^{(t+1)} + (1/x_I^2)] - neF_n^{HD} = 0 \qquad (5.15)$$

Substituting for σ and using equation (5.13) in equation (5.15), we may solve for F_n^{HD} producing:

$$F_n^{HD} = \{1/\gamma^2 - 1/\gamma^{(t+1)}\}.(n.e/16\pi\varepsilon_o a_n^2) \qquad (5.16)$$

which can be written as:

$$F_n^{HD} = \Gamma\,(n.e/16\pi\varepsilon_o a_n^2) \qquad (5.17)$$

where $\Gamma = \{1/\gamma^2 - 1/\gamma^{(t+1)}\}$ (5.18)

Values of Γ and γ, for values of t lying between 6 and 15 are shown in table (5.3).

Substituting the values of x_I and F_n in equation (5.14) we can obtain an absolute level of the standard ion potential energy U_n^* at the point of inflexion when the hump "just disappears". Then we obtain:

$$U_n^* = (H_n - n\Phi^E) + S_n^* \qquad (5.19)$$

where $S_n^* = \{(t+1)/t\gamma^t - 2/\gamma\}(n^2e^2/16\pi\varepsilon_o a_n)$ (5.20)

or

$$S_n^* = \theta \cdot (n^2 e^2 / 16\pi\varepsilon_0 a_n) \qquad (5.21)$$

where $\theta = \{(t+1)/t\gamma^t - 2/\gamma\}$ (5.22)

Table(5.3) also contains values of θ for values of t from 6 to 15.

TABLE (5.3)

Values of γ, T and θ for values of t from 6 to 15

t	γ	T	θ
6	1.285	0.433	-1.297
7	1.260	0.472	-1.361
8	1.290	0.506	-1.412
9	1.223	0.535	-1.451
10	1.209	0.560	-1.489
11	1.196	0.582	-1.520
12	1.186	0.602	-1.546
13	1.176	0.619	-1.570
14	1.168	0.636	-1.591
15	1.160	0.650	-1.609

Equation (5.21) has been approximated by excluding the F^2-term. If this is included, then S_n^* is given by:

$$S_n^* = \theta(n^2 e^2 / 16\pi\varepsilon_0 a_n) - (1/2)c_n (F_n)^2 \qquad (5.23)$$

5.2.3 Choice of repulsive power-law.

To help with the choice of the repulsive exponent t, we have used equations (5.13) and (5.17) to calculate x_I and F_n^{HD} values for tungsten for t-values from 6 to 15, for each value of n=1, 2, 3.

An a_n -value corresponding to the atomic radius of tungsten, namely 0.137nm, has been used. The resulting values of x_I and F_n^{HD} are shown in table(5.4).

TABLE (5.4)

The values of x_I, F_1^{HD}, F_2^{HD} and F_3^{HD} for tungsten for t-values from 6 to 15.

t	x_I(nm)	F_1^{HD}(V/nm)	F_2^{HD}(V/nm)	F_3^{HD}(V/nm)
6	0.176	8.33	16.66	24.99
7	0.172	9.20	18.40	27.60
8	0.177	9.74	19.48	29.22
9	0.167	10.29	20.58	30.87
10	0.165	10.78	21.56	32.34
11	0.163	11.20	22.40	33.60
12	0.162	11.58	23.16	34.74
13	0.161	11.91	23.82	35.73
14	0.160	12.24	24.48	36.72
15	0.158	12.51	25.02	37.53

From table (5.4), we can observe that the values of x_I and F_n^{HD} are not unduly sensitive to the values of 't'. Nevertheless, a choice has to be made here as to the value of the repulsive exponent 't'. From now on we shall present results only for the cases when t= 9 and 12.

5.2.4 Evaluation of F_n^{HD} values

From equation (5.17), it is possible to evaluate approximate values of F_n^{HD} for various species at different charged states.

Our F_n^{HD} expression involves the distance (a_n) of the ionic bonding-point from the electrical surface, in zero field. There are difficulties in choosing a value of a_n, because, as already indicated in chapter 2, the position of electrical surface is not well defined and also the effective ionic radii are not well defined. However, the assumption that the true value of a_n is somewhat greater than the radius of the external ion finds support by both the theoretical work of Lang and Kohn (1973) and the experimental work of Culbertson et al. (1979). As the first approximation, we assume that a_n is equal to the neutral atomic radius ρ_0 of the species. This assumption was also considered by Tsong and Mueller (1969). We shall look more closely at this assumption in section (5.5).

Tables(5.5) and (5.6) show the values of F_n^{HD} (n=1, 2, 3), for t=9 and 12 respectively, for most of the elements commonly employed in the conventional field ion techniques. The atomic radii have been stated to the nearest 0.0005 nm.

TABLE (5.5)

Values of x_I, F_1^{HD}, F_2^{HD}, F_3^{HD}, and atomic radii for t=9, for various species.

Species	ρ_0/nm	x_I/nm	F_1^{HD}(V/nm)	F_2^{HD}(V/nm)	F_3^{HD}(V/nm)
W	0.137	0.167	10.26	20.52	30.78
Ta	0.143	0.174	9.41	18.82	28.24
Re	0.137	0.167	10.26	20.52	30.78
Ir	0.1355	0.165	10.49	20.98	31.47
Hf	0.1565	0.191	7.86	15.72	23.58
Mo	0.136	0.166	10.41	20.82	31.23
Pt	0.139	0.169	9.96	19.93	29.89
Ru	0.1325	0.162	10.97	21.94	32.91
Au	0.144	0.176	9.28	18.57	27.86
Si	0.1175	0.143	13.95	27.90	41.85
Rh	o.1345	0.164	10.64	21.19	31.93
Co	0.125	0.152	12.32	24.65	36.97
Fe	0.124	0.151	12.52	25.05	37.56
Ti	0.1445	0.176	9.22	18.44	27.66
Ni	0.1245	0.152	12.42	24.85	37.27
Ge	0.1225	0.149	12.83	25.66	38.50
La	0.1865	0.228	5.53	11.07	16.61
Cu	0.128	0.156	11.75	23.51	35.26
Cr	0.125	0.152	12.32	24.65	36.97
Sn	0.140	0.171	9.52	19.65	29.47
Ag	0.1445	0.176	9.22	18.44	27.67
Al	0.143	0.174	9.41	18.83	28.25
Ga	0.122	0.149	12.94	25.88	38.82

TABLE (5.6)

Values of x_I, F_1^{HD}, F_2^{HD} F_3^{HD}, and atomic radii for t=12, for various species.

Species	ρ/nm	x_I/nm	F_1^{HD}(V/nm)	F_2^{HD}(V/nm)	F_3^{HD}(V/nm)
W	0.137	0.162	11.54	23.09	34.64
Ta	0.143	0.169	10.59	21.19	31.79
Re	0.137	0.162	11.54	23.09	34.64
Ir	0.1355	0.160	11.80	23.60	35.41
Hf	0.1565	0.185	8.84	17.69	26.54
Mo	0.136	0.161	11.71	23.43	35.15
Pt	0.139	0.164	11.21	22.43	33.65
Ru	0.1325	0.157	12.34	27.68	37.03
Au	0.144	0.170	10.45	20.90	31.35
Si	0.1175	0.139	15.69	31.39	47.09
Rh	o.1345	0.159	11.97	25.95	35.93
Co	0.125	0.148	13.87	27.74	41.61
Fe	0.124	0.147	14.09	28.18	42.28
Ti	0.1445	0.171	10.37	20.75	31.13
Ni	0.1245	0.147	13.98	27.96	41.94
Ge	0.1225	0.145	14.44	28.88	43.32
La	0.1865	0.221	6.23	12.46	18.69
Cu	0.128	0.151	13.22	26.45	39.68
Cr	0.125	0.148	13.87	27.74	41.61
Sn	0.140	0.166	11.05	22.11	33.17
Ag	0.1445	0.171	10.37	20.75	31.13
Al	0.143	0.169	10.59	21.19	31.79
Ga	0.122	0.144	14.56	29.12	43.68

5.3 Comparison of F_n^e (BIH) and F_n^{HD}

We are now in a position to perform a self-consistency test of the simple formalisms. This we do graphically.

It can be seen from equation (5.17) that F_n^{HD} is a function of only a_n, for given values of n and t, so F_n^{HD} can be plotted against a_n. Figs. (5.2a, b, c) show the cases n = 1 to n = 3, respectively. In each case plots are shown for t = 9 and t = 12.

Values of F_n^e(BIH) for various species are tabulated in Table (5.2). A comparison with F_n^{HD} values is made in the following way:

We select the ρ_0 for the given species and plot the F_n^e(BIH) value for this species at ρ_0 value, as a small circle. Thus, if the circle lies above the continuous plot, then F_n^e (BIH) is greater than the corresponding F_n^{HD}, and vice-versa. This has been done for all species.

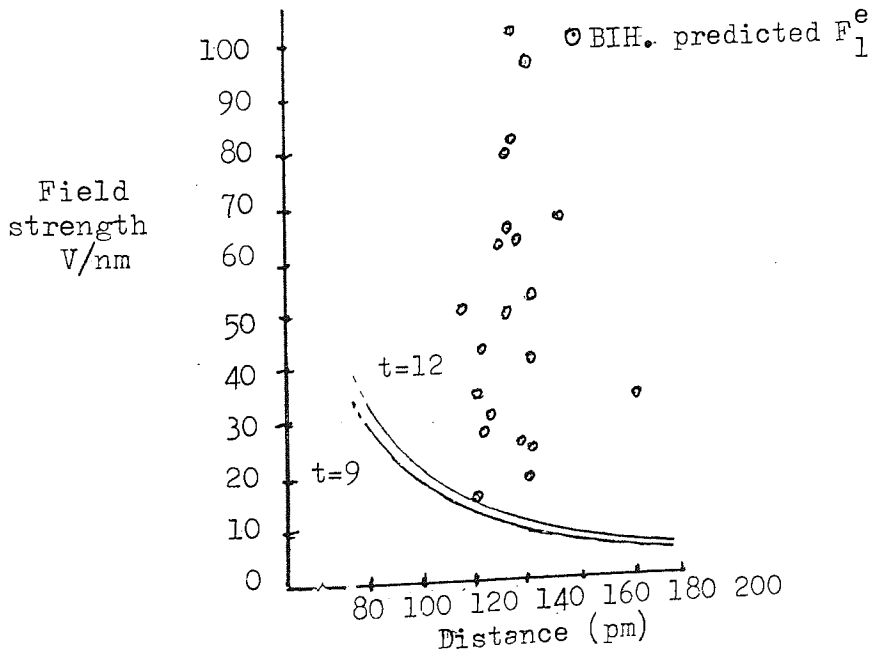

Fig. (5.2a) Comparison of F_1^{HD} with F_1^e

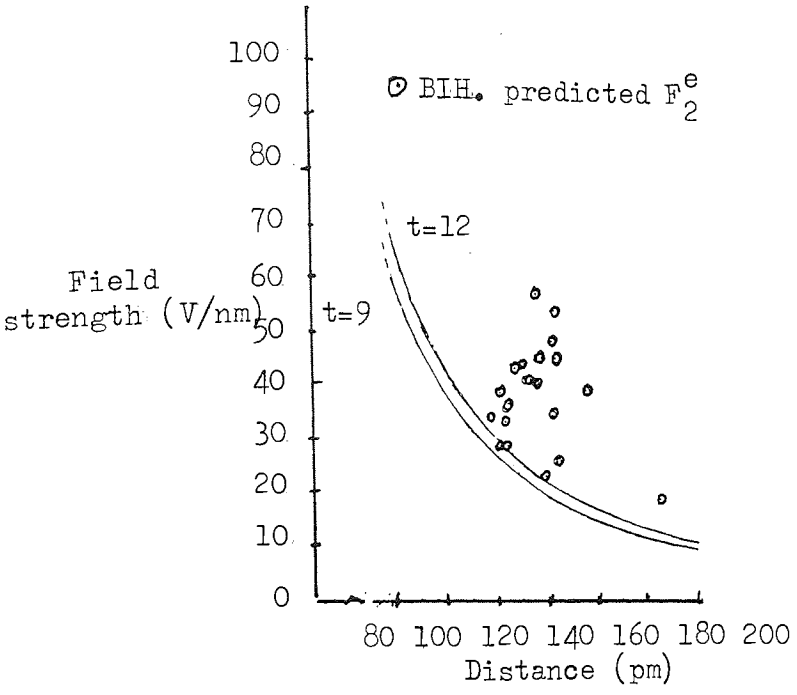

Fig. (5.2b) Comparison of F_2^{HD} with F_2^e

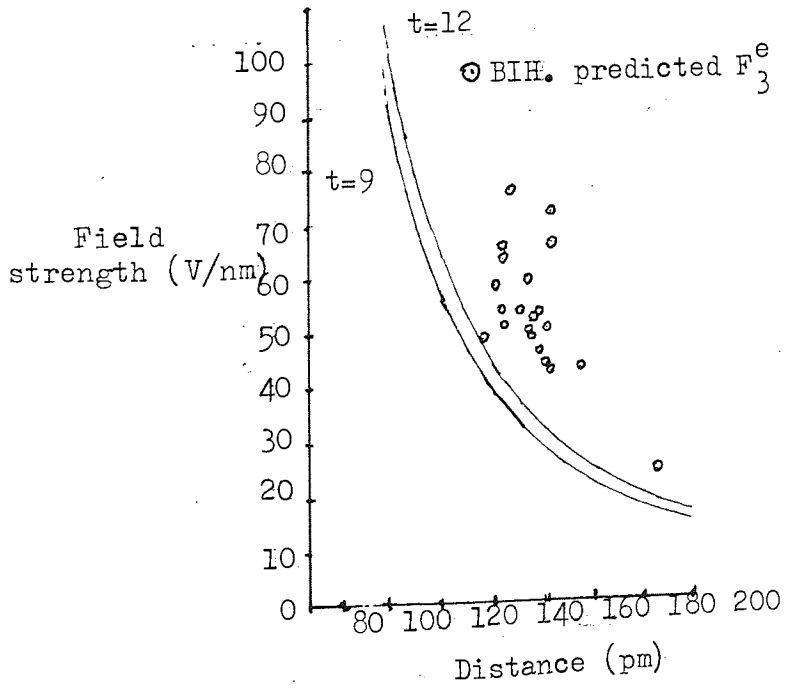

Fig. (5.2c) Comparison of F_3^{HD} with F_3^e

Inspection of Figs. (5.2a), (5.2b) and (5.2c) now shows that in nearly all cases the basic image-hump predicted value of F_n^e is greater than the field at which the hump disappears.

If the assumption that ρ_0 is a fair estimate of a_n is reasonable, then these findings give a clear indication that the basic formalism based on equation (5.2) is unphysical, certainly for most of the elements commonly employed in the field ion techniques.

Further, because the values of F_n^e predicted from equation (5.2) are expected to be higher than those predicted from equation (5.1), the addition of the F^2-term to the basic formalism will only make matters worse (i.e. it gives an evaporation field prediction even higher than the hump disappearance field).

These comparisons thus suggest that the simple formalisms that neglect the repulsive power interaction term are in most cases unphysical and cannot be applied to the metals typically employed in the low-temperature field-ion techniques.

5.4 Comparison of F_n^{HD} with observed evaporation fields

To infer that the Mueller mechanism cannot be operating in field evaporation it is necessary to make a comparison of observed evaporation fields with values of the field at which the Schottky hump disappears. If it can be shown that an observed evaporation field is greater than F_n^{HD}, and if our extended image hump formalism is realistic, then the Mueller mechanism cannot be operating for the species and charge state in question.

Table (5.2) shows the relevant observed evaporation field values (F^o) together with their sources in the literature. In

cases where different values are indicated in different sources, the lower value has been selected; and in cases where the variation of evaporation field with temperature is recorded the value corresponding to a temperature near 80 K has been taken.

With tin and gallium, the values taken correspond to the evaporation of an overlayer on a tungsten substrate; with aluminium, the value corresponds to evaporation near 55K; with silicon the value given is the lowest recorded for a doped specimen.

For the purpose of comparison with the observed evaporation fields we need F_n^{HD} against a_n curves only for the case when t=12, as this is a more demanding criterion than the case when t = 9. Fig.(5.3) shows the comparison. As before, there has been a problem over the lack of knowledge of the true values of a_n, and consequently the observed field values are plotted at the neutral-atom radius of the material in question.

Inspection of Fig.(5.3) shows that for most metals, the plotted points lie above the n = 2 curve; nearly all points lie above the n = 1 curve, but only about half the points lie above the n = 3 curve. However, the recent work on post-ionization, discussed in section (3.5), indicates that the low temperature escape charge-state is usually 1+ or 2+. So in reality it can be assumed that for all species well above the n = 2 curve, field evaporation cannot be taking place via the Mueller mechanism. But we need to examine the situation more closely for the species for which the F^o-plots lie below the n = 2 curve.

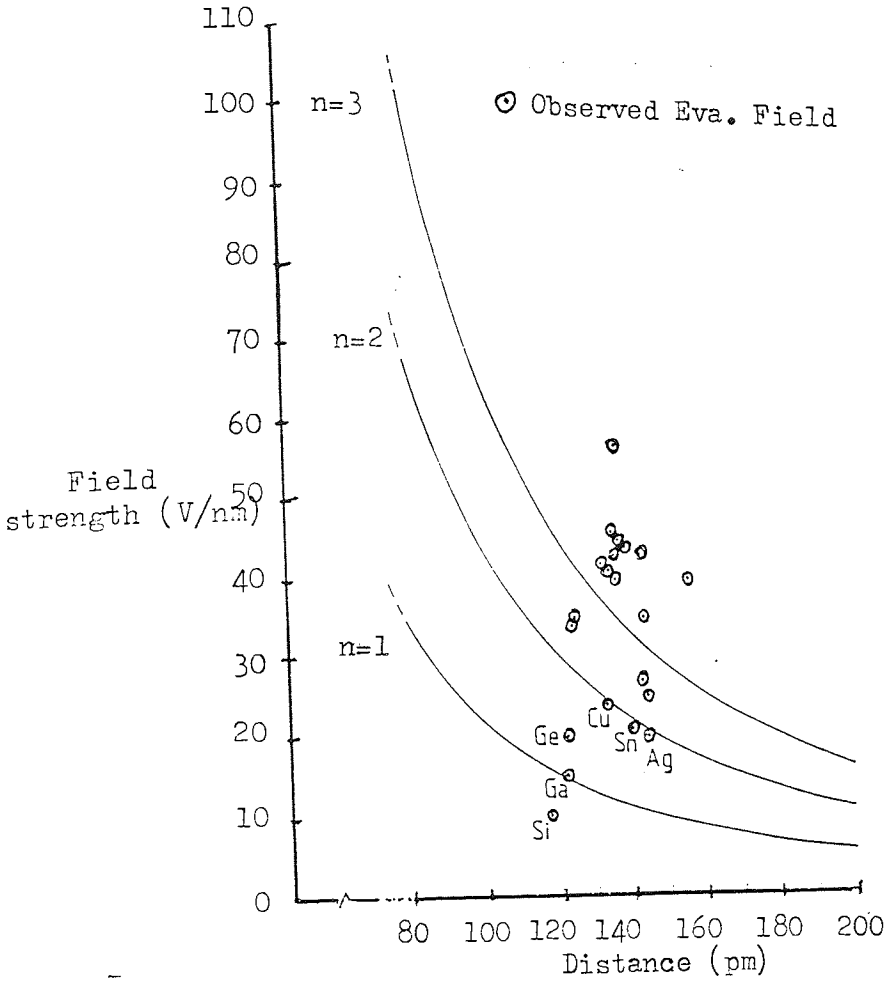

Fig. (5.3) Comparison of experimental evaporation fields with F_n^{HD}

Among the species, Cu, Sn, Mg, Ge and probably Ga lie just below the n=2 curve, but these are significantly above the n=1 curve.

These metals have been reported to field evaporate in a mixture of charge states (cf. Dixon et al. 1981) and with copper in particular, the proportion of Cu^{++} and Cu^{+} ions has been reported to decrease with increasing temperature. This is characteristic of an evaporation process in which copper escapes as Cu^{+} and then post-ionizes to Cu^{++}. Thus fig. (5.3) indicates that the Mueller mechanism is not operating for copper; also this still seems to be the case when the rather low radius of the Cu^{++}

ion is taken into account.

The thermodynamic data for silver, that are reflected in the BIH- predicted value for F_2^e in table (5.2), strongly indicate that any observed Ag^{++} would be formed by post ionization of Ag^{+}, and so silver too does not escape by the Mueller mechanism. Nor does Sn^{+} for the same reason. We have no information about the evaporation charge-state of germanium.

From Fig (5.3), we thus see that the Mueller mechanism is yet to be firmly eliminated only for silicon, gallium and germanium. However, these metals are not included in the discussion of mainstream evaporation escape mechanism.

5.5. Possible corrections.

5.5.1 Justification for choice of the a_n -value.

Our calculation of F_n^{HD} corresponds to taking a_n equal to the neutral atomic radius ρ_0. It is important that a_n should not be overestimated making F_n^{HD} unduly lower than it really should be. We justify our choice of a_n-value by the following arguments.

If the assumption that the metal's electrical surface lies inside the electron charge cloud of the substrate is realistic, then the true value of a_n is somewhat greater than the radius of the external ion. This assumption finds support from the theoretical work of Lang and Kohn (1973) on the calculation of the charge-profiles induced in a metal surface by the application of a uniform electric field. According to Lang and Kohn, for tungsten, the distance δ of the edge of electron cloud from the " effective metal surface"(in our terminology "electrical surface") is roughly 0.04 nm. Similar results can be found in the experimental work of Culbertson et al. (1979) on the field dependence of the appearance

energies of helium ions desorbed by electron stimulation from field-adsorption sites on a tungsten emitter. According to their deduction, the neutral-atom bonding distance of helium , as measured from the electrical surface of a tungsten emitter, is greater than the helium neutral-atom radius by between 0.042 nm to 0.058 nm. Thus we can generally suppose that the bonding distance a_n should be greater than the radius of an external particle by a distance greater than about 0.04 nm, i,e.:

$$\delta > 40 \text{ pm} \qquad (5.24)$$

The next problem is to determine proper values for the ionic radii. It seems difficult to find good values for metal ion radii, even in free space. However, some values taken from Moses (1978) are shown in table (5.7). Obviously the situation at the surface of a field ion emitter is very different from the context in which ionic radii are usually stated; so the cited values probably give only a broad indication of radii differences to be applied in the field-ion situation. Nevertheless, in the absence of anything better we shall make arguments based on these values.

TABLE (5.7)

Selected ionic radii, taken from Moses (1978).

Ionic species	Ionic Radii (nm)	ρ_0 (nm)
Mo(3+)	0.092	0.136
Au(1+)	0.137	0.144
Co(3+)	0.065	0.125
Fe(2+)	0.075	0.124
Ni(2+)	0.069	0.1245
La(3+)	0.106	0.1865
Cu(2+)	0.070	0.128
Ag(1+)	0.113	0.1445
Al(3+)	0.050	0.143
Ga(3+)	0.062	0.122

The general message from the results in table (5.7) seems to be as follows. For 2+ ions, the ionic radius ρ_2 is significantly smaller than the neutral-atom radius ρ_0, the difference being as much as 60 pm in some cases. For 1+ ions the differenece is somewhat smaller; for 3+ ions the difference may be even larger. We may reasonably assume that ions field evaporate in a 1+ or 2+ charged state. And with 2+ ions we may assume that:

$$\rho_0 - \rho_2 < 60 \text{ pm.}$$

or $\rho_2 - \rho_0 > -60$ pm (5.25)

Now the bonding distance a_2 is given by:

$$a_2 = \rho_2 + \delta$$
$$= \rho_0 + (\rho_2 - \rho_0) + \delta$$

Thus combining in equalities, we obtain:

$$a_2 - \rho_0 > -20 \text{ pm.}$$

What this means is that in the worst case we might need to shift the plotted points in the earlier diagrams to the left (relative to the n = 2 curve) by a distance not exceeding 20 pm.

This would have little effect on our arguments in most cases. The situation would be most critical for the species with low observed evaporation field, but it is precisely these species that tend to evaporate as 1+ ions.

For 1+ ions, the trend if anything is to shift the plotted points to the right (relative to the n = 1 curve). So for 1+ ions the arguments against the Mueller mechanism should if anything become stronger.

5.5.2 Overestimation of the correlation term

In the theories of field evaporation, the correlation term in the ion potential energy is taken as the image potential. The image potential and other relevant potential energy curves are shown in Fig. (5.4).

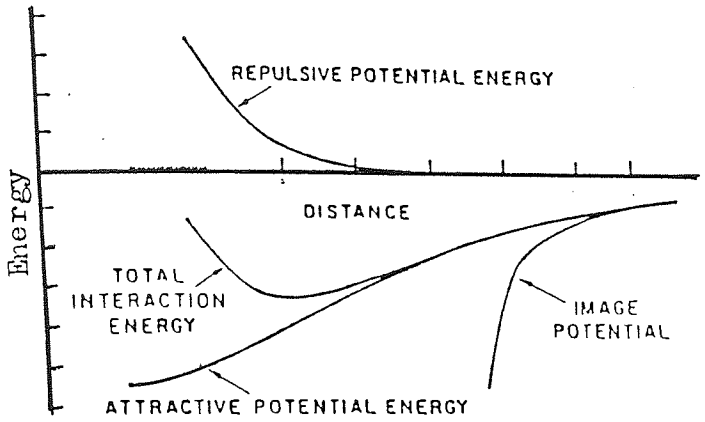

Fig. (5.4) Potential energy curves (Smith et al. 1973)

Smith et al. (1973) suggest that the image potential does in fact overestimate the magnitude of correlation energy. If this is the case, then to get some feeling for the likely effect, we can express the correlation term in the form:

$$- n^2e^2/16\pi\varepsilon_o x.\ 1/\varepsilon_1 , \qquad \text{where } \varepsilon_1 > 1$$

The factor ε_1, which will appear "next to ε_0" in any derived formula, reduces the magnitude of the correlation interaction.

Thus, equation (5.17) becomes:

$$F_n^{HD} = \Gamma'(n\ e\ /\ 16\pi\varepsilon_o\varepsilon_i a_n^2) \qquad (5.26)$$

It can be readily seen from equation (5.26) that the F_n^{HD}-value is reduced, and in this case, therefore, arguments against the

Mueller mechanism become stronger.

It is difficult to obtain a reliable estimate of the size of ε_1.

5.5.3 Use of revised repulsive potential form

5.5.3.1 Basic theory

In the theory as developed so far, we have assumed that the position 'x' of a desorbed atom is measured from the metal's electrical surface. But the repulsive component in the potential energy expression (cf. equation 5.7) is modelled on the atom-atom repulsive interactions in free space. So it is arguable that the denominator in the repulsive term, in equation (5.7), should actually involve the distance between the nucleus of a desorbed atom and that of a substrate atom on whose electron edge the desorbing atom sits just before evaporation.

More generally, a desorbing atom must be interacting with several substrate atoms prior to desorption. One might, therefore, seek to model this situation by a repulsive term of the form $G/(x+c)^t$, where 'c' is a parameter lying between 0 and the parameter d shown in (fig. 2.5). Thus, we modify equation (5.7) to the form:

$$U_n(x,0) = H_n - n\Phi^E - \sigma/x + G/(x+c)^t \qquad (5.27)$$

Where $\sigma = n^2e^2/16\pi\varepsilon_0$, as before. At the bonding point a_n, $\partial U_n/\partial x = 0$; therefore, we obtain:

$$G = \sigma\{(a+c)^{(t+1)}\}/(t \cdot a_n^2) \qquad (5.28)$$

In the presence of an external field F, the potential energy of an ion of charge n is given by:

$$U_n(x,F) = H_n - n\phi^E - \sigma/x + G/(x+c)^t - neFx \qquad (5.29)$$

The "hump disappearance" condition requires $\partial U_n/\partial x=0$ and $\partial^2 U_n/\partial x^2=0$ simultaneously. Accordingly, from equation (5.29), we obtain:

$$\partial U_n/\partial x = \sigma/x_I^2 - tG/(x_I + c)^{(t+1)} - neF \qquad (5.30)$$

so the field F_n^{HD} where the hump disappears is given by:

$$F_n^{HD} = \sigma/(ne \cdot x_I^2) - tG/\{ne(x_I + c)^{(t+1)}\} \qquad (5.31)$$

where x_I is the point of inflexion given by the condition:

$$0 = \partial^2 U_n/\partial x^2 = -2\sigma/x_I^3 + t(t+1)G/(x_I + c)^{(t+2)} \qquad (5.32)$$

This leads to an equation for x_I of the form:

$$x_I^3 + \beta(x_I+c)^{(t+2)} = 0 \qquad (5.33)$$

$$\text{where } \beta = -2a_n^2/\{(t+1)(a_n + c)^{(t+1)}\} \qquad (5.34)$$

Equation (5.33) has to be solved numerically.

5.5.3.2 Application to tungsten.

As already indicated, we assume that c lies between zero and repulsion distance d. For tungsten, d has been calculated by Forbes (1980) to be about 0.08 nm, this value being based on the experimental measurements by Culbertson et al. (1979).

Thus, taking n = 2, since these tungsten ions are found in more abundance than in any other charge states, and a_n =0.137 nm, equation (5.33) is solved for x_I using a computer program, for the cases t=6, 9, 12 and 15, and c=0 and 0.08 nm. Table (5.8) shows the values of x_I and F_n -values, derived from equation (5.31).

TABLE (5.8)

Values of x_I and F_n^{HD} for tungsten, for c= 0 and 0.08 nm; t=6, 9, 12, 15, and a_n =0.137 nm.

t	x_I/nm	F_n^{HD}(V/nm)	x_I/nm		F_n^{HD}(V/nm)
	c=0		c=0.08 nm		
6	0.176	16.60	0.191	15.99	15.99
9	0.167	20.52	0.179	19.83	19.83
12	0.162	23.09	0.172	22.35	22.35
15	0.158	24.93	0.167	24.20	24.20

Inspection of table (5.8) shows that choice of t-value makes little difference to the form of the results, in the sense that in each case there is little change in F_n^{HD} as c increases from zero to 80 pm, whatever the value of t. We thus concentrate on the cases t = 9 and t = 12 as before. The F_n^{HD}-values for a range of

c-values lying between c = 0 and c = 0.15 nm. are plotted in Fig. (5.5).

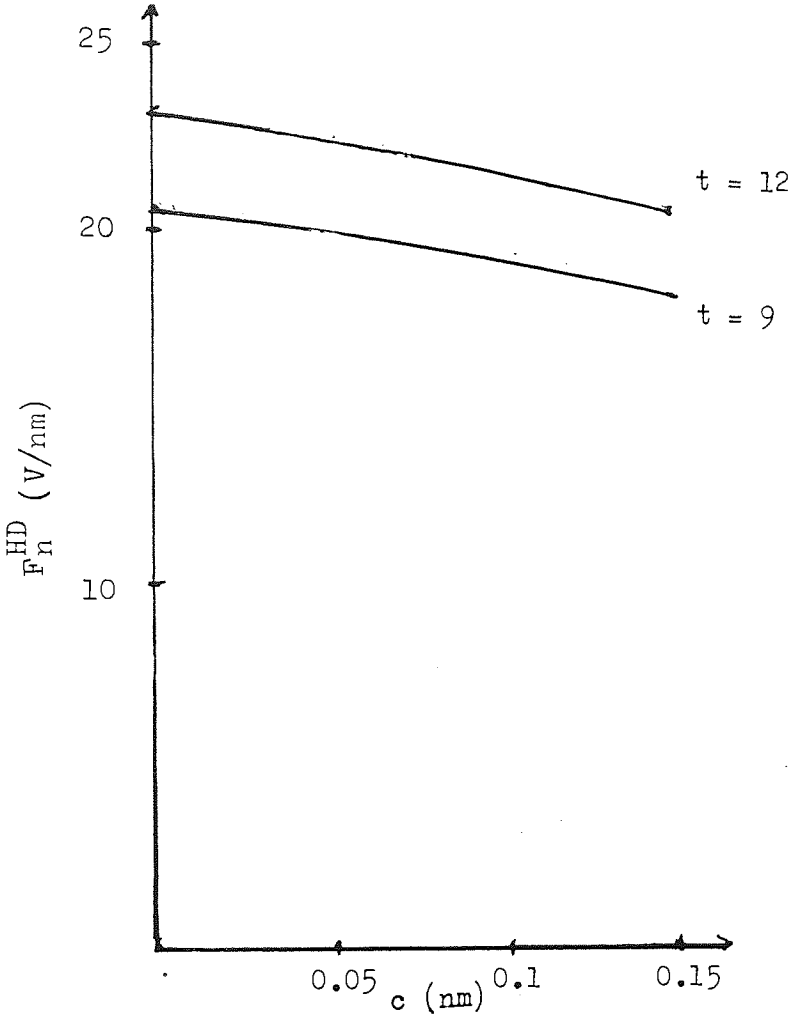

Fig. (5.5) Graph of F_n^{HD} vs. c for t = 9 and 12, for tungsten.

In all cases, the effect of making c greater than 0 is to reduce F_n^{HD}, which would make our argument against the Mueller mechanism even stronger. From the form of the equations, we expect this result whatever the value of a_n. This obviously raises a question whether it is worthwhile to introduce the correction factor 'c' in the repulsive interaction term G/x^t; in fact it would seem that our original assumption, about measuring distances from metal's electrical surface even for the repulsive term, was broadly satisfactory, and can be justified in terms of its

mathematical convenience.

Although we have investigated the effect of the repulsive interaction on F_n^{HD} for tungsten, generally similar results can be expected for other materials. In all cases the use of a (positive) c-value will make the case against the Mueller mechanism stronger.

5.5.4 Corrections - summary

The discussion, in this section, on possible corrections that may have any effect on our mathematical theory and arguments, can be summarised as follows:

(1) If anything, the image potential overestimates the correlation term in the ion potential energy. The effect, if anything, is to reduce the F_n^{HD}-values and make our arguments stronger.

(2) If the denominator in the repulsive term takes the form $(x + c)^t$, where $c>0$, then there is little change in F_n^{HD} values. If anything, our arguments become stronger.

(3) In the context of ionic bonding distances, our arguments should be valid if $a_n - \rho_0 > -20$ pm. This is the most critical of the corrections investigated, but the inequalitiy seems to be satisfied if n = 1 or 2, for most chemical species of interest.

In general terms, therefore, exploration of these corrections has not affected the validity of our arguments.

5.6 Conclusion

In this chapter we have shown the following with reasonable certainty:

1. The simple image-hump formalisms are not logically self-consistent.

2. The ability of the simple image-hump formalisms to approximately predict observed evaporation fields in no sense implies that field evaporation is taking place by means of the Mueller mechanism. Rather, it seems a reflection of the fact that the Mueller mechanism, like the Gomer mechanism, is thermally activated.

3. Further, for most metals used in the conventional field-ion techniques, observed evaporation fields seem to be significantly higher than the field at which the Schottky hump disappears. Therefore the Mueller mechanism cannot be operating for these metals.

Taken together, these first two findings firmly suggest that discussion of normal field evaporation in terms of the existing image-hump formalisms should be discontinued.

The fact that observed evaporation fields are higher than Schottky-hump disappearance fields also, of course, tends to discriminate against classical evaporation mechanisms that postulate that the evaporating atom is initially bound in the form of an ion.

CHAPTER 6

FURTHER ARGUMENTS AGAINST THE MUELLER MECHANISM

In the preceding chapters we have accumulated much evidence to show the inadequacies of Mueller's image hump mechanism in interpreting the field evaporation data. We have also shown theoretically that the image hump disappears at a much lower field than the conventionally calculated evaporation field or the experimental evaporation field. These findings show that there have been conceptual errors in developing the Mueller theory of field evaporation. However, since 1980 there have been other developments, theoretical as well as practical, in field evaporation, undertaken by various research workers. In this chapter, we look at some relevant contemporary work, and we also look further at the other types of possible test that were identified in chapter 3 (see section 3.11).

6.1 The a-priori prediction of escape mechanism.

We begin by looking at an argument developed by Forbes (1982c) on the basis of the work described in section 5.2.2.

6.1.1 Calculation of the energy level W_n^* of the ion.

At the field F_n^{HD} where the Schottky-hump disappears there is a plateau in the ionic potential curve, and the standard ionic

potential energy at the plateau is given by equation (5.19), namely:

$$U_n^* = (H_n - n\Phi^E) + S_n^* \qquad (6.1)$$

Where S_n^* is given by equation (5.21). Therefore with the F^2-term, we obtain:

$$S_n^* = \Theta.\ (n^2e^2/\ 16\pi\varepsilon_o a_n) - (1/2)c_n\ (F_n^{HD})^2 \qquad (6.2)$$

where the symbols have their usual meanings. The values of Θ for the repulsive exponent t-values from 6 to 15 are given in table (5.3).

It follows that the energy level W_n^* of the ion, at the plateau, relative to the bonding potential energy is:

$$W_n^* = (\Lambda^0 + H_n - n\Phi^E) + \Theta.(n^2e^2/\ 16\pi\varepsilon_o a_n) + (1/2)(c_\alpha - c_n)(F_n^{HD})^2 \qquad (6.3)$$

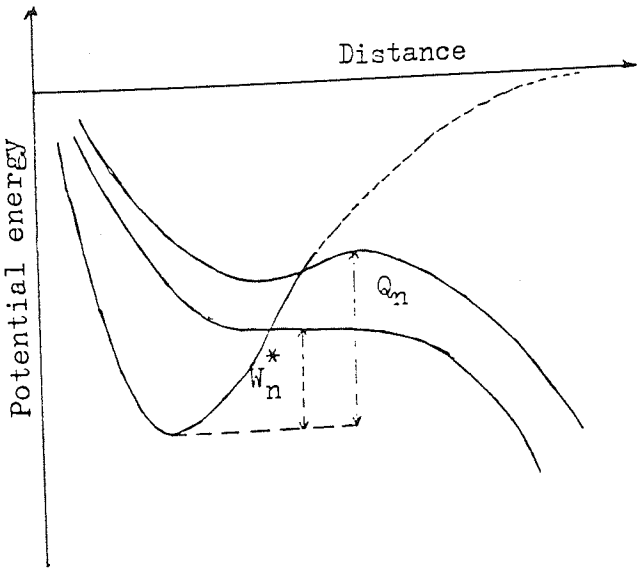

Fig. (6.1) The numerical criterion for Mueller mechanism, $Q_n > W_n^*$

Forbes' argument is that if the Mueller mechanism operates and a Schottky hump exists in the ionic potential curve, then the activation energy Q_n (as measured experimentally, or as predicted from the emission equation) must be greater than W_n^*. The situation is shown in Fig. (6.1).

This comparison should provide an a-priori numerical criterion for evaluating the Mueller mechanism.

In section (3.3) we have derived estimates of Q_n from experiments, using equation (3.15); these values lie between 155 meV and 185 meV, for J^o-values lying between 1 layer/s and 0.01 layer/s. Forbes, however, prefers the structure criterion $W_n^* > 1$ eV, for making a clear decision against the Mueller mechanism.

In equation (6.3), the parameter c_α is not known for most species, but all the other parameters are known. Forbes argues, however, that c_α must on general physical grounds be greater than c_n, so the F^2-term must be positive. If we use $W_n^*(NP)$ to denote W_n^* less the F^2-term, then $W_n^* > W_n^*(NP)$. Hence, if the criterion $W_n^*(NP) > 1$ eV is satisfied, then the criterion $W_n^* > 1$ eV certainly will be.

Table (6.1) shows values of $W_n^*(NP)$ for various species, for $n = 1$ and $n = 2$. As in chapter 5, a_n has been set equal to ρ_0. The species are arranged in order of descending $W_1^*(NP)$.

From table (6.1), it can be observed that for most species $W_n^*(NP) > 1$ eV. Therefore according to this numerical criterion, the Mueller mechanism cannot be operating for these species; rather, a Gomer-type mechanism must be operating. However, for some of the elements, eg. Si, Ge, Sn, Cr, Cs and Ga, either $W_1^*(NP)$ or $W_2^*(NP)$ is less than 1 eV. For these species the situation is less clear, and the test is indecisive. (It is worthy

of note that two of these species, gallium and caesium, are used in liquid-metal ion sources.)

TABLE (6.1)

Values of $W_n^*(NP)$, as given by equation (6.3), for most elements used in the field evaporation experiments. ρ_0 denotes the neutral-atom radius of the species in question. Species for which W_n^* (for n = 1 or 2) is less than 1 eV, are marked with an asterisk. The values are from Forbes (1982).

Species	ρ_0(nm)	$W_1^*(NP)$ (eV)	$W_2^*(NP)$ (eV)
W	0.137	8.1	9.4
Ta	0.143	7.9	8.0
Re	0.137	6.8	6.5
Ir	0.1355	6.6	6.0
Hf	0.1565	6.3	7.0
Mo	0.136	5.6	5.3
Pt	0.139	5.5	6.8
Ru	0.1325	5.3	4.9
Au	0.144	4.8	9.4
Rh	0.1345	4.3	5.2
La	0.1865	4.0	2.8

TABLE (6.1) Continued

Species	ρ_o(nm)	W_1^*(NP) (eV)	W_2^*(NP) (eV)
Ti	0.1445	3.8	1.8
Si**	0.1175	3.8	0.8
Co	0.125	3.4	2.7
Fe	0.124	3.3	1.6
Ni	0.1245	2.6	2.4
Ge**	0.1225	2.5	0.0
Cu	0.128	2.3	4.9
Pb	0.175	2.2	3.6
Sn**	0.140	2.1	0.4
Ag	0.1445	2.1	7.4
Cr	0.125	1.8	0.4
Al	0.143	1.3	4.4
Cs**	0.266	0.3	3.7
Ga**	0.122	0.1	2.8

6.1.2 Corrections to Forbes' treatment

A defect of Forbes' treatment is that it assumes the conventional forms for the image potential and the repulsive potential. The difficulties with these assumptions were discussed in chapter 5. Thus, in the light of section 5.5, we shall explore the effects of making certain corrections to Forbes' treatment. Since any such corrections are, of course, likely to affect the "marginal" cases more critically than the "relatively safe" cases, we shall concentrate mainly on the asterisked species in table (6.1).

In the light of sections 5.5.2 and 5.5.3, and neglecting F^2-terms, equation (6.3) can be replaced by:

$$W_n^*(NP) = K_n - 2\sigma/\xi_1 x_I + G.t[1/\{t.(x_I + c)^t\} + x_I/\{(x_I + c)^{(t+1)}\}] \qquad (6.4)$$

where the symbols have their previous meanings. The values of x_I are the numerical solutions of the equation (5.33) for various values of c within the range $0 < c < d$ where 'd' is the repulsion distance as used earlier. Note that, for $c = 0$, and $\xi_1 = 1$, equation (6.4) reduces to Forbes' treatment.

From equation (6.4), it can be clearly seen that, if $\xi_1 > 1$, then the second term in this equation will be reduced, and hence $W_n^*(NP)$ will be larger. Hence the argument against the Mueller mechanism will be even stronger than in Forbes' treatment.

To examine the effects of the c-variation we look first at the "marginal" cases. For c-values ranging from 0.01 nm to 0.14 nm, x_I-values were calculated for Si, Ge, Sn, Cr, Cs and Ga, and

subsequently, using respective x_I-values and corresponding c-values for these species $W_1^*(NP)$ and/or $W_2^*(NP)$ values were calculated. In our calculation we have assumed the repulsive exponent to be 12 (i.e t = 12). Results are shown in Fig. (6.2).

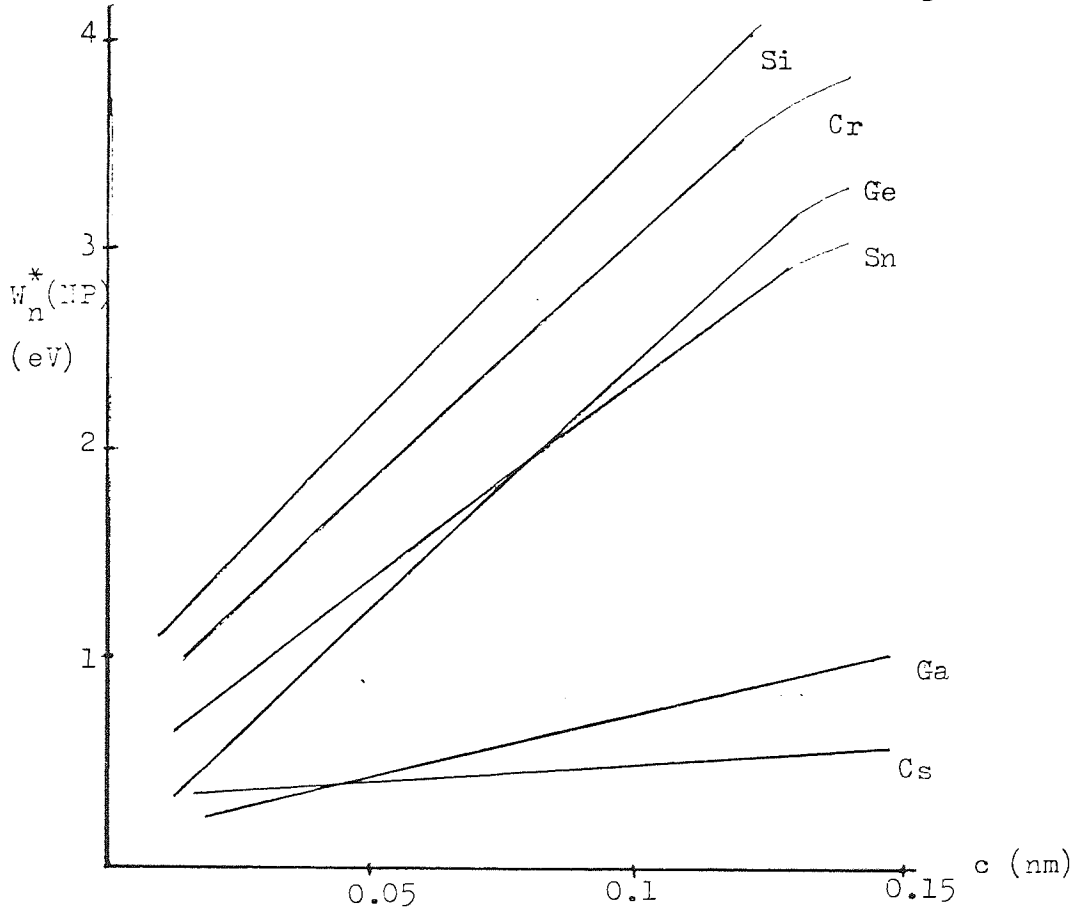

Fig. (6.2) Plot of W_n^* vs c for Si, Ge, Sn, Cr, Cs and Ga

In all cases the energy difference $W_n^*(NP)$ between the level of the ionic plateau and the bonding well level increases as c increases. In the case of Cr, Sn, Ge and Si the increases are significant and tend to strengthen our feeling that the Mueller mechanism is unlikely to be applicable to the field evaporation of these species. In the cases of Ga and Cs, there is also an increase in W_n^*, but this is less significant.

6.2 Q-F and T-F measurements

Whilst the work in this thesis was being carried out, Forbes (1982b) and Forbes and Chibane (1982) were developing relationships between Q and F, and T and F, in the framework of the charge-hopping mechanism. In this section we briefly describe their work, and develop/examine the equivalent tests for the Mueller mechanism.

6.2.1 Formulae for Gomer-type mechanisms

The activation-energy formula developed by Forbes (1982b) has the form:

$$Q_n = \Omega\{(F_n^e/F) - 1\}^2 \qquad (6.5)$$

where F_n^e (as earlier) is the zero-Q evaporation field and Ω is a parameter described as weakly dependent on F.

From this it follows that we expect $Q^{1/2}$ to be a linear function of 1/F. This has been confirmed by Chibane (1985), who has replotted the experimental results of Ernst (1979) for rhodium, Kellogg (1984) for tungsten, and Block (private communication) for silver. As an illustration, Fig. (6.3) shows Ernst's rhodium results replotted in the form $Q^{1/2}$ vs 1/F.

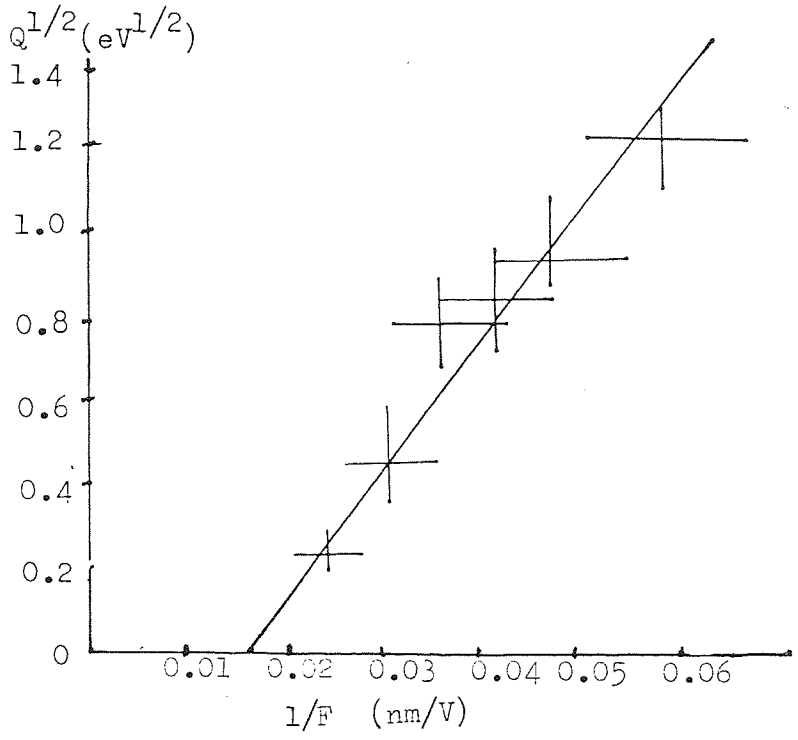

Fig. (6.3) Plot of $Q^{1/2}$ vs 1/F for rhodium (Forbes, Chibane and Ernst 1984).

It also follows that experimental plots of $T^{1/2}$ vs 1/F should be straight. This has been demonstrated over a range in temperature near 80 K, for example in the reanalysis by Chibane and Forbes (1982) of the experiments of Wada et al. (1980). Fig. (6.4) is taken from Forbes and Chibane (1982), and relates to tungsten and molybdenum.

The diagram shows, at low temperatures, a well defined "deviation temperature" at which departure from linearity occurs (and below which the classical emission equation fails). For tungsten, deviation occurs near 50 K, and for molybdenum near 35 K.

The observations, therefore, provide support for the common assumption that field ion emission is thermally activated when

carried out near 80 K. In section (3.4), we have emphasised that the field sensitivity experiments should be carried out in an "activation-dominated" regime.

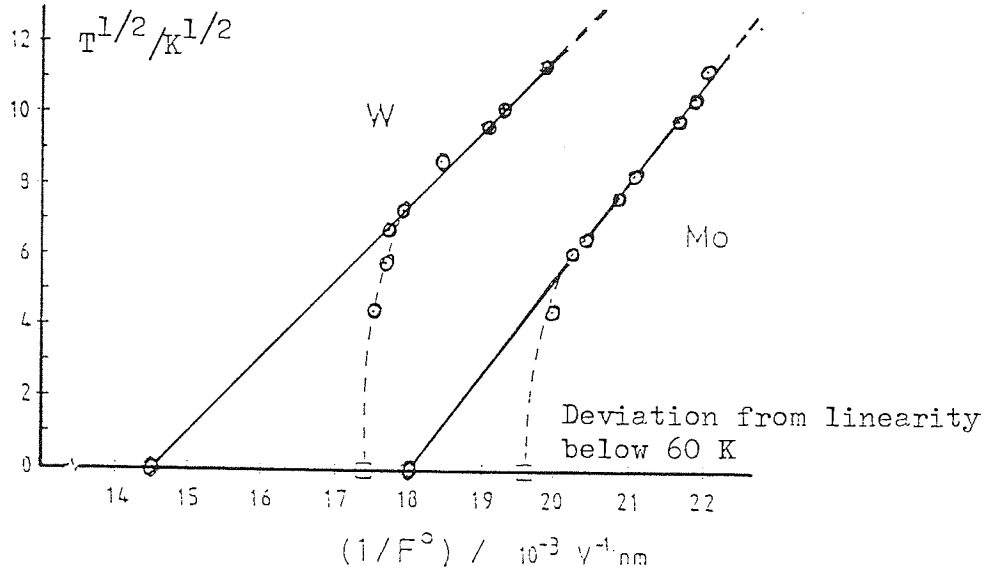

Fig. (6.4) Data from Wada et al. (1980) replotted in the form $T^{1/2}$ vs 1/F for tungsten and molybdenum (Forbes and Chibane 1982)

Thus what we have described in this section is held to confirm the plausibility of Gomer-type mechanisms, at least for the more refractory materials, over the temperature range normally considered.

6.2.2 Formulae for the Mueller mechanism

Not withstanding this apparent success of a Gomer-type mechanism it seemed useful to develop equivalent tests for the Mueller mechanism.

To find an approximate Q_n- F formula we first need to find an analytical expression for how the ionic potential at the Schottky hump (U_n^{Sh}) varies with field (F). From equation (5.6), the

potential energy $U_n(x,F)$ can be written in the form:

$$U_n(x,F) = H_n - n\,\phi^E + C(x) - neFx - (1/2)c_n F^2 \qquad (6.6)$$

where $C(x) = -\sigma/x + G/x^t$, and all the symbols have their previous meanings. The value of G is given by equation (5.8) namely:

$$G = (\alpha/t)\, a_n^{t-1} \qquad (6.7)$$

So C(x) can be written:

$$C(x) = \sigma(-1/x + a_n^{t-1}/t\, x^t) \qquad (6.8)$$

At the point of inflexion x_I:

$$(\partial^2 U_n/\partial x^2)\Big|_{x_I} = 0 \qquad (6.9)$$

or equivalently:

$$(\partial^2 C/\partial x^2)\Big|_{x_I} = 0 \qquad (6.10)$$

The position of the Schottky hump x_n^{Sh}, measured from the metal's electrical surface, is given by the requirement that:

$$\partial U_n/\partial x \Big|_{x_n^{Sh}} = 0 \qquad (6.11)$$

i.e. $$\partial C/\partial x \Big|_{x_n^{Sh}} - neF = 0 \qquad (6.12)$$

It follows that at the field F_n^{HD} at which the Schottky hump just disappears:

$$\partial C/\partial x\Big|_{x_n^{Sh}} = \partial C/\partial x\Big|_{x_I} = neF_n^{HD} \qquad (6.13)$$

At any lower field F, x_n^{Sh} can be written $x_n^{Sh} = x_I + \delta$, where δ denotes the distance between the hump and the intersection point. Also $(\partial C/\partial x)$ can be Taylor-expanded about x_I in the form:

$$(\partial C/\partial x)\Big|_{x_n^{Sh}} = (\partial C/\partial x)\Big|_{x_I} + (\partial^2 C/\partial x^2)\Big|_{x_I}.\delta + 1/2(\partial^3 C/\partial x^3)\Big|_{x_I}.\delta^2 + \ldots \qquad (6.14)$$

From equations (6.10), (6.12) and (6,13) we obtain:

$$neF = neF_n^{HD} + (1/2)(\partial^3 C/\partial x^3)\Big|_{x_I}.\delta^2 \qquad (6.15)$$

Hence δ is given (approximately) by:

$$\delta = (2ne/B)^{1/2}.(F_n^{HD} - F)^{1/2} \qquad (6.16)$$

where B is given by:

$$B = -\partial^3 C/\partial x^3\Big|_{x_I} = \sigma[\{(t+1)(t+2).a_n^{(t-1)}\}/(x_I^{t+3}) - 6/x_I^4] \qquad (6.17)$$

Finally, we write equation (6.16) as:

$$\delta = \phi\,(F_n^{HD} - F)^{1/2} \tag{6.18}$$

where $\phi = (2ne)^{1/2} \cdot B^{-1/2}$ (6.19)

Now from equation (6.6) and at field F_n^{HD} we have:

$$U_n^* = H_n - n\phi^E + C(x_I) - neF_n^{HD}x_I - (1/2)\,c_n\,(F_n^{HD})^2 \tag{6.20}$$

where U_n^* is the level of the hump when it just disappears. At any other field F we may Taylor-expand C(x) about x_I to give equation (6.6) in the form:

$$U_n^{Sh} = H_n - n\phi^E + C(x_I) + (\partial C/\partial x)\Big|_{x_I} \cdot \delta - neFx_n^{Sh} - (1/2)\,c_n\,F^2 \tag{6.21}$$

So, from equations (6.21), (6.20) and (6.13) we obtain:

$$\begin{aligned}(U_n^{Sh} - U_n^*) &= neF.x_I + neF_n^{HD}.\,\delta \\ &\quad - neFx_n^{Sh} + (1/2)c_n\{(F_n^{HD})^2 - F^2\} \\ &= ne(F_n^{HD} - F)(x_I + \delta) \\ &\quad + (1/2)c_n\{(F_n^{HD})^2 - F^2 \\ &= ne\,\gamma' a_n\,(F_n^{HD} - F) + \phi\,(F_n^{HD} - F)^{3/2} \\ &\quad + (1/2)c_n\{(F_n^{HD})^2 - F^2\}\end{aligned} \tag{6.22}$$

In general, Q_n is given by:

$$Q_n = U_n^{Sh} - U_\alpha^B = U_n^{Sh} + \Lambda^0 + (1/2)c_\alpha F^2 \tag{6.23}$$

where U^B is the bonding-point level. And at field F_n^{HD} we have:

$$W_n^* = Q_n(F = F_n^{HD}) = U_n^* + \Lambda^0 + (1/2)c_\alpha (F_n^{HD})^2 \qquad (6.24)$$

Approximating equation (6.22), it follows from equations (6.23) and (6.24) that:

$$Q_n(\text{approx.}) = W_n^* + ne\gamma a_n (F_n^{HD} - F) + \Phi.(F_n^{HD} - F)^{3/2} - (1/2)(c_\alpha - c_n)\{(F_n^{HD})^2 - F^2\} \qquad (6.25)$$

To continue the discussion we use rhodium as an example. Some relevant data are as in table (6.2).

TABLE (6.2)

a_1/nm	x_I/nm	Φ	W_1^*
0.135	0.160	0.011	4.3

To begin with, we ignore the F^2-terms. Table (6.3) shows the corresponding values of Q_n (approx.) and relevant relative sizes of the first two field-dependent terms in equation (6.25). For comparison we also show the activation-energy Q_n(full, NP) calculated from the full-Q expression (but omitting F^2-term):

$$Q_n(\text{full, NP}) = K_n - neFx_n^{Sh} + n^2e^2[\{(a_n^{(t-1)})/t.(x_n^{Sh})^t\} - 1/x_n^{Sh}) \qquad (6.26)$$

x_n^{Sh}-values can be found analytically.

TABLE (6.3)

Relative sizes of F-terms and Q_n, approx. and their variations with F for rhodium, taking F_n^{HD} = 11.97 V/nm. and W_1^* = 4.3 eV.

F	Q_n	Q_n	$ne\gamma a_n(F_n^{HD} - F)$	$\Phi(F_n^{HD}-F)^{3/2}$
V/nm	full/eV	approx/eV	eV	eV
0	6.20	6.69	1.92	0.472
1	6.04	6.47	1.76	0.414
2	5.88	6.26	1.60	0.358
3	5.72	5.05	1.44	0.306
4	5.56	5.83	1.28	0.256
5	5.40	5.63	1.12	0.210
6	5.24	5.42	0.96	0.166
7	5.08	5.22	0.80	0.126
8	4.92	5.03	0.64	0.090
9	4.76	4.84	0.48	0.058
10	4.60	4.66	0.32	0.031

The most obvious feature of table (6.3) is that Q_1(approx.)-values are unrealistically large. This was of course to be expected, in view of Forbes' results discussed in section (6.1). Leaving this aside, however, we note that Q_1(approx.)-values are reasonable estimates of the Q_1(full)-values. Also note that the term linear in (F_n^{HD}) is much the larger of the two, so in the first approximation the $(F_n^{HD} - F)^{3/2}$-term can be neglected. We also note that the F^2-term in equation (6.25) can be expanded in the form:

$$F^2\text{-term} \approx (c_\alpha - c_n)\, F_n^{HD}.\, (F_n^{HD} - F) \qquad (6.27)$$

For rhodium the value of $(c_\alpha - c_n).\, F_n^{HD}$ is 0.011 eV V^{-1} nm. In comparison, the value of $ne\gamma a_n$ is 0.16 eV V^{-1} nm, so the F^2-term is also small in comparison with the linear term. It follows that equation (6.25) can be further approximated as:

$$Q_n(\text{approx.}) = W_n^* + ne\gamma a_n(F^{HD} - F) \qquad (6.28)$$

In other words (for rhodium), the Mueller mechanism predicts a linear dependence of activation energy on field at small Q_n-values.

Obviously, in the case of rhodium where the Q_n-values are unrealistically large there is no point in attempting to test for this linear dependence in experimental data. However, in cases where Forbes' criterion is unable to distinguish between

evaporation mechanisms, tests based on theory developed here might conceivably prove useful. (And, obviously, an equivalent test, using a F - T relationship can be devised.)

6.3 Appearance energy variation with field

The use of appearance energies and their dependence on field as a test of field evaporation mechanism has already been discussed in section (3.8). However, we are now in a position to derive a proper formula for the field dependency of A.

The standard appearance energy $A_{\alpha nr}^{st}$ is given by equation (2.53), so identifying the point of escape x^p as the Schottky distance x_n^{Sh}; we have:

$$A_{\alpha nr}^{st} = H_r - U_n(x_n^{Sh}, F) = H_n - U_n^{Sh} \qquad (6.29)$$

Therefore, if $A_{\alpha nr}^{*}$ is the standard appearance energy when the hump disappears, then

$$A_{\alpha nr}^{*} = H_r - U_n^{*} \qquad (6.30)$$

Hence, combining these equations and using equation (6.22), we obtain an equation for the appearance energy difference:

$$(A_{\alpha nr}^{st} - A_{\alpha nr}^{*}) = -ne\gamma a_n(F_n^{HD} - F) - \Phi(F_n^{HD} - F)^{3/2} - (1/2)c_n\{(F_n^{HD})^2 - F^2\} \qquad (6.31)$$

We have seen in section (6.2.2) that the first term on the r.h.s.

of equation (6.31) is dominant. Therefore, we can express equation (6.31) approximately as:

$$A_{\alpha nr}^{st} - A_{\alpha nr}^{*} = -ne\gamma a_n (F_n^{HD} - F) \qquad (6.32)$$

This is an equation for the variation of appearance energy with field, within the framework of extended image-hump formalism. This equation can be used as follows. Within this framework $A_{\alpha nr}^{*}$ can be predicted from equation $A_{\alpha nr}^{*} = H_r - U_n^{*}$. On the other hand $A_{\alpha nr}^{st}$ can be derived from experiments. The former is an absolute measure of the level of the top of the Schottky-hump and the latter is an absolute measure of the level of the hump over which field evaporation actually takes place. If these two quantities are significantly different (say more than 1 eV), then field evaporation is not taking place via the Mueller mechanism. On the other hand, if the quantities are comparable, then conformity with equation (6.32) provides a test for the Mueller mechanism. It is probably best to apply this in the form:

$$d(A_{\alpha nr}^{st})/dF = ne\gamma a_n \qquad (6.33)$$

This, for example, is a test that might apply to asterisked materials in table (6.1). But relevant experimental results are not yet available.

6.4 The FWHM variation with field

Since 1980 some relevant theory has appeared in the literature. Mair et al. (1983) have argued that half-widths of energy distributions for various mechanisms of field evaporation should

be as follows:

(1) For the Mueller mechanism; it is either of the order of $k_B T$ (less than 0.1 eV at room temperature), or determined by the spread of bonding-site levels.

(2) For the charge-draining mechanism, either as for the Mueller mechanism, or determined by a theory that is not yet fully understood.

(3) For the charge hopping mechanism (with singly charged ion), as given by the formula:

$$FWHM = (0.0676\ eV^{3/2}.V^{-1})\ F.(\Phi^E)^{-1/2} \qquad (6.34)$$

where Φ^E is the emitter work function and F the relevant evaporation field.

We can use equation (6.34) to compare the theoretical predictions of FWHM with the experimental values. Table (6.4) shows the theoretically calculated values of FWHM for Ga, Ni, Cu and Fe. The values of experimental F^o and Φ^E are taken from tables (5.1) and (5.2). The experimental values are taken from the references Culbertson et al. (1979) for Ga and Ernst et al. (1979) for Ni, Cu and Fe.

TABLE (6.4)

Theoretical FWHM-values for Ga, Ni, Cu and Fe

Species	Φ^E/eV	F/Vnm^{-1}	FWHM/eV	FWHM (expt.)/eV
Ga	4.10	15	0.5	1.5
Ni	5.01	35	1.05	1.5
Cu	4.55	24	0.76	1.5
Fe	4.17	34	1.12	1.5

Clearly, the experimental values are well above k_BT. They are also above the theoretically predicted values shown in table (6.4). Conclusions to be drawn are; either the theory of field evaporation for energy half-widths is not properly understood or that some secondary process is occuring that is broadening the energy distribution. We note in passing that even larger FWHM-values are recorded for liquid-metal ion sources (see Swanson et al. 1981) and that it is known in this case that ion-ion interactions in the vacuum space are causing at least part of the broadening.

We may conclude that at this point of time, FWHM-measurements are not helpful in discriminating between escape mechanisms.

CHAPTER 7

SUMMARY, DISCUSSION AND IDEAS FOR FUTURE WORK

In this chapter, we summarise the achievements of this work and consider two further points relevant to this thesis. These are:

(a) Lack of explicit use of quantum mechanics in our treatment of field evaporation theory.

(b) The structured surface problem and probable non-linear trajectory of the emitted ion.

7.1 Achievements - summary and discussion

We began this work by formulating a consistent set of definitions, terminology and units of measurement for various field evaporation parameters, and discussion has been conducted within this framework.

A review of the literature and the further work described in this thesis have identified various types of experimental evidence and theoretical arguments that can help in determining the mechanism of field evaporation. Some of the evidence obtained from tests shows that the field evaporation is caused by thermal activation, some tests show that field-evaporated ions may undergo "post-ionization", and there are some specific tests that are capable of distinguishing between escape mechanisms. The situation can be summarised as follows.

(1) Field evaporation is caused by thermal activation; this is demonstrated by:

(a) the evaporation field prediction (F_n^e).

(b) the quasi-thermodynamic tests.

(c) estimation of the appearance energy.

The fact that a plot of ln(J) vs. 1/T is a straight line (at least over a relevant range of temperature) is also a evidence of this. Such plots have been used by Ernst (1979) and Kellogg (1984) to derive values of Q_n. We have also noted that prediction of evaporation field by the Mueller formula is not a valid test of escape mechanism. (2) The existence of "post-ionization" can be demonstrated by measurement of the evaporation charge-state distribution and its variation with field (taken in conjunction with appearance energy measurements). The evidence concerning charge states reveals that field evaporation is a two stage process (discussed in detail in section 3.5).

(3) For distinguishing between mechanisms the following tests are identified as appropriate:

(a) Calculation from potential curves of minimum theoretical Q_n (Q_n^{obs} vs. W_n^*).

(b) Calculation from potential curves of maximum theoretical evaporation field (F^{obs} vs. F_n^{HD}).

(c) Calculation from potential curves of maximum standard appearance energy (A^{obs} vs A^*).

(d) Tests based on estimation of partial energies from the experimental field-sensitivity data. The procedures need the mechanism dependent and mathematically correct expression for the field dependence of activation-energy.

(e) Study of variation of the evaporation field with temperature. Again, this procedure needs the mechanism dependent Q_n - F expression.

(f) Study of variation of Q_n with field. This needs the mechanism dependent explicit Q_n - F expression and also reliable experimental measurements of Q_n.

(g) Study of the appearance energy variation with field. This is also mechanism dependent because it needs the explicit Q_n-F expression.

(h) Study of FWHM variation with field. This needs a mechanism dependent FWHM expression, but it seems that reliable expressions are not available, so this test is not currently of any use.

The survey of the literature also brought out two other general points. First, that tests applied to distinguish between evaporation mechanisms have emerged in parallel with the experimental methods. The earliest were methods for determining the evaporation field values. These are followed by tests involving field sensitivities. It is only relatively recently that tests involving the explicit field dependence of activation energy and appearance energy have been considered. Second, it was also clear that there have been significant deficiencies in the theories of field evaporation in the literature, namely, the neglect of the dx^p/dF term (particularly in the context of the charge-hopping mechanism), and neglect of the repulsive term in the theory of both Mueller and Gomer-type mechanisms.

A major contribution of my work, as described in this thesis, has of course been to incorporate the repulsive term into the theory of the Mueller mechanism and to examine the consequences of

so doing.

More careful consideration of the tests listed suggests that these can be divided into two categories:

(1) Category A tests - 3(a) to 3(c) - these involve calculation of some parameter from potential curves and these calculated values are then compared with their corresponding observed values - comparison of F_n^{HD} with F^{obs} typifies a good example of this kind.

(2) Category B tests - 3(d) to 3(g) - these tests involve variation of one parameter with respect to another and are, in effect, based on comparison of theoretical and experimental values of the relevant rate of change. Thus, for example, the field sensitivity tests are really based on the rate of change of evaporation flux (J) with field F, although we have chosen to represent these in terms of partial energies.

The test concerning FWHM has to be considered in its own right (but, as already said, is not currently useful).

It should be noticed that the category A tests are in a sense clearer and more decisive than the category B tests; also that experimental parameters involved in category A tests can be measured reasonably well without significant complications; and that, for a species, these tests can provide a clear indication that the Mueller mechanism does not operate.

Although the category B tests have a tendency to be less decisive because of the experimental uncertainties in determining relevant parameters, these may be useful where the category A tests are indecisive.

Because the category A tests are considered to be more important, we have, in chapters 5 and 6, paid considerable

attention to the validity of the underlying theoretical assumptions.

As regards application of the tests, our conclusion is that in determining the escape mechanism the category A tests should be applied first; if, in a particular situation, these tests are found to be inconclusive, then category B tests should be applied.

As regards the species used in field evaporation experiments, our conclusion is that most materials do not field-evaporate via the Mueller mechanism. This conclusion is based on the category A tests as utilised in chapter 5 and in section 6.1, and details concerning particular materials will be found in the tables and figures in these sections.

7.2 On the validity of the basic assumptions

Assessment of the achievements of this work clearly reminds the reader that our treatment of field evaporation mechanism - like nearly all other treatments - is based on the suppositions that:

(1) It is permissible to use potential energy expressions in the classical form.

(2) Use of the flat-surface model is satisfactory.

(3) Evaporation can be treated as if it is taking place at right angles to the emitter surface and is independent of the detailed atomic structure of the emitter.

However, we must now look at these suppositions and assess how necessary these have been in developing a useful classical model for the Mueller mechanism.

7.2.1 Quantum mechanical considerations

Contemplation of the application of quantum mechanics to the field evaporation situation raises two doubts: whether it is plausible for an integrally charged ion to exist close to the metal surace; and, if such an ion exists, then whether its interaction with the metal electrons can be adequately described by the classical potential energy expressions used in this thesis.

If it is not plausible to assume that an integrally charged ion can exist at the point of escape then one has to assume that the ion is partially charged. This would tend to imply that the escape mechanism in field evaporation is some form of charge draining process. Full quantum mechanical calculations (if these were possible) would of course resolve this point. But it is precisely because such calculations were not possible in 1980 (and are still somewhat unreliable - Forbes, private communication), that a detailed study of the Mueller mechanism has been undertaken in this thesis.

However, let us assume that an integrally charged external ion can exist. Strictly, one should calculate its interaction with the surface quantum-mechanically. But, whatever the results of quantum mechanical calculations of potential energy contributions associated with the external ion, these can be put into approximate analytical mathematical forms even if these are applicable only over small ranges of distances. For the maximum theoretical F and minimum theoretical Q_n tests, we have looked at how our physical conclusions would be affected by changes in the

paramaterisation of the potential energy expressions, and we have found (in chapters 5 and 6) that our conclusions were not unduly sensitive to such changes. We therefore trust that expressions derived from quantum mechanical arguments would translate to approximate mathematical forms lying within the parameter ranges.

7.2.2 Structured surface considerations

In the structured surface situation the field varies with position lateral to the surface. Therefore, there is a possibility that the ion trajectory is partly parallel to the surface. There is experimental evidence that this is in fact the case, namely the aiming errors observed in field desorption microscopy (Waugh et al. 1976).

The suggestion is that as the electric field is raised over an emitter surface, a kink site atom leaves the normal lattice site and rolls to a position more exposed to the field before leaving the surface. We now have to consider two possibilities, that ionization takes place immediately after the atom has rolled to the field exposed site or while it is still rolling towards it. Therefore, with such a trajectory escape may occur either on the lateral part of the path or at the normal part of the path. The question is: how does this affect our arguments?

Let us consider the "normal escape" situation first. The most important test that we have performed on the escaping ion relies on the energy difference between the bonding level and the hump level. The theory determines the level of the hump relative to absolute zero. In the structured surface situation, one has to think in terms of ion potential energy variation along a line

passing through a protruding substrate atom over which field evaporation takes place. There will, of course, be some field variation along this line and an average field of some kind will appear in the electrostatic term. That average field may not correspond to the measured field (but is probably slightly higher).

As regards the field at the bonding point, this field is less than that used to determine the hump level. If F is the latter field then the corresponding field at the bonding position is given by:

$$F' = \eta F \text{ where } \eta < 1 \qquad (7.1)$$

Now consider the expression for W_n^* discussed in section (6.1) (or any similar expression). In this we can interpret F as some average field above a protruding surface atom. But a different field ηF should now appear in the "$(1/2)c_\alpha F^2$" term. However, since the parameter c_α is basically an empirical one, it is probably best to leave the theory in its existing form but to interpret c_α as taking into account local field differences as well as polarisation and partial ionization effects.

In reality, in applications of the theory, either c_α is determined empirically, or the F^2 - term is neglected. Thus most of the theoretical arguments used previously (and certainly those relating to the "Category A" tests) are applicable to the structured surface situation.

Let us look more closely at the "maximum theoretical evaporation field" test discussed in chapter 5. The experimental values quoted for "evaporation field" correspond to values of the "external" field some little way above the surface. But on the

line through the protruding atom, the "effective" field at the position of the hump will necessarily be higher than this external field. On the other hand, the calculated F_n^{HD} values are values for the effective field. So if the "observed" external field is higher than F_n^{HD}, then this implies that the "experimentally derived" effective field will be even higher than F_n^{HD}. So in this situation our arguments against the Mueller mechanism become stronger.

It is also true that, if escape takes place on the normal part of a path lying above a protruding atom, then there should be less uncertainty in determining the value of a_n, since the situation corresponds to the helium field ionization results (Culbertson at al. 1979). Arguments relating to the size of ions become more straight-forward. Again, if anything, our arguments seem to become stronger.

Now consider the alternative situation in which escape occurs on the lateral part of the trajectory. Whilst the atom is rolling on the surface, it must be in close contact with it. However, it is now believed that an integrally charged ion cannot exist close to the surface; so we need to assume that any particles that are in contact with the emitter surface are partially charged. Thus, if escape occurs when the atom is rolling then the mechanism involved in field evaporation cannot possibly be the Mueller mechanism. Most probably it would be some complicated form of charge draining mechanism.

The general conclusion, therefore, is that our arguments against the Mueller mechanism should be reasonably robust, both against the introduction of quantum-mechanical arguments, and against the abandonment of the flat-surface assumption. It should

remain true that most species do not escape via the Mueller mechanism.

7.3 Some ideas for future work

It is clear, from the analysis of this thesis, that more experimental and theoretical work would be useful in a number of areas. To improve our understanding of theories of field evaporation we need to establish a better view on the behaviour of charged surfaces and the trajectory of the field evaporated ions. It is important that better surface models are available to predict local field and potential variations, taking into account the local atomic and electronic structures.

On the basis of an appropriate charged surface structure, a better theoretical basis for the charge-draining mechanism has to be developed.

There should be more experimental work in field evaporation, especially on measurement of the temperature dependence of evaporation field, of the field dependence of activation energy (using a wide range of materials), and of the field dependence of $n_{hr}A$. Although, in our theretical work, we have not considered the field dependence of $n_{hr}A$, we think that it has an interesting part to play in field evaporation theories, and possible theoretical reasons for the field-dependence in $n_{hr}A$ should be explored.

Perhaps the strongest implication of our work, however, is that one should now put aside the Mueller mechanism, and concentrate more on the urgent need of a good quantum mechanical treatment of the charge-draining mechanism.

REFERENCES

Andren H. O., Henjered A. and Kingham D. R." On the charge state of tungsten ions in the pulsed-field atom probe", Surface Sci. 138 (1984) 227 - 234

Birdseye P. J. Ph.D. Thesis, University of Oxford, (1972)

Brandon D. G."The resolution of atomic structure; recent advances in the theory and development of the field-ion microscope." Brit. J. Appl. Phys. 14 (1963) 474 - 485

Brandon D. G."The structure of field evaporated surfaces" Surface Sci. 3 (1964), 1-18

Brandon D. G. "The analysis of field evaporation data from field-ion microscope experiments". Brit. J. Appl. Phys. 16 (1965) 683 - 692

Brandon D. G. "The field evaporation of dilute alloys." Surface Sci. 5 (1966a) 137 - 145

Brandon D. G. "On field evaporation" Phil. Mag. 14 (1966b) 803 - 820

Brenner S. S. and McKinney J. T. "On the ionization state of field evaporated atoms as measured in the FIM atom probe" Appl. Phys. Letters, 13 (1968) 29 - 33

Chambers R. S. Ehrlich G. and Vesely M. in 17th Field Emission Symposium, Yale University (1970).

Chambers R. S. Ph.D. Thesis, University of Illinois at Urbana; Champainy, (1975).

Chibane K. Ph.D. Thesis, University of Aston in Birmingham, (1985)

Culbertson R. J., Sakurai T. and Robertson, G. H. " Field ionization of surface adsorbates". Phys. Rev. B19 (1979) 4427 - 4434

Ehrlich G. and Kirk C.F." Binding and field desorption of individual tungsten atoms". J. Chem. Phys. 48 (1968) 1465- 1473

Ernst N. "Experimental investigation of field evaporation of singly and doubly-charged rhodium" Surface Sci. 87 (1979), 469-82

Ernst N., Bozdech and Block J. H. "Field ion appearance spectroscopy" Surface Sci. 80 (1979) 645-655

Ernst N. and Block J. H. "Comparison of Debye temperature for rhodium surface atoms determined during field evaporation and low energy electron diffraction" Surface Sci. 91 (1980) L27-L31

Ernst N. and Jentsch T.H. "Post-field-ionization of singly charged rhodium: an experimental and theoretical study". Phys. Rev. B24 (1982) 6234-41.

Forbes R. G. "An alternative theoretical approach to field evaporation rate sensitivities". Surface Sci. 46 (1974) 577 - 601

Forbes R. G. "A generalised theory of standard field ion appearance energies" Surface Sci. 61 (1976) 221-244

Forbes R. G. Unpublished report (1977)

Forbes R. G. "Negative work-function correction at a positively-charged surface" J. Phys. D: Appl. Phys. 11 (1978a) L161 - L165

Forbes R. G. "Field evaporation theory: the atomic-jug formalism" Surface Sci. 70, (1978b) 239-54

Forbes R. G. "Charge-hopping and charge-draining: two mechanisms of field desorption" Surface Sci. 102 (1981) 255-262

Forbes R. G. "Electrothermodynamical cycles applied to ionic potentials and to field evaporation" J. Phys. D.: Appl. Phys. 15 (1982a) 1301-22

Forbes R. G. "A new formula for predicting low-temperature evaporation field". Appl. Phys. Letters, 40 (1982b) 277 - 279

Forbes R. G. "Towards a criterion for the a-priori prediction of field evaporation mechanism" J. Phys. D.: Appl. Phys. 15 (1982c) L99-L104

Forbes R. G. and Chibane K. "A fresh look at the electric-field dependence of surface atom binding energy" Surface Sci. 121 (1982a) 275 - 289

Forbes R. G. and Chibane K. "The temperature dependence of evaporation field for Gomer-type field evaporation mechanism" Surface Sci. 122 (1982b) 191 -215

Forbes R. G., Biswas R. K and Chibane K. "Field evaporatio theory: A re-analysis of published field sensitivity data". Surface Sci. 114 (1982) 498 - 514

Forbes R. G., Chibane K. and Ernst N. "Derivation of bonding distance and vibration frequency from field evaporation experiments" Surface Sci. 141 (1984) 319 - 340

Forbes R. G. and Wafi M. K. "An array model for the field adsorption of helium on tungsten(111)" Surface Sci. 93 (1980) 192 - 212

Goldenfield I. V., Korostyshevsky I. Z. and Mischadchuk B. G. "Analysis of field-ion energies in a mass spectrometer" Intern. J. Mass Spectrom. Ion Phys. 13 (1974) 297 - 309

Gomer R. "Field desorption". J. Chem. Phys. 31 (1959) 341 - 345

Gomer R. "Field emission and field ionization" (OUP, London, 1961).

Gomer R. and Swanson L.W. "Theory of field desorption". J. Chem. Phys. 38 (1963) 1613 - 1625

Haydock R. and Kingham D. R. "Post-ionization of field evaporated ions" Phys. Rev. Letters, 44 (1980) 1520-23

Kellogg G. L. "Measurement of the charge state distribution of field evaporated ions: evidence for post-ionization". Surface Sci. 120 (1982) 319 - 327

Kellogg G. L. " Measurent of activation energies of field evaporation of tungsten ions as a function of electric field" Phys. Rev. B 29 (1984) 4304 - 4312

Kellogg G. L. and Tsong T. T. J. Appl. Phys. 51 (1980) 1184 - 1193

Kingham D. R. "The post-ionization of field evaporated ions: a theoretical explanation of multiple charge states" Surface Sci. 116 (1982a) 273-301

Kingham D. R. "The mechanism of charge transfer during field evaporation". Proc. 29th IFES, Goeteborg, Sweden, (1982b)

Kreutzer H. J. and Nath K. J. D. Physique 47, Colloque C7 (1986) 3 - 6

Knor Z. Surface and defects properties of solids Vol. 6 (1977) 139 - 152

Lang N. D. and Kohn W. "Theory of metal surfaces: induced surface charge and image potential". Phys. Rev. B7 (1973) 3541- 3545

McKinstry D. "An examination of field evaporation theory". Surface Sci. 39 (1972) 37 - 59

Mair G. L. R., Forbes R. G., Latham R. V. and Mulvey T. "Energy spread measurements on a liquid metal ion source" Microcircuit Engineering (1983), ed. by H. Ahmed, J. R. A. Cleaver, Jones G. A. C. 171 - 178

Menand A. and Kingham D. R. "Isotopic variations in field evaporation charge-state of Boron ions". J. Phys. D.: Appl. Phys. 17 (1984) 203-208

Mueller E. W. "Tearing off adsorbed ions by high electric field strengths". Naturwissenschaften 29 (1941) 533 - 541

Mueiier E. W. "Field desorption" Phys. Rev. 102 (1956) 618 - 630

Mueller E. W. "Field-ionization and field-ion microscopy" Adv. Electr. and Electron Phys. 13 (1960) 83 - 98

Mueller E. W. "The effect of polarization, field and gas impact on the topography of field evaporated surfaces". Surface Sci. 2 (1964) 484 - 493

Mueller E. W., Panitz J. A. and McLane S. B. "The atom-probe field-ion microscope" Rev. Sci. Inst. 39 (1968) 83- 99

Mueller E. W. and Tsong T. T. "Field-ion microscopy; principles and applications" (Elsevier: New York 1969)

Mueller E. W. and Tsong T. T. Prog. Surface Sci. 4 (1974) 1 - 11

Mueller E. W. and Krishnaswamy S. V. "High ionic charges on field evaporating 5d transition metals". Phys. Rev. Letters, 37 (1976) 1011 - 1020

Nakamura S. "Field evaporation of metals in field-ion microscope". J. of Electron microscopy, 4 (1966) 279-285

Nakamura S. and Kuroda T. "On field evaporation endforms of a bcc metal surface observed by a field-ion microscope" Surface Sci. 17 (1969) 346 - 358

Patel C., M.Sc. Thesis, University of Aston in Birmingham (1974)

Plummer E. W. and Rhodin T. N. "Atomic binding of transition metals on clean single crystal tungsten surfaces" J. Chem. Phys. 49, No.8 (1968) 3479-96

Reviere J. C. "Solid state Sci." Vol. 1, ed. M. Green, (Dekker, New York 1969) 179

Sakurai T. and Mueller E. W. "Field calibration using the energy distribution of field-ionization" Phys. Rev. Letters, 30, No.12 (1973) 532 - 538

Smith J. R. Ying S. C. and Kohn W. "Charge densities and binding energies in hydrogen chemisorption". Phys. Rev. Letters, 30, No. 13 (1973) 610 - 619

Smoluchowski R. "Anisotropy of the electronic work-function of metals" Phys. Rev. 60 (1941) 661 - 669

Swanson L. W. "Microcircuit Engineering" (1980) Amsterdam

Swanson L. W., Schwind G. A. and Bell A. E. J. Appl. Phys. 51 (1980) 3453 - 3455

Taylor D. M., Ph.D. Thesis, Cambridge University (1970)

Theophilou A. K. and Modinos A. " Metallic field effect and its consequences in field emission, field ionization and capacitance of a capacitor" Phys. Rev. B6 (1972) 801 - 809

Tsong T. T. "On the mechanism of field evaporation" Surface Sci. 10 (1968), 102 - 117

Tsong T. T. "16th. Field emission symposium", Pittsburgh Pa. (1969)

Tsong T. T. "Measurement of the polarizabilities and field evaporation rates of individual tungsten atoms" J. Chem. Phys. 54 (1971) 4205 - 4216

Tsong T. T. "Field ion image formation". Surface Sci. 70 (1978a) 211 - 218

Tsong T. T. "Measurement of field evaporation rate of several transition metals". J. Phys. F. (Metal Phys.) 8 (1978b) 1349 - 1351

Tsong T. T. and Mueller E. W. "Effects of static penetration and polarisability on the capacity of a capacitor, field evaporation and field ionization processes". Phys. Rev. 181 (1969) 530 - 535

Tsong T. T. and Mueller E. W." Field evaporation rates of tungsten" Phys. Stat. Sol. (a). 1 (1970) 513 - 533

Tsong T. T. and Mueller E. W. "Field adsorption of inert gas atoms", J. Chem. Phys. 55 (1971) 2884 - 2891

Vesley M. and Ehrlich G. "Field evaporation: model and experiments" Surface Sci. 34 (1973) 547 - 560

Wada M., Konishi M. and Nishikawa O. "Binding states of Ga and Sn on W and Mo: structures, evaporation field and its temperature dependence". Surface Sci. 100 (1980) 439 - 445

Wafi M. K., Ph. D. Thesis, The University of aston in Birmingham, (1981)

Walko R. J. and Mueller E. W. "Self imaging of a surface by field evaporation" Phys. Stat. Sol. (1972) 99K9

Waugh A. R., Boyes E.D. and Southon M. J. "Investigations of field evaporation with a field desorption microscope" Surface Sci. 61 (1976) 109-142.